

Transmembrane Signalling: Structural and Functional Studies on Histidine Kinase CitA

Dissertation

for the award of the degree

Doctor rerum naturalium

of the Georg-August University Göttingen

within the doctoral program *Biomolecules: Structure - Function -*

Dynamics

of the Georg-August University Graduate School of Science (GAUSS)

submitted by

Benjamin Schomburg

from Löhne

Göttingen 2014

Thesis Committee

Prof. Dr. Christian Griesinger
Dept. of NMR-based Structural Biology
Max-Planck-Institute for Biophysical Chemistry, Göttingen

Prof. Dr. Claudia Steinem
Institute for Organic and Biomolecular Chemistry, University of Göttingen

Prof. Dr. Blanche Schwappach
Dept. of Biochemistry I, University of Göttingen Medical School

Examination Board

Referee: Prof. Dr. Christian Griesinger
Dept. of NMR-based Structural Biology, Max-Planck-Institute for Biophysical Chemistry, Göttingen

2nd Referee:

Prof. Dr. Claudia Steinem
Institute for Organic and Biomolecular Chemistry, University of Göttingen

Further members of the Examination Board

Prof. Dr. Blanche Schwappach
Dept. of Biochemistry I, University of Göttingen Medical School

Prof. Dr. Patrick Cramer
Dept. of Molecular Biology, Max-Planck-Institute for Biophysical Chemistry, Göttingen

Prof. Dr. Michael Meinecke
Dept. of Cellular Biochemistry, University of Göttingen Medical School

Dr. Martin Kollmar
Dept. of NMR-based Structural Biology, Max-Planck-Institute for Biophysical Chemistry, Göttingen

Date of oral examination: 28.01.2015

Affidavit

I hereby declare that I wrote this thesis *Transmembrane Signalling: Structural and functional Studies on Histidine Kinase CitA* on my own and without the use of any other than the cited sources and tools.

.....

Place, Date

.....

Signature

Contents

Contents	v
1 Introduction	1
1.1 Stimulus perception in cells	1
1.2 Structural features of histidine kinases	4
1.3 Two-component systems	6
1.4 PAS domains	7
1.5 CitA family	9
1.6 <i>Geobacillus thermodenitrificans</i>	11
1.7 NMR assignment strategy	11
2 Materials and Methods	15
2.1 Chemicals and equipment	15
2.2 Construct selection	15
2.3 Strains, plasmids and primers	15
2.4 Cloning techniques	18
2.4.1 Polymerase chain reaction (PCR)	18
2.4.2 Agarose gel electrophoresis	18
2.4.3 Restriction digestion of DNA	18
2.4.4 Ligation of DNA fragments	19
2.4.5 Plasmid purification	19
2.4.6 DNA sequencing	19
2.4.7 Site-directed mutagenesis	19

2.5	Transformation and cultivation of <i>Escherichia coli</i>	20
2.5.1	Unlabelled protein	20
2.5.2	Selenomethionine-labelled protein	21
2.5.3	^{13}C - ^{15}N labelled protein	22
2.6	Protein purification	24
2.6.1	PAS domains	24
2.6.2	Gt CitApc solid-state NMR samples	26
2.7	Crystallisation of PAS domains	29
2.8	Liquid-state NMR experiments	30
2.8.1	General procedures	30
2.8.2	Secondary structure determination	30
2.8.3	Ligand affinity determination	31
2.9	Solid-state NMR experiments	33
2.9.1	PDSO spectra	33
2.9.2	Triple-resonance spectra	34
2.9.3	INEPT spectra	36
3	Results	37
3.1	The periplasmic PAS domain (PASp)	37
3.2	The cytosolic PAS domain (PASc)	43
3.3	Liposome-embedded CitApc	49
4	Discussion	57
4.1	The periplasmic PAS domain (PASp)	57
4.1.1	Citrate binding and activation of PASp	59
4.2	The cytosolic PAS domain (PASc)	62
4.3	Liposome-embedded CitApc	64
4.3.1	CitApc in Asolectin	64
4.3.2	CitApc R93A in DMPC	66
4.3.3	Citrate affinity of PASp	71
4.3.4	Signalling effects in the cytosolic PAS domain	73

4.3.5	PASc in context of full-length CitA	75
4.3.6	Signal transduction model	77
4.4	Outlook	79
5	Abstract	83
	Bibliography	85
6	Acknowledgements	99
7	List of abbreviations	101
8	Appendix	105
8.1	Expression vectors	105
8.2	PASc crystal data collection, phasing and refinement statistics	107
8.3	NMR assignments	108
8.4	Pulse programs	132
8.4.1	Liquid-state NMR	132
8.4.2	Solid-state NMR	138

1 Introduction

1.1 Stimulus perception in cells

In an ever-changing environment, the ability to adapt is key to the survival of all organisms. To be able to monitor and react to environmental stimuli, signal uptake and processing needs to be executed by cells. Hence chemical signals, like changes in osmolarity, availability of nutrients or toxic conditions have to be communicated across the cellular plasma membrane. To this end, a variety of different classes of receptors are utilised, including G-protein coupled receptors, ion channels and enzyme-linked receptors. In the class of enzyme-linked receptors, receptor kinases constitute a large family of proteins that allow for interwoven signalling networks in which different pathways can interact with each other.

Receptor kinases are employed by virtually all organisms and are characterised by a kinase domain that phosphorylates specific amino acid residues (primarily serine/threonine, tyrosine or histidine) either of an effector protein or within the receptor itself (Hanson and Schulman, 1992). Signal processing through phosphorylation has the advantage of being reversible, adaptable and efficient, using a small modification to a protein for a recognisable effect on structural and thus functional properties (Westheimer, 1987). The reversibility is provided by protein phosphatases that selectively dephosphorylate the phosphoprotein. Since the kinases and phosphatases can be triggered by different inputs, crosstalk between different pathways is easily achieved. The net state of phosphorylation is determined by the activity of all relevant kinases and phosphatases and can thus be more complex than a simple on/off switch (Bray, 1995). The adaptability is generated by a large pool of receptor domains that selectively recognise input molecules and

kinases/phosphatases that then selectively modify target proteins. Lastly, a phosphorylation mechanism is efficient through its use of ATP as a high energy phosphate donor to ensure a thermodynamically favourable reaction, while the dephosphorylation is readily achievable through bulk water allowing for energetically favourable hydrolysis.

Histidine phosphorylation, the main phosphorylation mechanism in prokaryotes, was unknown until 30 years after initial findings of protein phosphorylation (Boyer *et al.*, 1962). Signalling through protein phosphorylation was therefore believed to be absent in prokaryotes, mostly because of the susceptibility of phosphoramidates of phosphorylated histidines in activated prokaryotic kinases to hydrolysis in the acidic assays used at the time. The first evidence for prokaryotic histidine phosphorylation can be credited to *in vitro*-studies of the histidine kinases (HKs) NtrB (Ninfa *et al.*, 1988) and CheA (Hess *et al.*, 1988). HKs and their signalling targets, the response regulators (RRs), have since emerged as the most abundant signalling system in prokaryotes. HKs are found in virtually all bacterial species, with only few exceptions (Koretke *et al.*, 2000). In addition, around five percent of all known histidine kinases are found in fungi, amoebae and plants (Thomason and Kay, 2000).

In prokaryotes, the roles of histidine kinase signalling systems include sensing of nutrients, chemoattractants, osmotic conditions, cell density and more. In eukaryotes, histidine kinases have been found governing hormone-dependent developmental processes. Since HKs are not found in animal genomes, one major research interest is the potential for developing new classes of antimicrobial drugs. Instead of toxic effects to bacteria, binding to HKs could be used in these new antibiotics to trigger an immune response to HKs. Alternatively, HKs important for microbial toxicity could be inhibited. These indirect drugs would cause less side effects and, more importantly, would be less likely to evoke resistance compared to classical antibiotics (Wolanin *et al.*, 2002).

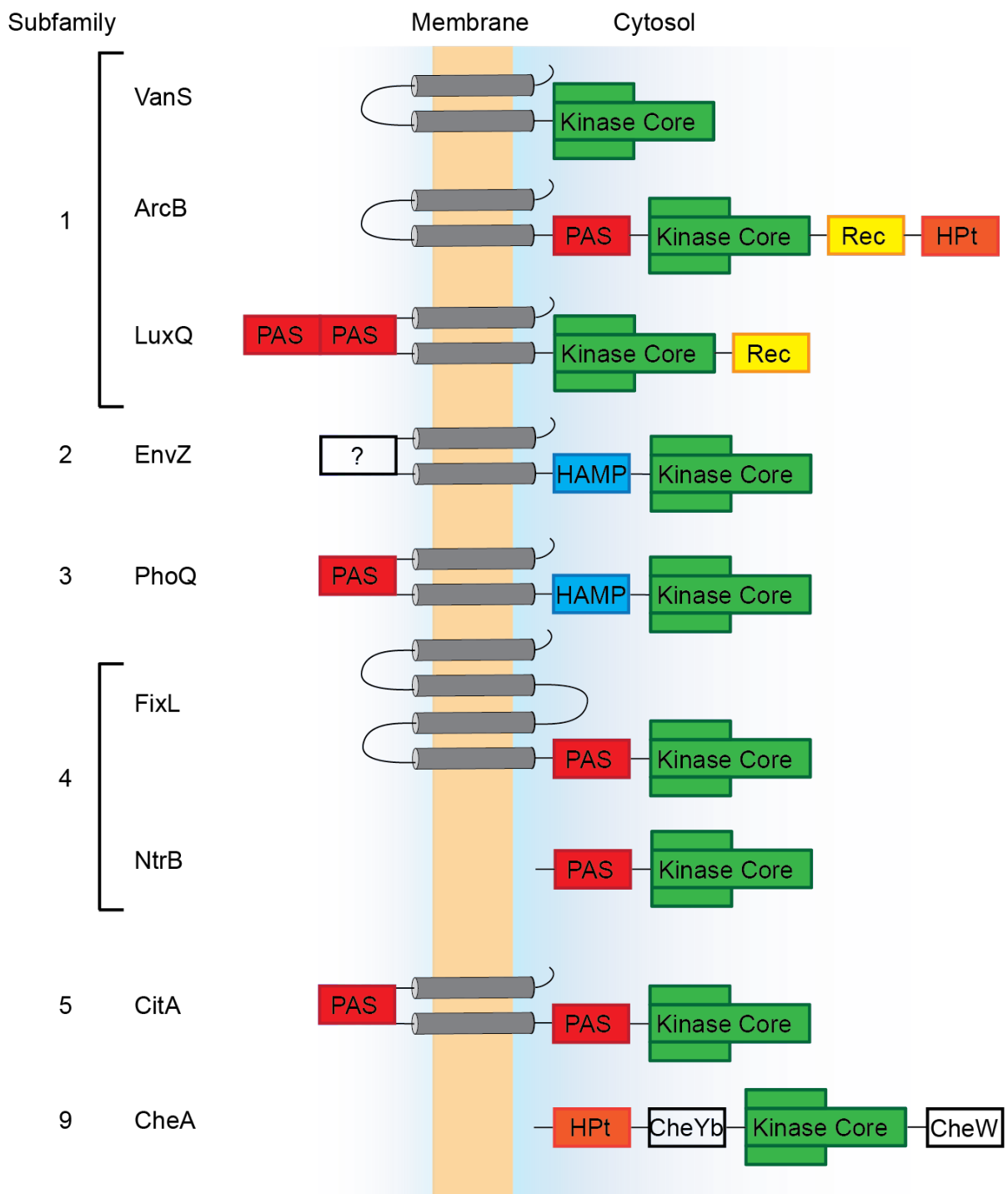


Figure 1.1: Domain organisation of selected histidine kinases. Different HK subfamilies can be classified based on conserved homology motifs in the kinase core. Even within one family, the domain organisation varies greatly, as exemplified for subfamily 1. 83 % of HKs contain transmembrane segments and relay signals across the cellular membrane.

HKs are an extremely diverse class of proteins with modular design. They are classified by a conserved kinase core consisting of a dimerisation and histidine phosphorylation domain (DHp) and the catalytic, ATP-binding kinase (CA). Based on conserved homology motifs in both DHp and CA domains, HKs can be divided into 11 distinct subfamilies (see figure 1.1) (Grebe and Stock, 1999). Subfamily 1 is the most common type of HK, comprising around 20 % of all known sequences and including all eukaryotic HKs. It also contains almost all hybrid HKs. One distinct class of HK is subfamily 9 in which one of the homology motifs, the H-box (containing the phosphorylatable histidine), is missing. Therefore, signal transduction through DHp phosphorylation is not possible. The subfamily 9 HKs are exclusively found in chemotaxis systems, in which they interact with auxiliary sensory components (Borkovich and Simon, 1991). Other HK subfamilies are characterised solely based on homology motifs and cannot be assigned to specific functional groups.

In general, HK subfamilies do not share domain architectures, but are characterised by the aforementioned homology motifs around the phosphorylatable histidine and the active site of the CA domain. As a result, different classes of HKs bind to different, specific classes of RRs based on structural motifs in the protein-protein interface (Grebe and Stock, 1999).

1.2 Structural features of histidine kinases

Over the last years, a number of structures have been solved of the complete kinase core (DHp + CA), isolated DHp and CA domains as well as of RRs and HK-RR domain complexes for various HKs, revealing details on the activation and phosphate transfer mechanism (for a selection of available structures, see (Zapf *et al.*, 2000; Marina *et al.*, 2005; Albanesi *et al.*, 2009; Casino *et al.*, 2009; Yamada *et al.*, 2009; Podgornaia *et al.*, 2013; Wang *et al.*, 2013)). The DHp domain consists of two anti-parallel helices forming a four-helix bundle through dimerisation. The CA domains are loosely attached to DHp by a flexible linker, allowing for different orientations of CA towards the conserved histidine in DHp domains. Unlike catalytic domains of Ser/Thr or Tyr kinases, the CA domain

of HKs is structurally related to the GHL ATPase superfamily, named after its members GyrB, Hsp90 and MutL (Dutta and Inouye, 2001) and thus not evolutionarily related. The kinase core structures reveal two distinct histidine phosphorylation routes, either *cis* or *trans*, with one kinase phosphorylating the histidine residue either of the same or of the other monomer. Recently, the helix bundle loops connecting the two α -helices in DHp have been identified as the determinant for *cis* or *trans* autophosphorylation (Ashenberg *et al.*, 2013). The length of this loop determines the helix bundle handedness, which in turn dictates the accessible phosphorylation site. In all structures solved to date that catch the CA domain in a kinase competent state, the phosphorylation reaction is asymmetric. While one of the CA domains approaches the activated histidine, the other is far away. Based on these structures, alternating reaction cycles for the individual CA domains in the dimer are proposed. In the crystal structures solved to date, the asymmetry of the CA domains is reflected in an asymmetric DHp assembly. Nonetheless, the asymmetry in DHp might be a result of crystal packing artefacts, which is suggested by symmetrical solution NMR structures of chimeric constructs including the EnvZ DHp domain (Ferris *et al.*, 2012).

Both the asymmetry and the flexibility involved complicate structural studies on the kinase core. However, a mechanistic model for autophosphorylation was recently proposed based on structure-guided functional analysis (Casino *et al.*, 2014). In this model, a nucleophilic attack of histidine on the γ -phosphate in ATP is made possible by a conserved aspartate in DHp acting as a general base. The γ -phosphate of ATP is positioned for the nucleophilic attack by conserved CA residues and shielded by a coordinated magnesium ion. The active site is thus formed by both the DHp and the CA domains. The phosphorylation mechanism seems to be comparable in *cis* or *trans*. In addition to kinase and phosphotransferase functionality, most HKs act as phosphatases on RRs. Depending on switching between states in the receptor domain, the net state of the protein is either kinase/transferase or phosphatase (Perego and Hoch, 1996; Hsing *et al.*, 1998).

1.3 Two-component systems

In a prototypical system, a HK forms a two-component system (TCS) with its cognate RR which is activated by the kinase and triggers cellular responses to extracellular stimuli. Since approximately 83 % of HKs are transmembrane proteins (Cock and Whitworth, 2007), a soluble RR is essential for transducing signals to cytosolic cell components. In the most simple case, the HK autophosphorylates on a conserved histidine upon signal recognition, creating a high-energy phosphoramidate. The phosphate is consecutively transferred to a conserved aspartate in the receiver domain (REC) of the cognate RR (see figure 1.2). Both HKs and RRs are highly modular proteins, allowing for integration of a wide variety of input signals and output responses. The prototypical RR consists of an *N*-terminal REC domain and a variable *C*-terminal effector domain. The REC domain is conserved in all known RRs with an average sequence identity of 26 %. In contrast, effector domains are structurally and functionally diverse. The most prominent class of RRs (63 %) contains DNA-binding effector domains of various structural families to alter gene expression levels. Other roles of effector domains include RNA binding, protein binding, and enzymatic functions (Gao and Stock, 2009).

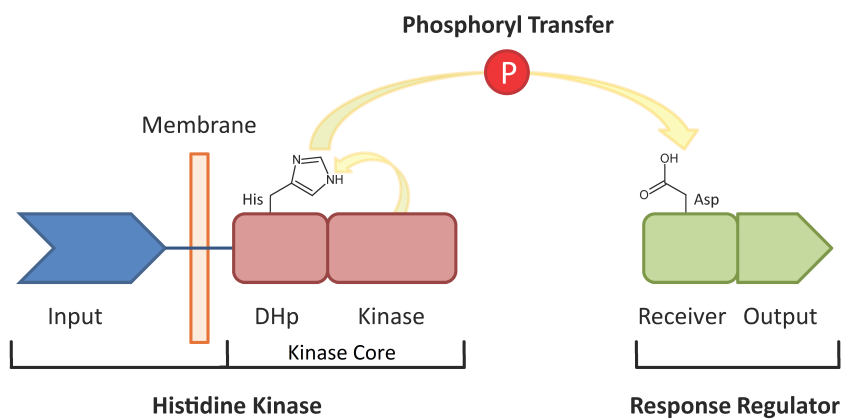


Figure 1.2: Schematic diagram of a minimal two-component system. The histidine kinase consists of a stimulus receiving receptor domain (input), the dimerisation and histidine phosphorylation domain (DHp) and the kinase domain. DHp and kinase form the conserved kinase core. Upon activation a conserved histidine in DHp is phosphorylated and the phosphoryl group consecutively transferred to an aspartate residue in the receiver domain (REC) of a response regulator. The activated response regulator then triggers cellular response through the output domain.

Additionally, RRs consisting of stand-alone REC domains lacking effector domains have been identified. These either function in chemotaxis systems by binding directly to motor proteins, or as part of a phosphorelay system. Phosphorelay systems are more complex than prototypical TCSs and involve several His-Asp phosphate transfer steps. HKs of phosphorelay systems contain REC domains and are termed hybrid HKs. Upon activation, phosphate is transferred from the conserved histidine in DHp to an aspartate residue of the internal REC domain. The phosphate of the REC domain is then transferred to a histidine phosphotransfer (HPt) domain, which is structurally related to DHp and can either be part of a soluble protein or of the kinase itself to create a phosphorylation cascade. From the HPt domain, the phosphorylation signal can be transferred to another REC domain, for example on a RR (Ogino *et al.*, 1998; Perego, 1998). Hybrid HKs are found in around 25 % of TCSs and open up possibilities for integration of different signalling pathways and multiple checkpoints along the phosphate transfer pathway.

1.4 PAS domains

For perceiving stimuli, HKs utilise a wide variety of different receptor domains. A presentation of all types of receptors is beyond the scope of this introduction; signal perception mechanisms are reviewed in detail elsewhere (Szurmant *et al.*, 2007; Krell *et al.*, 2010). The most abundant class of sensor domains is the PAS domain which can be found in at least 33 % of HKs (Gao and Stock, 2009). PAS domains are named after the first proteins in which the structural motif was first recognised, PER (period clock protein in *Drosophila melanogaster*), ARNT (aryl hydrocarbon receptor nuclear translocator of vertebrates) and SIM (single-minded protein in *D. melanogaster*). In prokaryotes, PAS domains are mainly found in HKs and serve as receptors associated with a wide range of stimuli, including light, redox potential, oxygen, small ligands and the overall cellular energy level (Taylor and Zhulin, 1999). In addition to HKs, PAS domains play a role in Ser/Thr kinases, circadian clock proteins, voltage-gated ion channels and cyclic nucleotide phosphodiesterases in both prokaryotes and eukaryotes.

Given that the PAS fold is found in all kingdoms of life, it is not surprising that the sequence homology is fairly low and prediction of PAS domains was almost impossible before the advent of algorithms like PSI BLAST (Altschul *et al.*, 1990). In fact, several PAS domains, for example receptor domains of HKs CitA, DcuS and PhoQ, have only been identified based on 3D structures and not on the primary sequence (Reinelt *et al.*, 2003; Pappalardo *et al.*, 2003; Cho *et al.*, 2006). The PAS fold consists of an N-terminal helix cap, a central β -scaffold of five anti-parallel strands and a varying number of short helices on one face of the β -sheet (see figure 1.3). The N-terminal cap is least conserved, both structurally (Vreede *et al.*, 2003) and based on amino acid sequence (Taylor and Zhulin, 1999).

Signal perception through PAS domains is possible through several different mechanisms. Most frequently, small molecule ligands bind to a cavity in the centre of the PAS core (the PAS fold excluding the N-terminal cap), as evident from structural and functional analysis on CitA (Kaspar *et al.*, 1999; Reinelt *et al.*, 2003; Sevvana *et al.*, 2008) or TodS (Mosqueda *et al.*, 1999; Lacal *et al.*, 2006). Another widely used mechanism of signal recognition through PAS domains involves bound cofactors. Cofactor-mediated stimulus perception is mainly found in systems associated with redox potential, oxygen concentration and light perception (Taylor and Zhulin, 1999). Bound cofactors include flavine adenine dinucleotide (Key *et al.*, 2007) and heme (Gong *et al.*, 2000). A third mode of stimulus perception is oxidation of cysteine-containing PAS domains to alter domain dynamics. In the HK ArcB, oxidative stress leads to inactivation of the kinase by the formation of two intermolecular cysteine bonds in PAS domains of a HK dimer, thus rigidifying the domain (Malpica *et al.*, 2004). In PhoQ, yet another stimulus perception

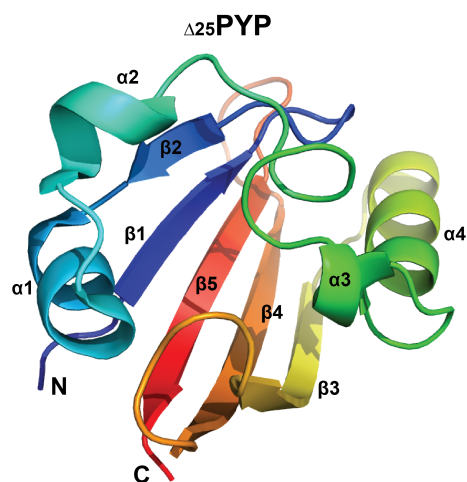


Figure 1.3: The PAS domain core. The photoactive yellow protein is viewed as a prototypic PAS domain. Deleting the N-terminal helix leaves an independently folding PAS core. Structural elements are labelled. PDB accession code: 1ODV (Vreede *et al.*, 2003)

mechanism is described, in which divalent cations bind at the PAS - membrane interface to trigger different conformations (Cho *et al.*, 2006; Cheung *et al.*, 2008).

In addition to stimulus perception, PAS domains also seem to be involved in signal propagation. Several HKs, including LuxQ (Neiditch *et al.*, 2006) and CitA (Etzkorn *et al.*, 2008) contain PAS domains that are not involved in ligand binding. The role of these PAS domains is difficult to study, as structural rearrangements cannot be triggered by ligand binding. Functional studies of these non-ligand binding PAS domains therefore have to be carried out in context of the multi-domain kinases, which is one of the aims of the study presented here.

1.5 CitA family

As shown above, the most prevalent domain organisation in HKs is characterised by a periplasmic sensory domain flanked by two transmembrane helices, with a cytosolic, C-terminal kinase core (see figure 1.1). In addition, PAS domains are the most widely used receptor domain. The CitA HK family with a periplasmic, citrate binding receptor domain and a second, cytosolic PAS domain preceding the kinase core is therefore an ideal candidate for structural studies on HKs. Over the last two decades, two proteins of the CitA family, DcuS and CitA itself, have been extensively studied.

DcuS is a C₄-dicarboxylate receptor first identified in 1998 as part of the DcuS-DcuR TCS (Zientz *et al.*, 1998). The DcuS-DcuR system is responsible for activating genes for dicarboxylate transport and fermentation in response to the availability of aspartate, fumarate, malate, maleate and succinate (Zientz *et al.*, 1998; Golby *et al.*, 1999). Fumarate-dependent activation, phosphoryl transfer to DcuR and binding of DcuR to DNA was shown *in vitro* (Janausch *et al.*, 2002; Abo-Amer *et al.*, 2003). With the availability of liquid-state NMR - (Pappalardo *et al.*, 2003; Kneuper *et al.*, 2005) and X-ray crystal structures (Cheung and Hendrickson, 2008) of the periplasmic, ligand binding domain, a first view of structural reorganisations in the periplasmic PAS domain is possible. However, as a model protein for a two-state signalling system DcuS is less than ideal as it requires the presence of dicarboxylate transporters DctA or DcuB to reach a ligand re-

sponsive state. Without either of the transmembrane transporters, DcuS is constitutively switched ON (Steinmetz *et al.*, 2014).

Like DcuS, the citrate receptor CitA contains one periplasmic (PASp) and one cytosolic PAS domain (PASc). The expression of citrate transporters and fermentation proteins is controlled by the CitA/CitB TCS (Bott *et al.*, 1995). Unlike DcuS, CitA ligand binding is highly selective; closely related isocitrate and tricarballoylate are not recognised by PASp (Kaspar *et al.*, 1999; Kaspar and Bott, 2002). Crystal structures available for *Klebsiella pneumoniae* CitA PASp in both citrate-free and citrate-bound forms (Reinelt *et al.*, 2003; Sevvana *et al.*, 2008) reveal major structural rearrangements. Upon citrate binding, the PASp β -sheet tightens around the citrate binding pocket, executing a pull on the C-terminal strand and the adjacent second transmembrane helix. This finding is in line with a potential piston-movement model for signalling (Ottemann *et al.*, 1999; Sevvana *et al.*, 2008). In contrast to DcuS, CitA can be described in both signalling states without the presence of an accessory binding protein. Additional proteins may well be involved in the signalling process, but the active as well as the inactive receptor state can be prepared both *in vitro* and *in vivo*.

Structural studies on membrane-embedded constructs of CitA-family HKs were so far inconclusive as to the signalling mechanism. Solid-state NMR studies on membrane-bound *Escherichia coli* DcuS (Etzkorn *et al.*, 2008) were complicated by the unavailability of the inactive receptor state and structural information on the cytosolic PAS domain. As an alternative system, CitA is available in both signalling states, but like in DcuS, isolated PASc of *K. pneumoniae* CitA is not stable in solution for NMR or crystallisation studies. With *E. coli* CitA PASc, a CitA-family cytosolic PAS domain was isolated in solution for the first time and assigned *via* liquid-state NMR in the course of this study. However, only the periplasmic receptor domain was visible in solid-state NMR experiments of membrane-embedded *E. coli* CitA constructs, necessitating the characterisation of a different HK candidate for structural studies.

1.6 *Geobacillus thermodenitrificans*

Proteins from thermophilic organisms are popular targets in structural biology owing to the increased rigidity over mesophilic proteins (Razvi and Scholtz, 2006). As structural studies on *E. coli* DcuS, *K. pneumoniae* CitA and *E. coli* CitA were inconclusive, CitA homologues were sought in thermophiles. While PAsC was not stable in solution for DcuS and *K. pneumoniae* CitA, *E. coli* CitA PAsC was assigned in solution, but could not be detected in solid-state spectra of membrane-embedded CitA constructs. By switching to thermophilic systems, PAsC dynamics could be expected to decrease at ambient temperatures compared with mesophilic systems allowing the detection in solid-state spectra.

A CitA homologue was found in *Geobacillus thermodenitrificans*, a thermophile first described as *Denitrobacterium thermophilus* (Ambroz, 1913) and later characterised based on metabolic and genomic properties (White *et al.*, 1993). *G. thermodenitrificans* is found in soil samples all over the world and in various habitats, including hot springs, shallow marine vents and deep subterranean oil reservoirs (Maugeri *et al.*, 2002; Feng *et al.*, 2007; Chamkha *et al.*, 2008; Adiguzel *et al.*, 2009; Yao *et al.*, 2013). Interest in *G. thermodenitrificans* is mostly fuelled by the potential of gaining biotechnologically important enzymes, namely alkane degradation enzymes (Feng *et al.*, 2007). As a possible source of a more rigid CitA homologue, *G. thermodenitrificans* was also identified as an ideal target for this study.

1.7 NMR assignment strategy

Histidine kinases are large, multi-domain membrane proteins with a dimeric functional assembly. These properties make them difficult targets for liquid-state NMR or crystallisation. While liquid-state NMR is limited by molecular tumbling times that increase with particle size, crystallography of membrane proteins is limited to proteins that form tight three-dimensional packings in artificial membrane systems. To overcome the limitations of those two techniques alone, a combination approach analogous to the one described by Etkorn *et al.* was employed (Etkorn *et al.*, 2008). The CitA receptor family is selected

as a target for various reasons: first, PAS domains are the most abundant receptor domain in HKs and the CitA domain organisation (a periplasmic sensor domain flanked by two transmembrane helices) is most common among HKs. Second, the function of cytosolic PAS domains not involved in signal recognition (like in chemotaxis sensors or oxidative stress receptors) is unclear and can be studied in the CitA model system. Third, unlike in most other HKs, the small molecule ligand for CitA is known and binding well characterised; both signalling states of the receptor are experimentally accessible. Last, CitA contains two PAS domains with a high content of β -sheets, resulting in well dispersed ^{13}C and ^{15}N NMR resonances facilitating assignment.

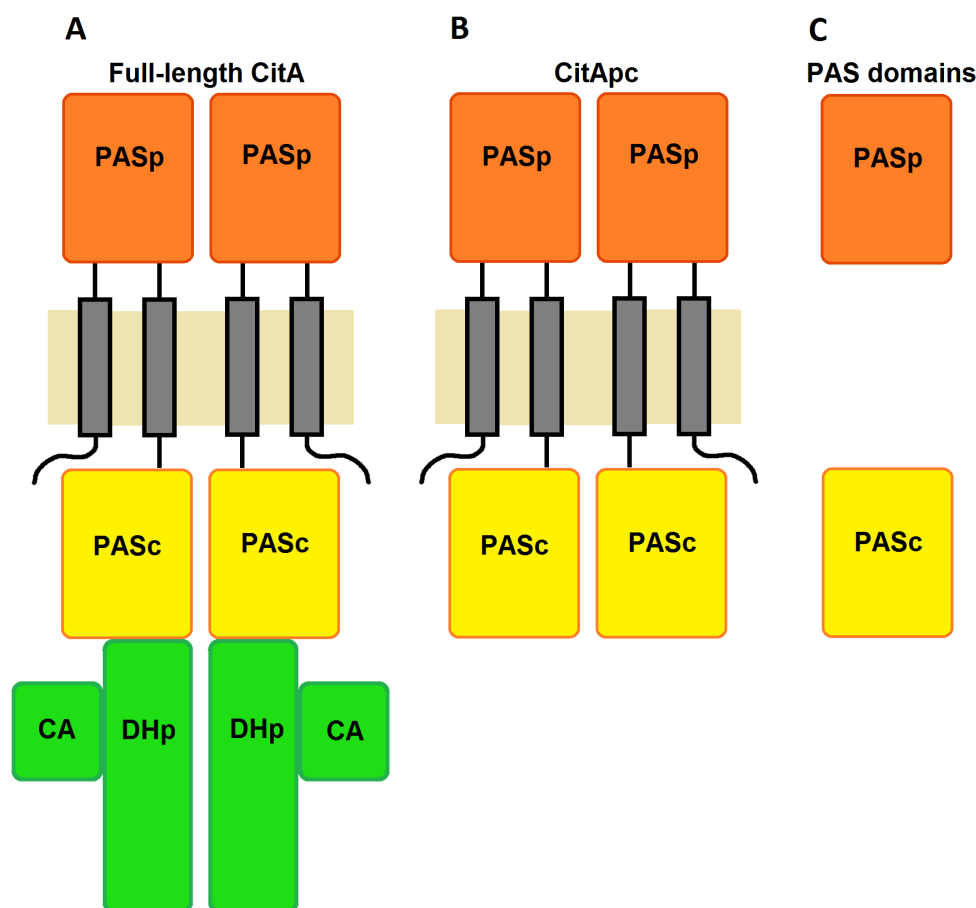


Figure 1.4: Construct design for structural studies. Full-length CitA with a molecular weight of 59 kDa per monomer (A) was shortened by removing the kinase core (DHp and kinase domains), yielding the 34 kDa CitApc construct used for solid-state NMR studies (B). The individual PAS domains were produced as soluble proteins with a molecular mass of 14 and 13 kDa for PASp and PASc, respectively (C).

As the key question of this study is concerning signal transduction across the membrane and not kinase activation, the DHp and CA domains were omitted from all studied protein constructs. Excluding the kinase core reduces the molecular weight from 59 to 34 kDa per monomer. This shortened construct, termed CitApc (for periplasmic and cytosolic PAS domains), is used for solid-state NMR spectroscopy on liposome-embedded protein samples. As the remaining 321 amino acid CitApc construct is still challenging to assign *de novo* by solid-state NMR, the individual PAS domains were produced as isolated, soluble proteins (see figure 1.4). The isolated domains can be assigned *via* liquid-state NMR and used for crystallisation trials to aid in interpreting the solid-state NMR results. Based on liquid-state resonance assignments, peak positions can be predicted for solid-state spectra (see figure 1.5), provided that the structure does not undergo major changes in context of the transmembrane helices. Ideally, the PAS domains can then be assigned in CitApc based on liquid-state data and the remaining, unassigned resonances can be attributed to the transmembrane helices. As these resonances are only a small subset of the full spectrum, a *de novo* assignment of the transmembrane helices can then be carried out based on three-dimensional solid-state NMR experiments. In cases where the isolated domains experience different local structure in context of the transmembrane helices, these differences will also be revealed by incompatibility of liquid-state assignments and solid-state peak positions as well as by sequential assignment.

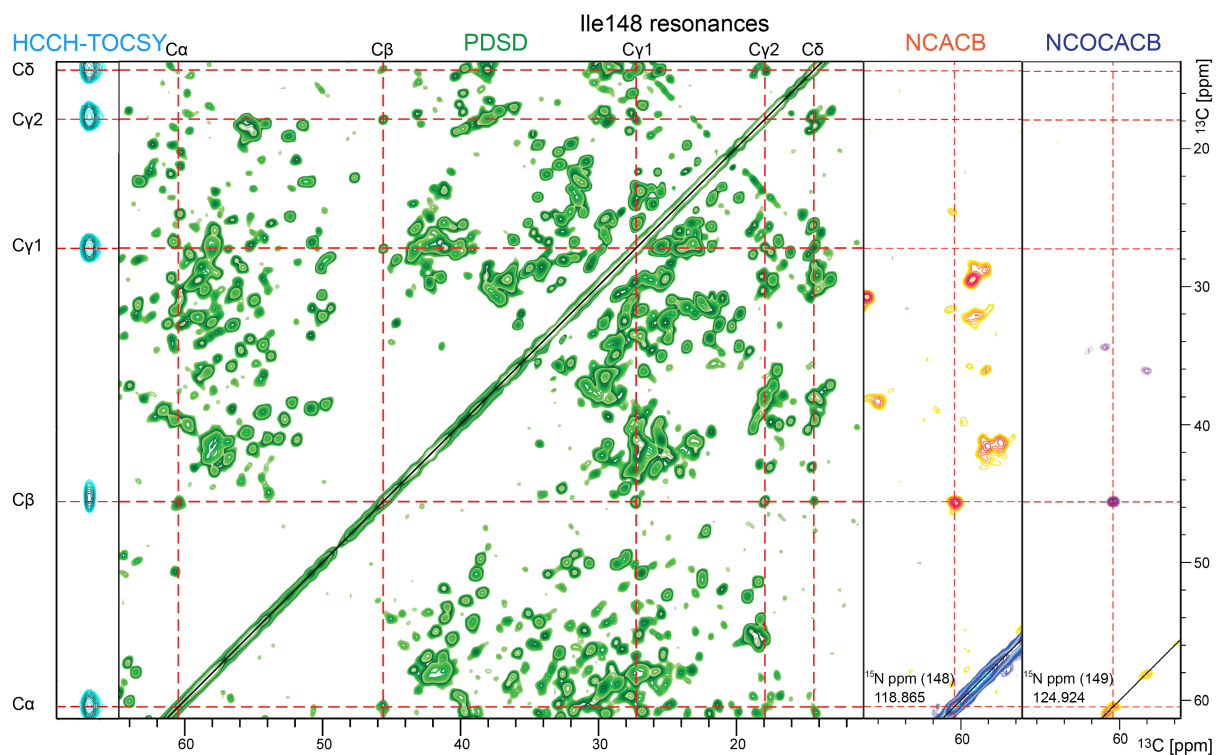


Figure 1.5: Assignment strategy for membrane-embedded CitApc. Liquid-state NMR assignments of isolated PAS domains were used to facilitate solid-state NMR assignments of CitApc. Expected peak positions in solid-state spectra can be predicted from liquid-state chemical shifts (red line intersections) in carbon and nitrogen dimensions. The strategy is exemplified for 2D PDSD, 3D NCACB and 3D NCOCACB assignments of Ile 148 based on liquid-state assignments in an HCCH-TOCSY. In 3D spectra, the corresponding nitrogen plane for Ile 148 (NCACB) and Val 149 (NCOCACB) are shown.

2 Materials and Methods

2.1 Chemicals and equipment

Chemicals for the preparation of buffers, solutions and media were obtained from the companies CARL ROTH GMBH & CO. KG (Karlsruhe, GER), SIGMA-ALDRICH CHEMIE GMBH (Steinheim, GER), and MERCK MILLIPORE (Darmstadt, GER) unless otherwise stated. Restriction enzymes were acquired from THERMO FISHER SCIENTIFIC FERMEN-TAS (Vilnius, LIT) and NEW ENGLAND BIOLABS (Ipswich, USA). Preparation of plasmid DNA, DNA extraction from gels and PCR purification were carried out using kits from MACHEREY-NAGEL (Dueren, GER).

2.2 Construct selection

Constructs for *Geobacillus thermodenitrificans* CitA PAsp (residues 33-161), PAsc (residues 200-309) and CitApc (residues 1-309) were selected based on secondary structure and fold prediction using Phyre2 (Kelley and Sternberg, 2009) paired with domain prediction using InterProScan 5 (Zdobnov and Apweiler, 2001; Goujon *et al.*, 2010).

2.3 Strains, plasmids and primers

G. thermodenitrificans CitA DNA was kindly provided by the group of Prof. Gottfried Unden, Johannes Gutenberg-Universität Mainz, GER. *Escherichia coli* XL 2-blue (*endA1 supE44 thi-1 recA1 gyrA96 relA1 lac*) was used for cloning, *E. coli* BL21(DE3) (*B dcm ompT hsdS_{rB-mB}- gal Λ DE3*) for PAS domain protein expression.

For production of selenomethionine containing protein, methionine auxotroph *E. coli* 834 cells (*hsdS metE gal ompT*) were used. Membrane-embedded constructs for solid-state NMR spectroscopy were expressed in *E. coli* C43(DE3) cells (*F⁺ ompT gal dcm hsdS_B(r_B-m_B-)(DE3)*). Expression constructs for solid-state samples (CitApc₁₋₃₀₉) were cloned into pET16bTEV, individual domains (PASp₃₃₋₁₆₁ or PASc₂₀₀₋₃₀₉) into pET28aZ2 vectors (MERCK MILLIPORE). Oligonucleotides for construct generation and mutagenesis were obtained from SEQLAB (Göttingen, GER) and are listed in table 2.1.

Table 2.1: Primers for construct design

Primer	Nucleotide sequence 5' → 3'	Restriction site	T _M [°C]
CitA (N1)	GCT TCT AGA CAT ATG AAG CTT CAG ACA AGG TTA ATG GTC	NdeI	69.4
PASp(N33)	GTC GAA TTC GGA TCC ACA CTG AAA GAG CAA ATC GGA ATG C	BamHI	72.5
PASp (C161)	GCT CTC GAG AAG CTT TCA GGT GCG CTG AAT ATC TTC TAA CAA AAA C	HindIII	73.0
PASc (N200)	GTC GAA TTC GGA TCC CCG GAA GAA ATC GGC TTG TTG TAC	BamHI	73.6
PASc (C309)	CTG GAA TTC CTC GAG ATT ACT TGT TGC GAA ACG TCG ATA CCG	XhoI	73.3
R93A mutagenesis	GGC AAC CGA CAA GGC ATT GCT TAT GCC CAT CCG CTG AC	-	79.8
R218A mutagenesis	CAG GCA ATT TTA GAG GCG ATT GCT GAA GGA ATC GTC GCC	-	79.0
E219G mutagenesis	GCA ATT TTA GAG GCG ATT CGT GGA GGA ATC GTC GCC GTC AAT C	-	84.4
V285A mutagenesis	GTT TTA GGA GGA GAG ACC GTC ATT GCG AAC AGG ATT CCG	-	82.7
N288D mutagenesis	GAG GAG AGA CCG TCA TTG CGG ACA GGA TTC CGA TCA AAA AC	-	83.6
R289D mutagenesis	GGA GAG ACC GTC ATT GCG AAC GAC ATT CCG ATC AAA AAC AAG CAA G	-	79.9
R307A mutagenesis	GGA GCG GTA TCG ACG TTT GCC AAC AAG TCG GAG TTG TAC	-	81.1

2.4 Cloning techniques

2.4.1 Polymerase chain reaction (PCR)

DNA for CitA constructs was amplified *via* polymerase chain reaction (Saiki *et al.*, 1988) using the Phusion High Fidelity PCR Kit from NEW ENGLAND BIOLABS. Reactions were set up with 5× reaction buffer, 100 ng template DNA, 0.25 mM of each dNTP, 500 nM forward and reverse primers and 2 U polymerase in a total volume of 40 µL. PCR reactions were carried out in a PCR Sprint thermal cycler from THERMO SCIENTIFIC HYBAID (Ashford, UK). The reaction setup was heated to 98 °C for 30 seconds, followed by 25 cycles of denaturation (98 °C, 10 seconds), annealing (55 °C, 30 seconds) and elongation (72 °C, 30 seconds). In a final step, the setup was kept at 72 °C for 10 minutes. The PCR products were subsequently purified using a NucleoSpin Gel and PCR Clean-Up Kit from MACHEREY-NAGEL following the supplier's instructions.

2.4.2 Agarose gel electrophoresis

Purified PCR products were mixed with 6× DNA loading dye (40 % Ficoll 400, 0.5 % bromphenol blue, 0.5 % xylene cyanol) and separated on agarose gels (Aaij and Borst, 1972) containing 2 % agarose in TAE buffer (40 mM Tris-Cl, 20 mM acetic acid, 1 mM EDTA, pH 8.0) and 0.005 % ethidium bromide, using DNA marker (GeneRuler 1 kB DNA Ladder (THERMO FISHER SCIENTIFIC FERMENTAS)) as a reference. The gel was run in TAE buffer at 100 V for 60 minutes. DNA bands of PCR products were excised from the gel and purified using a NucleoSpin Gel and PCR Clean-Up Kit following the supplier's instructions.

2.4.3 Restriction digestion of DNA

The blunt ends of the purified PCR products as well as the target vectors were digested using restriction endonucleases specified in table 2.1 (Nath and Azzolina, 1981). Restriction enzymes and buffers were obtained from FERMENTAS and NEW ENGLAND BIOLABS. For digestion, 3 - 5 µg of vector/PCR product were added to 10× reaction buffer containing

5 U endonuclease adjusted to a final volume of 50 μL and incubated at 37 $^{\circ}\text{C}$ for 2 hours. The reaction was then purified using a NucleoSpin Gel and PCR Clean-Up Kit following the supplier's instructions.

2.4.4 Ligation of DNA fragments

The cleaved DNA fragments from PCR were ligated with the prepared vectors using T4 ligase and buffer from NEW ENGLAND BIOLABS (Sugino *et al.*, 1977). Ligation reactions were set up at a vector/insert ratio of 1:1 in a total volume of 20 μL and incubated at 14 $^{\circ}\text{C}$ over night. The reaction was subsequently terminated by heating up to 65 $^{\circ}\text{C}$ for 10 minutes. 5 μL of the ligation set-up were used to transform XL2-blue cells.

2.4.5 Plasmid purification

Plasmids were purified from overnight cultures of XL2-blue cells (see 2.5) by means of midi-prep. Cells were spun down by centrifugation and plasmids purified using a NucleoBond Xtra Midi purification kit by MACHEREY-NAGEL following the company's manual.

2.4.6 DNA sequencing

DNA sequencing (Sanger and Coulson, 1975) was carried out by SEQLAB (Göttingen, GER). Samples for sequencing contained 500 - 600 ng plasmid DNA and 20 pmol of either T7 promoter or T7 terminator primer in a total volume of 7 μL , adjusted with water.

2.4.7 Site-directed mutagenesis

Mutants of *G. thermodenitrificans* PASp and PASc constructs were generated *via* site-directed mutagenesis utilising the primers shown in table 2.1. Mutagenesis PCR reactions were set up using a QuikChange II Site-Directed Mutagenesis Kit (AGILENT TECHNOLOGIES, Santa Clara, USA). 25 ng of template PAS-domain plasmid and 150 ng of both forward and reverse primers were added to 2.5 U PfuUltra DNA polymerase and 1 μL dNTP mix in 10 \times reaction buffer with a total volume of 50 μL .

PCR reactions were carried out in a PCR Sprint thermal cycler. The reaction mix was heated to 95 °C for 30 seconds, followed by 12 cycles of denaturation (95 °C, 30 seconds), annealing (55 °C, 1 minute) and elongation (68 °C, 6 minutes). In a final step, the setup was kept at 68 °C for 10 minutes. The PCR products were subsequently purified using a NucleoSpin Gel and PCR Clean-Up Kit following the supplier's instructions.

2.5 Transformation and cultivation of *Escherichia coli*

2.5.1 Unlabelled protein

All *E. coli* cells were transformed using 50 µL aliquots of cells that were thawed on ice. 0.5 µL plasmid DNA was added, followed by another 30 minutes incubation on ice. Cells were transformed by heat shock (45 seconds at 42 °C) and kept on ice for another two minutes. 50 µL of 2× YT medium (1.6 % tryptone, 1 % yeast extract, 0.5 % NaCl adjusted to pH 7.0 with NaOH) was added and the cells were incubated at 37 °C for one hour. Cells were harvested by centrifugation (7,500 g for 5 minutes at room temperature) and re-suspended in 30 µL 2× YT medium. The cell suspension was plated out on Luria-Bertani (LB) agar plates (1 % tryptone, 0.5 % yeast extract, 1 % NaCl, 1.5 % agar) containing the appropriate antibiotic (0.01 % ampicillin for pET16bTEV, 0.007 % kanamycin for pET28aZ2) and incubated over night at 37 °C.

Over-night suspension cultures of *E. coli*, both for midi-prep and for production of unlabelled protein, were set up by picking a colony from an agar plate and resuspending it in 1 mL LB medium (1 % tryptone, 0.5 % yeast extract, 1 % NaCl adjusted to pH 7.2 with NaOH) with the appropriate antibiotic. Cells were cultivated for 5 - 6 hours at 37 °C in an incubator shaker. 20 µL cell culture were subsequently transferred to 100 mL LB medium with the appropriate antibiotic and incubated over night at 37 °C in an incubator shaker.

350 µL of the 1 mL day culture were added to 150 µL 50 % glycerol for setting up glycerol stocks. Cells were harvested by centrifugation (15 minutes at 4,300 g, 4 °C) either to be used in midi-preps (see 2.4.5) or for production of protein samples for crystallisation.

Protein sample production was carried out by adding 25 mL of the overnight culture

to 1 L of fresh LB medium with 0.007 % kanamycin and incubating at 37 °C in an incubator shaker until an optical density at 600 nm (OD_{600}) of 0.5 was reached. Afterwards, the temperature was decreased to 30 °C and the culture was grown until an OD_{600} of 0.7 was reached. Protein expression was then induced by adding 0.5 mM isopropyl β -D-1-thiogalactopyranoside (IPTG) and cells were harvested 5 hours after induction by centrifugation (20 minutes at 7,400 g, 4 °C). Pellets were stored at -80 °C until purification.

2.5.2 Selenomethionine-labelled protein

For production of selenomethionine (SeMet)-labelled protein for crystallisation (Hendrickson *et al.*, 1990), plasmids were transformed into methionine auxotroph *E. coli* B834(DE3) (NOVAGEN, Darmstadt, GER). Day cultures were set up from agar plates using 1 mL of minimal medium (see table 2.2) containing 50 μ g L-methionine. After 6 hours, over-night cultures were set up by adding 50 μ L of day culture to 100 mL of minimal medium supplemented with 5 mg of L-methionine. The whole over-night culture was subsequently added to 1 L of minimal medium with 50 mg L-methionine and grown at 37 °C until OD_{600} of 0.6 was reached. The temperature was then reduced to 30 °C, and the cells were harvested at an OD_{600} of 1.0 by centrifugation (20 minutes at 7,400 g, 4 °C). Cells were then re-suspended in 1 L of minimal medium without methionine and incubated for 6 hours at 30 °C. After addition of 50 mg seleno-L-methionine, protein expression was induced after another 30 minutes by addition of 0.5 mM IPTG. Cells were harvested five hours after induction by centrifugation (20 minutes at 7,400 g, 4 °C) and stored at -80 °C.

Table 2.2: Minimal medium for SeMet protein expression

SeMet minimal medium	
100× Trace elements	1 %
20 % Glucose	2 %
MgSO ₄	1 mM
CaCl ₂	0.3 mM
Thiamine·HCl	1 mg / L
NH ₄ Cl	1 g / L
L-Methionine	50 mg / L
10× M9 Salts	10 %
100× Trace elements	
Na-ethylenediaminetetraacetate (EDTA)	5 g / L, pH 7.5
FeCl ₃ ·6 H ₂ O	0.83 g / L
ZnCl ₂	84 mg / L
CuCl ₂ ·2 H ₂ O	13 mg / L
CoCl ₂ ·6 H ₂ O	10 mg / L
H ₃ BO ₃	10 mg / L
MnCl ₂ ·6 H ₂ O	1.6 mg / L
10× M9 Salts, pH 7.4	
Na ₂ HPO ₄	80 g / L
KH ₂ PO ₄	40 g / L
NaCl	5 g / L

2.5.3 ¹³C-¹⁵N labelled protein

Uniform doubly labelled samples for liquid-state NMR were produced in *E. coli* BL21(DE3) cells in M9 minimal medium (McIntosh and Dahlquist, 1990). Day cultures were set up analogous to 2.5.1, over-night cultures were grown in 50 mL minimal medium (see table 2.3) containing ¹³C-glucose and ¹⁵N-ammonium chloride. For protein expression, 25 mL over-night culture was added to 1 L minimal medium and grown at 37 °C until an OD₆₀₀ of 0.5 was reached, the temperature was then reduced to 30 °C. Expression was induced with 0.5 mM IPTG at an OD₆₀₀ of 0.7. Cells were harvested 5 hours after induction.

For solid-state samples, expression constructs were transformed into *E. coli* C43(DE3) as described in 2.5.1. Day cultures in 1 mL 2× YT medium were transferred to 100 mL minimal medium and grown over night as detailed above. For expression culture, the over-night culture was diluted 1:30 in 3 L of fresh minimal medium containing ¹³C-glucose and

^{15}N -ammonium chloride. Cells were grown to an OD_{600} of 0.4 at $37\text{ }^\circ\text{C}$, the temperature was then reduced to $20\text{ }^\circ\text{C}$ and expression induced at an OD_{600} of 0.9 - 1.0 with 0.5 mM IPTG. Cells were harvested after growing over-night at $20\text{ }^\circ\text{C}$.

Table 2.3: Minimal medium for ^{13}C - ^{15}N labelled protein expression

NMR minimal medium	
100× Trace elements	1 %
20 % ^{13}C -glucose	2 %
MgSO_4	2 mM
CaCl_2	0.1 mM
Thiamine·HCl	30 mg / L
^{15}N - NH_4Cl	1 g / L
5× M9 Salts	20 %
100× Trace elements	
Na-ethylenediaminetetraacetate (EDTA)	5 g / L
$\text{FeSO}_4 \cdot 7\text{ H}_2\text{O}$	6 g / L
$\text{MnCl}_2 \cdot 4\text{ H}_2\text{O}$	1.15 g / L
$\text{ZnSO}_4 \cdot 7\text{ H}_2\text{O}$	700 mg / L
$\text{CuCl}_2 \cdot 2\text{ H}_2\text{O}$	300 mg / L
$\text{CoCl}_2 \cdot 6\text{ H}_2\text{O}$	10 mg / L
H_3BO_3	20 mg / L
$(\text{NH}_4)_6\text{Mo}_7\text{O}_{24} \cdot 4\text{ H}_2\text{O}$	250 mg / L
5× M9 Salts, pH 7.4	
Na_2HPO_4	33.9 g / L
KH_2PO_4	15 g / L
NaCl	2.5 g / L

2.6 Protein purification

2.6.1 PAS domains

Cell lysis

All PASp and PASc constructs were purified following the same protocol. Cell pellets from 1 L expression cultures were re-suspended in 60 mL lysis buffer (20 mM Tris·HCl pH 7.9, 300 mM NaCl, 10 mM imidazole, 0.5 mM phenylmethylsulfonylfluoride (PMSF)) on ice. Per 100 mL of lysis buffer, one cOmplete (EDTA free) protease inhibitor cocktail tablet (ROCHE DIAGNOSTICS, Basel, CH) was added. Cells were ruptured by sonication, cellular debris was removed by centrifugation (45 minutes at 48,000 g, 4 °C).

Ni-NTA purification

In a first purification step, Ni-NTA (nitrilotriacetic acid) resin (QIAGEN, Hilden, GER) was used to enrich histidine-tagged PAS domains. 2.5 mL resin were equilibrated with 50 mL lysis buffer before adding the supernatant from cell lysis. The suspension was mixed on a tilting shaker for one hour at 4 °C and transferred to a disposable plastic column (THERMO FISHER SCIENTIFIC). The flow-through was collected and the resin washed with 100 mL lysis buffer. Target proteins were eluted with 8 × 2 mL elution buffer A (20 mM Tris·HCl pH 7.9, 300 mM NaCl, 100 mM imidazole) and 8 × 2 mL elution buffer B (20 mM Tris·HCl pH 7.9, 300 mM NaCl, 500 mM imidazole). Purification was monitored with SDS-PAGE (Sodium dodecyl sulfate polyacrylamide gel electrophoresis). Gels were run for 60 minutes at 120 V (see table 2.4). Protein fractions containing the target protein were pooled and dialysed over night in 2 L TEV-buffer (50 mM Tris·HCl pH 7.9, 0.5 mM EDTA, 150 mM NaCl, 1 mM dithiothreitol (DTT), 0.5 mM PMSF) at 4 °C.

Table 2.4: 17.5 % SDS-PAGE gels

Stacking gel	
30 % acrylamide	10 %
Tris·HCl pH 6.8 (1 M)	12.5 %
10 % sodium dodecylsulfate (SDS)	1 %
10 % ammonium persulfate (APS)	1 %
tetramethylethylenediamine (TEMED)	0.08 %
H ₂ O	75.42 %
Separating gel	
30 % acrylamide	60 %
Tris·HCl pH 8.8 (1 M)	37.6 %
10 % SDS	1 %
10 % APS	1 %
TEMED	0.05 %
H ₂ O	0.35 %
running buffer	
Tris base	25 mM
glycine	192 mM
SDS	0.1 %

TEV-cleavage of His-tag

Protein concentration of dialysed protein was approximated from UV-absorption spectra. The *N*-terminal His-tag was cleaved by adding 1 mg TEV protease per 100 mg protein and incubating for six hours at room temperature without stirring. Successful cleavage was verified by SDS-PAGE. The protein sample was then added to 2.5 mL of Ni-NTA agarose (equilibrated with 50 mL SEC buffer: 20 mM sodium phosphate pH 6.5, 150 mM NaCl) and incubated for one hour. The resin was washed with 10 mL SEC buffer, flow-through and wash fractions were pooled and dialysed over night at 4 °C against 2 L of SEC buffer.

Size exclusion chromatography

The dialysed protein samples were concentrated to 1.5 mL using Vivaspin 20 (10 kDa) spin concentrators (SARTORIUS, Göttingen, GER). The protein concentration was monitored *via* UV absorption spectra. Concentrated samples were purified *via* size exclusion chromatography (SEC) on a Superdex 75 16/60 column (GE LIFE SCIENCES, Little Chalfont,

UK). The column was equilibrated with two column volumes SEC buffer, protein fractions were analysed by SDS-PAGE and fractions containing pure protein were pooled. The final PAS domain samples were dialysed over night at 4 °C against 2 L of NMR buffer (20 mM sodium phosphate pH 6.5, 50 mM NaCl). The buffer was used both for liquid-state NMR experiments and crystallisation set-ups. In a final step, samples were concentrated to 1.4 - 1.8 mM using Vivaspin 20 (10 kDa molecular weight cut-off) concentrators and 0.01 % sodium azide was added. All samples were stored at 4 °C when not used in experiments.

For determining the oligomeric state of proteins, analytical SEC was carried out on a Superdex 75 10/300 column (GE LIFE SCIENCES). 100 μ L protein samples at concentrations of 1 mM and the SEC buffer described above were used. To calculate the sample molecular weight based on elution volume, a standard protein mix (Gel filtration calibration kit LMW, GE LIFE SCIENCES) was separated on the same column. 1.5 mg each of conalbumin, carbonic anhydrase, ribonuclease A and aprotinin were suspended in 500 μ L SEC buffer; 100 μ L of this sample was used for SEC.

2.6.2 Gt CitApc solid-state NMR samples

Solid-state NMR samples were kindly provided by Karin Giller (Department of NMR-based structural biology, Max-Planck-Institute for Biophysical Chemistry, Göttingen, GER) using the following protocol.

Cell lysis

Cell pellets were re-suspended on ice in 225 mL TKMD buffer (50 mM Tris·HCl pH 7.0, 200 mM KCl, 5 mM MgCl₂, 5 mM β -mercaptoethanol, one spatula tip of DNaseI, two cOmplete (EDTA free) protease inhibitor cocktail tablets, 0.5 mM PMSF) using a POTTER-ELVEHJEM homogeniser. The suspension was stirred at 4 °C for one hour before cell lysis utilising three cycles in a french pressure cell (20,000 psi). Cell debris was pelleted by centrifugation (30 minutes at 4 °C and 27,500 g), the supernatant was spun down in an ultracentrifuge (90 minutes at 4 °C and 102,089 g). The ultracentrifugation pellet was re-suspended in 180 mL Ni-NTA-buffer (20 mM Tris·HCl pH 7.9, 500 mM NaCl, 10 mM imidazole) with 5 mM β -mercaptoethanol, two cOmplete (EDTA free) protease inhibitor

cocktail tablets, 0.5 mM PMSF and 4 % Triton X-100 (v/v) using a POTTER-ELVEHJEM homogeniser.

The suspension was stirred for three hours at 4 °C and subjected to ultracentrifugation a second time (one hour at 4 °C and 109,251 g). The supernatant was diluted to an end volume of 900 mL using Ni-NTA-buffer with three cOmplete (EDTA free) protease inhibitor cocktail tablets and 0.5 mM PMSF to set the final concentration of Triton X-100 at 0.8 % (v/v).

Ni-NTA purification

The protein solution was loaded over-night onto a 5 mL Ni-NTA column (GE LIFE SCIENCES) at 0.7 mL/min and 4 °C. The column was washed with Ni-NTA-buffer (supplemented with half a tablet of cOmplete (EDTA free) protease inhibitor cocktail per 100 mL, 1 mM β -mercaptoethanol, 0.5 mM PMSF and 0.2 % (v/v) Triton X-100) at 3 mL/min until a baseline was reached. The detergent was changed on-column by washing with 80 mL of Ni-NTA-buffer supplemented with half a tablet of cOmplete (EDTA free) protease inhibitor cocktail per 100 mL, 1 mM β -mercaptoethanol, 0.5 mM PMSF and 1 % (v/v) lauryldimethylamine-oxide (LDAO) at 3 mL/min.

One-step elution was carried out by washing with elution buffer (20 mM Tris-HCl pH 7.9, 500 mM NaCl, 500 mM imidazole) supplemented with one tablet of cOmplete (EDTA free) protease inhibitor cocktail per 100 mL, 1 mM β -mercaptoethanol, 0.5 mM PMSF and 1 % (v/v) LDAO at 2 mL/min. 2 mL fractions were collected and analysed by SDS-PAGE.

Size exclusion chromatography (SEC)

Pure protein fractions were pooled and concentrated to 2.5 mL using Vivaspin 20 (30 kDa) spin concentrators. The protein concentration was monitored *via* UV absorption spectra. Concentrated samples were purified *via* size exclusion chromatography on Superdex 200 26/60 columns (GE LIFE SCIENCES). The column was equilibrated with two column volumes gel filtration buffer (20 mM Tris-HCl pH 7.4, 150 mM NaCl, 1 mM DTT, 0.3 % LDAO) and 2 mL fractions were collected. Protein fractions were analysed by SDS-PAGE

gel electrophoresis and pure protein was pooled.

Reconstitution in liposomes

1,2-dimyristoyl-*sn*-glycero-3-phosphocholine (DMPC)- or asolectin lipid films were set up by dissolving the appropriate amount of lipids for a protein/lipid molar ratio of 1:100 in 2 mL of chloroform and methanol (1:1). The solvent was removed in a nitrogen gas stream followed by lyophilisation over-night. The lipid film was sonicated (3×15 minutes) in 1 mL gel filtration buffer before adding ultrafiltered protein samples. The mixture was incubated for two hours at room temperature on a tilting shaker. LDAO was subsequently removed by incubation with 2 g Bio-Beads SM-2 (BIO-RAD LABORATORIES, Hercules, USA) per 66 mg LDAO on a tilting shaker at 4 °C over night. The sample was diluted to 40 mL with gel filtration buffer without LDAO and the Bio-Beads were removed on a disposable plastic column which was washed with 2×10 mL gel filtration buffer without LDAO.

The liposomes were pelleted by ultracentrifugation (two hours at 4 °C and 109,251 g) and the pellet washed and re-suspended with 60 mL of 20 mM Tris·HCl pH 7.4. Ultracentrifugation was repeated (one hour at 4 °C and 109,251 g) and the pellet re-suspended in 10 mL of 20 mM Tris·HCl pH 7.4. After another ultracentrifugation step (one hour at 4 °C and 109,251 g), the pellet was re-suspended in 1 mL of 20 mM Tris·HCl pH 7.4. This step was repeated, following a final centrifugation run (one hour at 4 °C and 109,251 g) after which the supernatant was removed, leaving $\tilde{20}$ μ L of buffer. The sample was spun down another 30 minutes at 4 °C and 109,251 g and stored at 4 °C before transferring to solid-state NMR rotors.

For producing citrate-bound *G. thermodenitrificans* CitApc R93A, the same protocol was used, adding 5 mM sodium citrate to every buffer following cell lysis.

2.7 Crystallisation of PAS domains

Crystallisation trials of PASp and PASc constructs were set up using the following samples:

Construct	Concentration
PASp (native)	1.4 mM
PASp R93A (native)	1.4 mM
PASp R93A (SeMet)	1.4 mM
PASp R93A + 6-fold citrate (native)	1.4 mM
PASc (native)	1.0 mM
PASc (SeMet)	1.0 mM
PASc R218A (SeMet)	1.5 mM
PASc E219G (native)	1.4 mM
PASc V285A (native)	1.4 mM
PASc V285A (SeMet)	1.5 mM
PASc N288D (native)	1.5 mM
PASc N288D (SeMet)	1.5 mM
PASc R289D (native)	1.6 mM
PASc R289D (SeMet)	1.5 mM
PASc R307A (native)	1.5 mM
PASc R307A (SeMet)	1.5 mM

All protein samples used for crystallisation were buffered with 20 mM sodium phosphate, pH 6.5 and 50 mM NaCl. Initial crystallisation attempts were set up employing the sparse matrix screens Index HT, PEGion HT, Crystal Screen 1+2 (HAMPTON RESEARCH, Aliso Viejo, USA), PEGs Suite, JCSG+ Suite (QIAGEN) and Wizard 1+2 (RIGAKU REAGENTS, Bainbridge Island, USA). Drops were set up in 96-well plates (GREINER BIO ONE GMBH, Frickenhausen, GER) using the sitting drop vapour diffusion method. For each crystallisation condition, 200 nL of protein sample were mixed with 200 nL reservoir solution (Mosquito Crystal, TTP LABTECH LTD., Hertfordshire, UK) and equilibrated against 100 μ L reservoir solution.

In a second step, set-ups yielding crystals were optimised by constructing grid screens around the initial crystallisation conditions by varying ingredient concentrations and buffer pH. The grid screens were carried out in 96-well plates. The collection of X-ray diffraction datasets and solution of crystal structures was carried out by Dr. Stefan Becker (Department of NMR-based Structural Biology, Max-Planck-Institute for Biophysical Chemistry, Göttingen, GER).

2.8 Liquid-state NMR experiments

2.8.1 General procedures

Liquid-state NMR experiments were recorded on samples in 5 mm Shigemi tubes (SHIGEMI INC., Allison Park, USA) at concentrations between 1.4 and 1.7 mM. The experiments recorded for each sample are listed in table 2.5. All spectra were recorded at 25 °C on Bruker spectrometers and processed using NMRpipe (Delaglio *et al.*, 1995). Assignment was carried out using the CcpNMR Analysis software (Vranken *et al.*, 2005; Stevens *et al.*, 2011) and triple resonance backbone and side-chain assignment (Bax *et al.*, 1990; Ikura *et al.*, 1990; Frueh, 2014).

2.8.2 Secondary structure determination

Protein $C\alpha$ -chemical shifts are indicative of secondary structure and tend to shift upfield in β -strands and downfield in α -helices when compared to random coil chemical shifts. For $C\beta$ -chemical shifts, the opposite trend can be observed (Metzler *et al.*, 1993). By subtracting random coil chemical shifts (δC_{coil}) from experimental values (δC_{exp}), protein secondary structure can be predicted. $C\alpha$ - and $C\beta$ secondary shifts were merged by subtracting $C\beta$ - from $C\alpha$ -secondary shifts. In this notation, negative values correspond to β -strand structure while positive values reflect α -helical conformation. For calculating the $C\alpha$ - $C\beta$ -secondary chemical shifts, random coil chemical shifts based on statistical analysis (Wang and Jardetzky, 2002) were used.

Table 2.5: Liquid-state NMR experiments

Gt CitA PASp		
Spectrum	Field [MHz]	Recording time
¹⁵ N-HSQC	800	20 m
¹⁵ N-HSQC-NOESY	800	3 d
HNCA	700	2 d 21 h
CBCACONH	600	2 d 18 h
HNCO	600	2 d 16 h
HCCH-TOCSY	700	2 d 16 h
¹³ C-HSQC-NOESY	700	4 d 21 h
Gt CitA PASp R93A		
Spectrum	Field [MHz]	Recording time
¹⁵ N-HSQC	800	20 m
¹⁵ N-HSQC-NOESY	900	2 d 2 h
HNCA	700	1 d 19 h
CBCACONH	600	2 d 19 h
HNCO	600	23 h
HCCH-TOCSY	600	5 d 1 h
¹³ C-HSQC-NOESY	800	3 d 21 h
Gt CitA PASp R93A + citrate		
Spectrum	Field [MHz]	Recording time
¹⁵ N-HSQC	700	20 m
¹⁵ N-HSQC-NOESY	900	2 d 2 h
HNCA	700	1 d 19 h
CBCACONH	900	2 d 17 h
HNCO	700	19 h
HCCH-TOCSY	700	2 d 16 h
¹³ C-HSQC-NOESY	700	3 d 17 h
Gt CitA PASc		
Spectrum	Field [MHz]	Recording time
¹⁵ N-HSQC	800	20 m
¹⁵ N-HSQC-NOESY	800	3 d 6 h
HNCA	900	1 d 21 h
CBCACONH	900	2 d 15 h
HNCO	800	15 h
HCCH-TOCSY	600	2 d 20 h
¹³ C-HSQC-NOESY	800	6 d 15 h

2.8.3 Ligand affinity determination

The shift of ¹⁵N-HSQC peaks in a ligand titration experiment can be utilised to determine dissociation constants (Ryan T *et al.*, 1999; Auguin *et al.*, 2004; Coudeville *et al.*, 2008).

The dissociation constant K_D is defined as

$$K_D = \frac{[P][L]}{[PL]} \quad (2.1)$$

where $[P]$, $[L]$ and $[PL]$ are the free protein, free ligand and protein-ligand complex concentrations.

The total protein and ligand concentrations ($[P_{tot}]$ and $[L_{tot}]$, respectively) employed in the experiment can be expressed as the sum of the free and complex-bound concentrations. Substituting these expressions in equation 2.1 yields

$$K_D = \frac{([P_{tot}] - [PL])([L_{tot}] - [PL])}{[PL]} \quad (2.2)$$

After reorganisation, equation 2.2 can be solved for $[PL]$.

$$[PL] = \frac{[P_{tot}] + [L_{tot}] + K_D \pm \sqrt{([P_{tot}] + [L_{tot}] + K_D)^2 - 4[P_{tot}][L_{tot}]}}{2} \quad (2.3)$$

For monomeric proteins with one binding site, a linear variation of the chemical shift $\Delta\delta ppm$ with the proportion of protein in the bound state as compared to the total protein concentration can be assumed.

$$\Delta\delta ppm = \Delta\delta ppm_{Max} \frac{[PL]}{[P_{tot}]} \quad (2.4)$$

$\Delta\delta ppm_{Max}$ represents the chemical shift difference between the ligand-free and ligand-bound states at saturation. Substitution of equation 2.4 in equation 2.3 yields

$$\Delta\delta ppm = \Delta\delta ppm_{Max} \frac{[P_{tot}] + [L_{tot}] + K_D \pm \sqrt{([P_{tot}] + [L_{tot}] + K_D)^2 - 4[P_{tot}][L_{tot}]}}{2[P_{tot}]} \quad (2.5)$$

Plotting the chemical shift difference $\Delta\delta ppm$ as a function of ligand concentration allows for determination of K_D and $\Delta\delta ppm_{Max}$ based on equation 2.5.

Experiments were carried out at 20 °C with a protein concentration of 1.4 mM. The solution was kept at pH 6.5 throughout the titration. Citrate was added in steps of 0.16 mM, 0.33 mM, 0.66 mM, 1.33 mM, 2 mM, 2.66 mM and 3.33 mM (final concentrations).

2.9 Solid-state NMR experiments

2.9.1 PDS D spectra

Solid-state NMR spectroscopy at magic angle spinning (MAS) allows for acquisition of high-resolution spectra of samples where lack of fast isotropic motions makes liquid-state NMR impossible. CitApc samples embedded in liposomes were analysed by predicting solid-state peak positions in proton-driven spin diffusion (PDS D) spectra based on liquid-state assignments of the isolated PAS domains (see figure 1.5).

PDS D can be used to detect ^{13}C - ^{13}C correlation spectra by exploiting the dense proton spin network. Magnetisation is transferred from proton to ^{13}C *via* cross-polarisation. Proton resonances are decoupled during t_1 evolution and ^{13}C resonances consecutively stored on the z -axis for spin diffusion during a mixing time t_{mix} . During t_{mix} , proton decoupling is switched off to allow for diffusion enhancement through the proton bath (Suter and Ernst, 1985; Dumez *et al.*, 2011). After mixing, ^{13}C magnetisation is transferred back to the xy -plane for detection. Depending on t_{mix} , the information content of PDS D spectra can be varied. With short mixing times only short distance, intra-residual correlations can be detected, while longer mixing times allow for increased spin diffusion and the detection of inter-residual and long-range correlations. However, the signal/noise ratio at longer mixing time decreases and spectra get more crowded due to the additional inter-residual peaks. Because of the protein size, only short mixing-time (20 ms) PDS D spectra of CitApc constructs were acquired. The MAS speed was set to 11.4 kHz at 850 MHz base frequency or 11 kHz at 800 MHz base frequency to remove spinning sidebands from the aliphatic region of the spectra (see figure 2.1).

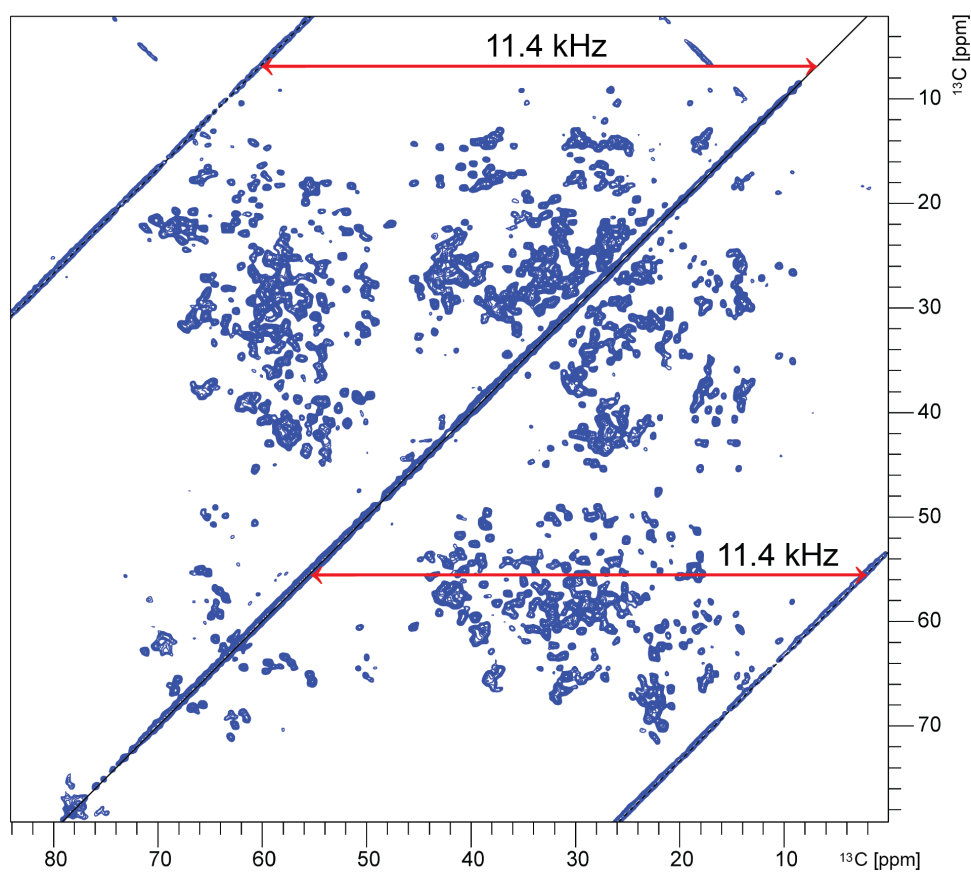


Figure 2.1: Aliphatic region in a 20 ms PDS spectrum of wild-type CitApc. Most regions in a short mixing-time PDS spectrum of CitApc experience peak overlap. Experiments with longer mixing times were therefore not recorded as overlap is expected to increase. At the MAS speed of 11.4 kHz and a base frequency of 850 MHz the spinning sidebands do not interfere with peaks in the aliphatic spectral region.

2.9.2 Triple-resonance spectra

For sequential assignment, spectra with intra-residual (residue i) and neighbouring-residue ($i-1$ or $i+1$) specific correlations are needed. In this work, CitApc sequential assignments were achieved by combining information from 3D NCACB, NCOCA and NCOCACB-spectra. Ambiguities in the sequential assignment could be resolved with the additional information on $\text{C}\alpha$ - $\text{C}\alpha$ -sequential contacts in a 2D CAncoCA spectrum (see figure 2.2).

The *de novo* sequential assignment in solid-state spectra depends on high-resolution 3D spectra with sufficient signal/noise. The signal/noise is generally relatively low for membrane proteins compared to crystalline material due to the diluting factor of the lipids.

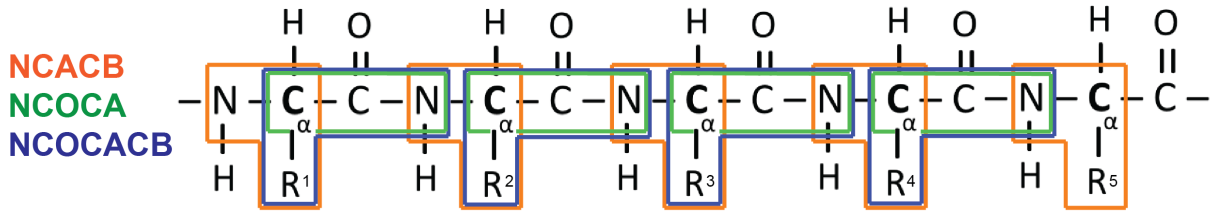


Figure 2.2: Sequential assignments based on solid-state spectra. Sequential assignments are made possible by combining intra-residual information from an NCACB experiment (orange) with inter-residue correlations to the preceding ($i-1$) residue from NCOCA (green) and NCOCACB (purple) spectra.

For CitApc, a protein/lipid molar ratio of 1/100 is used, increasing the experimental time for high-quality spectra compared to crystalline protein samples. This is especially critical for experiments relying on homonuclear magnetisation transfer between CO and $C\alpha$ (most used for correlating N of a given residue to $C\alpha$ of the preceding residue) with a generally low transfer efficiency (Chevelkov *et al.*, 2013b). Band-selective homonuclear cross-polarisation (BSH-CP) yields favourable 33 % transfer efficiency at moderate MAS frequencies of ~ 21 kHz for protonated proteins (Chevelkov *et al.*, 2013a; Shi *et al.*, 2014), allowing for sequential assignment of CitApc constructs.

Most efficient recoupling using BSH-CP is obtained at effective radio-frequency (RF) fields ω_{rf} on CO and CA of twice the MAS frequency ω_r ,

$$\sqrt{\Omega^2 + \omega_{rf}^2} + \omega_{rf} = 2\omega_r \quad (2.6)$$

where Ω is the CO chemical shift offset (with the carrier frequency on $C\alpha$).

For CO-CA transfer in 3D NCOCA and NCOCACB and 2D CAncoCA experiments, CO-magnetisation is flipped to the effective field using a hard trim pulse before BSH-CP with the flip angle

$$\theta = 90^\circ - \arctan(\omega_{rf}/\Omega) \quad (2.7)$$

All triple-resonance experiments were set up at 21 kHz MAS.

2.9.3 INEPT spectra

To detect mobile regions of CitApc, J-coupling based refocused ^1H - ^{13}C -INEPT spectra (Fyfe *et al.*, 1995; Soubias *et al.*, 2002) can be acquired. Since proton-proton dipolar couplings in solid samples are not averaged out, effective transverse dephasing times for rigid protein regions are very short. Therefore, only flexible protein regions where averaging of dipolar couplings is possible through rapid internal motions are detectable.

Solid-state NMR experiments were carried out on the spectrometers and at spinning speeds detailed below.

Table 2.6: Solid-state NMR experiments

Gt CitApc wild-type (asolectin)					
Spectrum	Field [MHz]	Rotor \varnothing [mm]	Spinning speed [kHz]	Recording time	Temperature [°C]
PDS 20 ms	850	4.0	11.4	3 d 8 h	7
NCOCA 2D	850	3.2	21	1 d 10 h	6
NCOCA 3D	850	3.2	21	2 d 23 h	6
NCACB 3D	850	3.2	21	6 d 23 h	6
NCACO 2D	850	3.2	21	1 d 10 h	6
NCACO 3D	850	3.2	21	5 d 13 h	6
CANCO 3D	850	3.2	21	5 d 7 h	5
NCOCACB 2D	850	3.2	21	4 d 19 h	6
NCOCACB 3D	850	3.2	21	8 d 7 h	6
Gt CitApc R93A (DMPC, citrate-free)					
Spectrum	Field [MHz]	Rotor \varnothing [mm]	Spinning speed [kHz]	Recording time	Temperature [°C]
PDS 20 ms	850	4.0	11.4	6 d 13 h	7
HC-INEPT 2D	850	4.0	8.333	20 h	7
NCACB 2D	850	3.2	21	20 h	9
NCACB 3D	850	3.2	21	5 d 21 h	9
NCOCA 2D	850	3.2	21	19 h	9
NCOCA 3D	850	3.2	21	7 d 22 h	9
NCOCACB 3D	850	3.2	21	10 d	9
Gt CitApc R93A (DMPC, citrate-bound)					
Spectrum	Field [MHz]	Rotor \varnothing [mm]	Spinning speed [kHz]	Recording time	Temperature [°C]
PDS 20 ms	800	4.0	11	7 d 6 h	9
HC-INEPT 2D	850	4.0	8.333	20 h	6
NCACB 2D	850	3.2	21	21 h	7
NCACB 3D	850	3.2	21	5 d 19 h	7
NCOCACB 3D	850	3.2	21	7 d 20 h	7
CAncOCA 2D	850	3.2	21	6 d 21 h	7

3 Results

3.1 The periplasmic PAS domain (PASp)

Samples of *Geobacillus thermodenitrificans* PASp₃₃₋₁₆₁ were purified as described in 2.6. From SEC elution profiles it is evident that PASp is monomeric in solution (see figure 3.1). Crystallisation attempts with *G. thermodenitrificans* PASp were unsuccessful, but based on crystal structures of homologous *Klebsiella pneumoniae* CitA PASp (PDB ID: 2V9A and 2J8O; identity: 40 %, homology: 59 %), both ligand-free and ligand-bound domain structures could be predicted using the I-TASSER protein fold prediction server (Zhang, 2008).

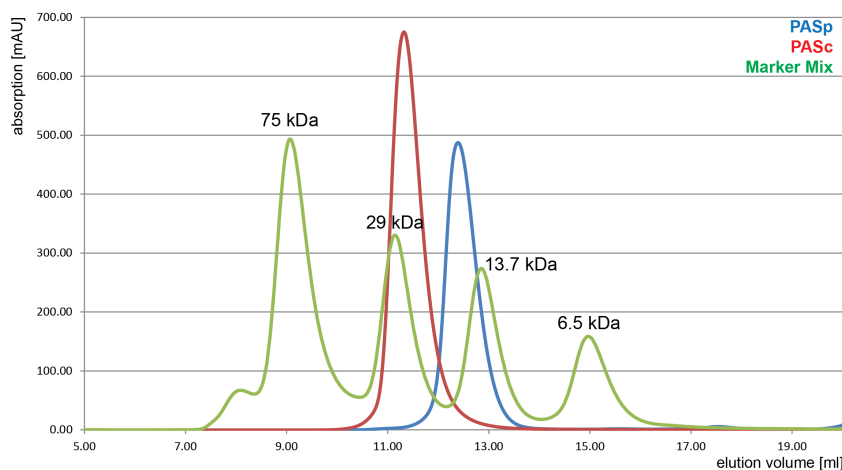


Figure 3.1: Size exclusion chromatography profiles of PAS constructs. The apparent molecular weight of PASp (blue) and PASc (red) can be calculated based on the elution profiles of proteins of known size (green). The apparent molecular weight of PASc corresponds to a dimeric state in solution. Peaks for isolated domains would be expected at 13.0 and 13.3 ml for PASp and PASc, respectively.

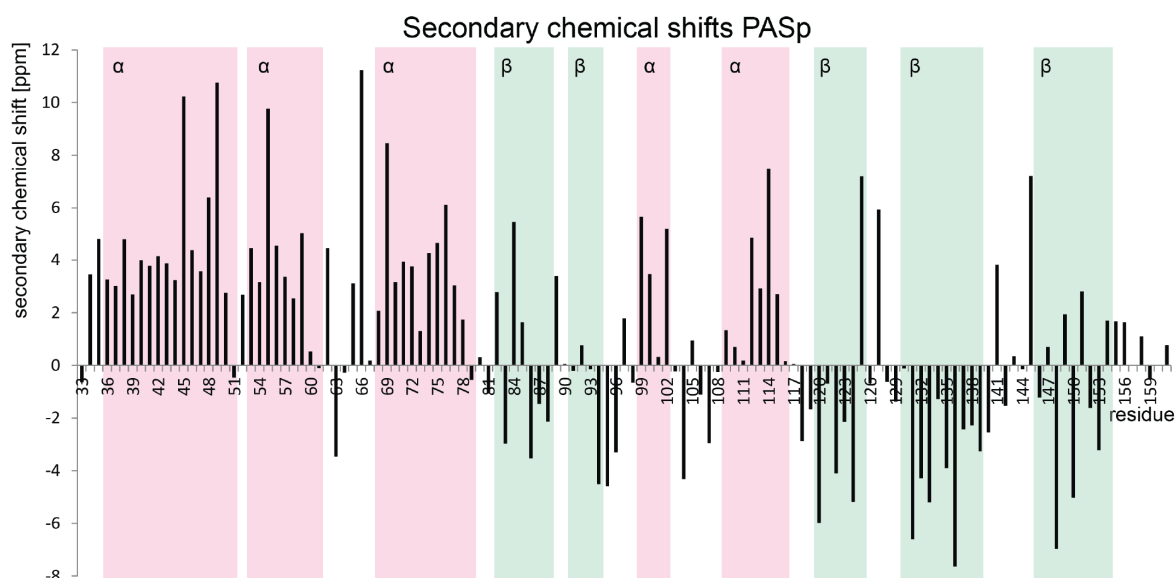


Figure 3.2: $C\alpha$ - $C\beta$ -secondary shift analysis of PAsp in solution. The secondary chemical shifts reflect secondary structure propensity, with positive values indicating α -helix, negative values corresponding to β -strands. The secondary structure elements of the PAsp model are superimposed (red: α -helix, green: β -strand). PAsp was assigned in the citrate-bound state as citrate-free PAsp is not experimentally accessible.

Uniformly ^{13}C - ^{15}N -labelled *G. thermodenitrificans* PAsp was assigned based on liquid-state NMR experiments (see table 2.5). In total, 96 % of proton, 90 % of carbon and 74 % of nitrogen resonances were assigned. The backbone assignment reached 98 % completeness, the remainder being proline amides. The I-TASSER model of PAsp could be validated by comparing secondary structure elements in the model to $C\alpha$ - $C\beta$ -secondary chemical shifts in solution (see figure 3.2).

To quantify citrate binding capacity, an NMR titration experiment was carried out based on ^{15}N -HSQC experiments (Ryan T *et al.*, 1999; Auguin *et al.*, 2004; Coudeville *et al.*, 2008). Surprisingly, even a 10-fold excess of citrate did not show any effect on the HSQC spectra. Likewise, no binding was observed in an isothermal titration calorimetry experiment (Pierce *et al.*, 1999). However, citrate binding of full-length *G. thermodenitrificans* CitA was shown *in vivo* (see figure 3.3) by the group of Prof. Gottfried Uden (Gutenberg-Universität Mainz, GER).

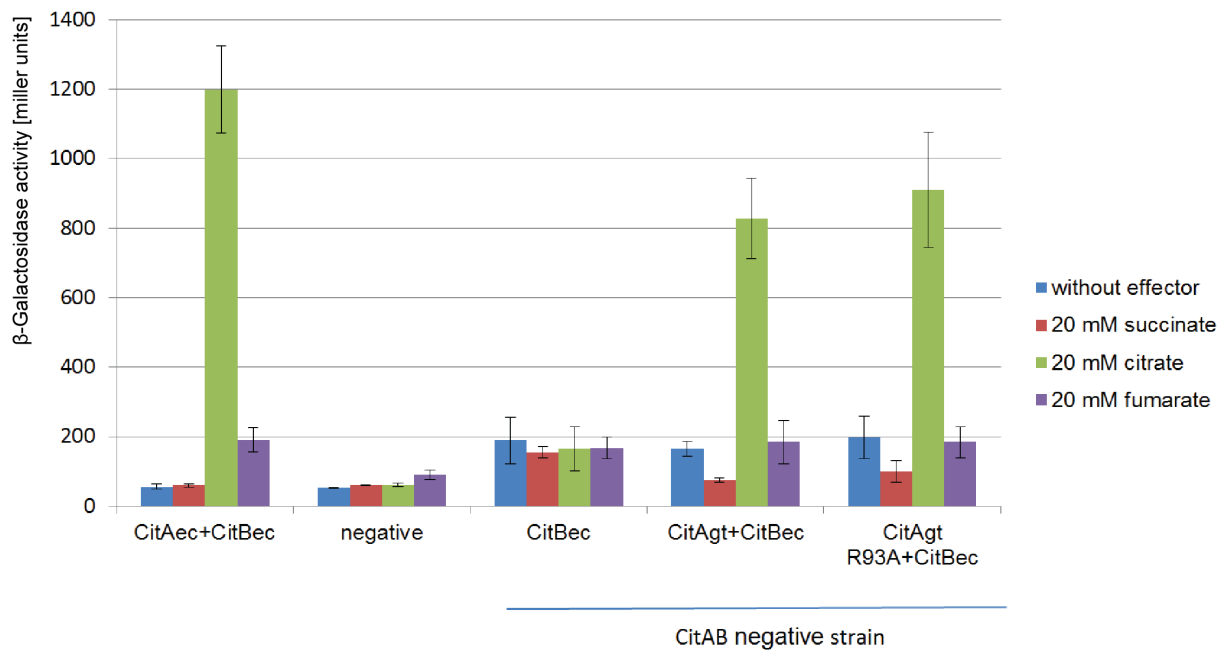


Figure 3.3: Activity and substrate specificity of *Geobacillus thermodenitrificans* CitA. *G. thermodenitrificans* CitA was verified as a citrate receptor *in vivo*. RR CitB-dependent reporter gene activity (β -Galactosidase) was monitored as a function of different small molecule ligands in *Escherichia coli* cells. The native *E. coli* CitA/CitB system displays selective activation upon citrate addition, while a CitA/CitB negative *E. coli* strain did not show any activity (left). The CitA/CitB negative *E. coli* strain complemented with RR CitB in absence of the cognate HK was inactive even in presence of ligands (centre). Complementation of the negative strain with either *G. thermodenitrificans* CitA (wild-type) or *G. thermodenitrificans* CitA R93A restored TCS activity and citrate specificity (right). The figure was kindly provided by Prof. Uden (Gutenberg-Universität Mainz, GER).

This led to the assumption that isolated PASp might bind citrate with very high affinity, so that the citrate-free state is not observable. This hypothesis is underpinned by high ligand affinity of the homologous PASp-domain in *K. pneumoniae* CitA (Kaspar *et al.*, 1999) and the presence of citrate in the crystal structure of *Escherichia coli* CitA PASp, although no citrate was added during purification and crystallisation. Based on the I-TASSER structural model, an R93A mutation was introduced in the citrate binding pocket. The selected arginine 93 is part of the conserved residues constituting the binding pocket of citrate-binding PAS domains (Gerharz *et al.*, 2003) (see figure 3.4). From crystal structures of *K. pneumoniae* and *E. coli* CitA PASp it is evident that the conserved arginine sidechain forms two hydrogen bridges to citrate. An alanine mutation

```

Geobacillus thermodenitrificans CitA VRLQPPFAERIRQKTGAEYVVIGNRQGI RYALPLTERIGKSMIGG NKVEVLKKGKSIISEAV 125
Escherichia coli CitA -RLATIANKLQRDTDFDYVVIGDRHSI RLYHPNPEKIGYPMQFTKQGALKESYFITGK 139
Klebsiella pneumoniae CitA -RIKALIDPMRSFSDATYITVGDSAGQ RLYFVNPDEIGKSM EGG SDEALINAKSYVSVR 141
Salmonella enterica CitA -RIKALIDPMRSFSDATYITVGNEKGG RLYFVNPDEIGKY EGG SDDALYNAKSYVSVR 136
Escherichia coli DcuS SGIQATAEAVRKRNDLLFIVVTDMQSL RYSFPEAQRIGQPFKGD ILKALNGEENVAINR 139
Klebsiella pneumoniae DcuS QIIQPLAQAITRRNDLLYAIVTDMQGI RYSF PDSSIIGKPFIGHT IQPTLQKENVAINH 141

```

Figure 3.4: Alignment of CitA-family HK PASp domains. BLAST Alignment of selected CitA-family PASp domains reveals a conserved arginine (red) which can be identified as part of the ligand binding pocket in PASp crystal structures. Other conserved residues in the binding pocket are highlighted green. A conserved methionine (M106 in *Geobacillus thermodenitrificans* CitA) is only present in CitA HKs and lacking in DcuS systems.

is therefore assumed to weaken the PASp-citrate hydrogen bond network and reduce the binding affinity. In the course of this project, the effect of the conserved arginine mutation was evaluated for *E. coli* CitA, where the K_D of wild-type PASp could be determined. Mutation of the conserved arginine, in this case R107, to alanine increased the dissociation constant from 240 nM to 150 μ M.

Like for wild-type PASp, $^{13}\text{C}^{15}\text{N}$ -labelled samples were produced for liquid-state NMR studies. PASp R93A is monomeric in solution as seen in the SEC elution profile. The protein was again assigned based on 3D-experiments (see table 2.5). In total, 72 % of proton, 80 % of carbon and 70 % of nitrogen resonances were assigned. 91 % of backbone resonances could be identified.

As with wild-type PASp, PASp R93A was titrated with sodium citrate (see figure 3.5). In contrast to wild-type protein, PASp R93A spectra exhibit strong binding-induced chemical shift changes. The appearance of intermediate peaks between citrate-free and saturated citrate-bound peak positions during the NMR titration is indicative of fast exchange of citrate and PASp. Based on the NMR titration, the overall K_D value was determined to be 624 ± 21 μ M. The dissociation constant of *G. thermodenitrificans* CitA PASp R93A is therefore in the same range as the K_D of *E. coli* CitA PASp R107A, the corresponding mutant in this system. Like wild-type CitA, the receptor functionality of CitA R93A was verified *in vivo* by the group of Prof. Uden (see figure 3.3). The NMR assignment protocol was repeated for citrate-bound PASp R93A with a protein/citrate ratio of 1:6. In total, 75 % of proton, 83 % of carbon and 70 % of nitrogen resonances were assigned, the backbone assignment was completed to 95 %.

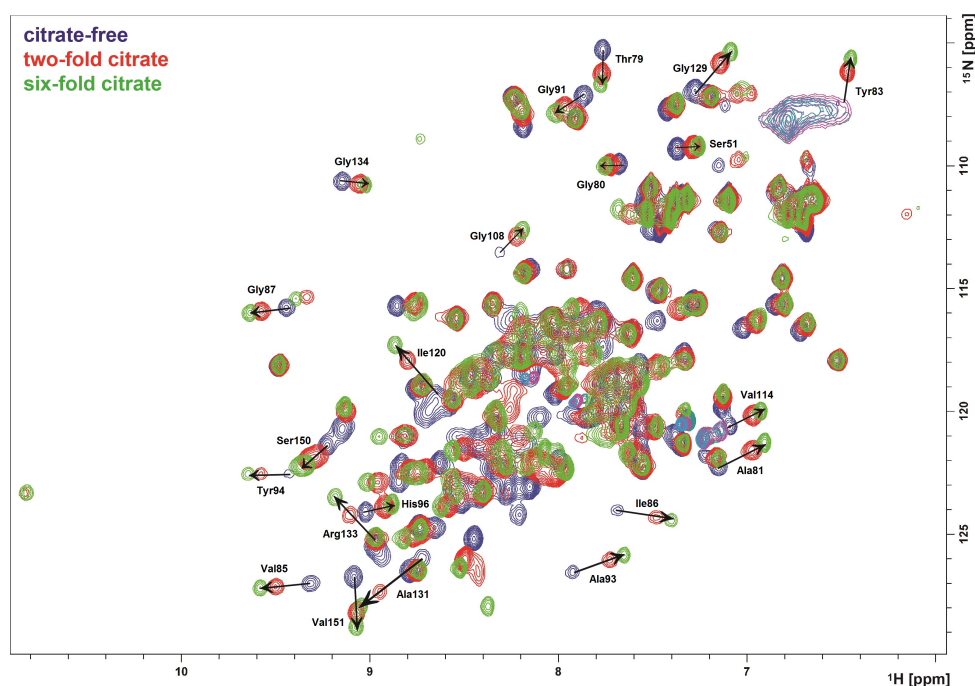


Figure 3.5: ^{15}N -HSQC titration of PASp R93A with citrate. Three representative ^{15}N -HSQC spectra of a titration of CitA PASp R93A with citrate. With increasing citrate concentration, several peaks shift significantly (some highlighted with arrows). Saturation is reached at six-fold excess of citrate, the calculated K_D was $624\ \mu\text{M}$.

With the assignment of PASp R93A in both citrate-free and citrate-bound state, it is possible to compare the secondary structure features of the different constructs. In order to do so, secondary chemical shifts were calculated for PASp wild-type, citrate-free PASp R93A and citrate-bound PASp R93A. The difference in chemical shifts can then be determined for all pairings of PASp constructs (see figure 3.6). The chemical shift differences between citrate-free and citrate-bound PASp R93A are consistent with the shift changes between wild-type PASp and citrate-free PASp R93A, indicating that wild-type PASp is in a citrate-bound state. Comparison of citrate-bound PASp R93A and wild-type PASp displays less chemical shift alterations which suggests similar conformations of the two states. Although crystallisation attempts were carried out for PASp R93A (both citrate-free and citrate-bound), no diffracting crystals could be produced.

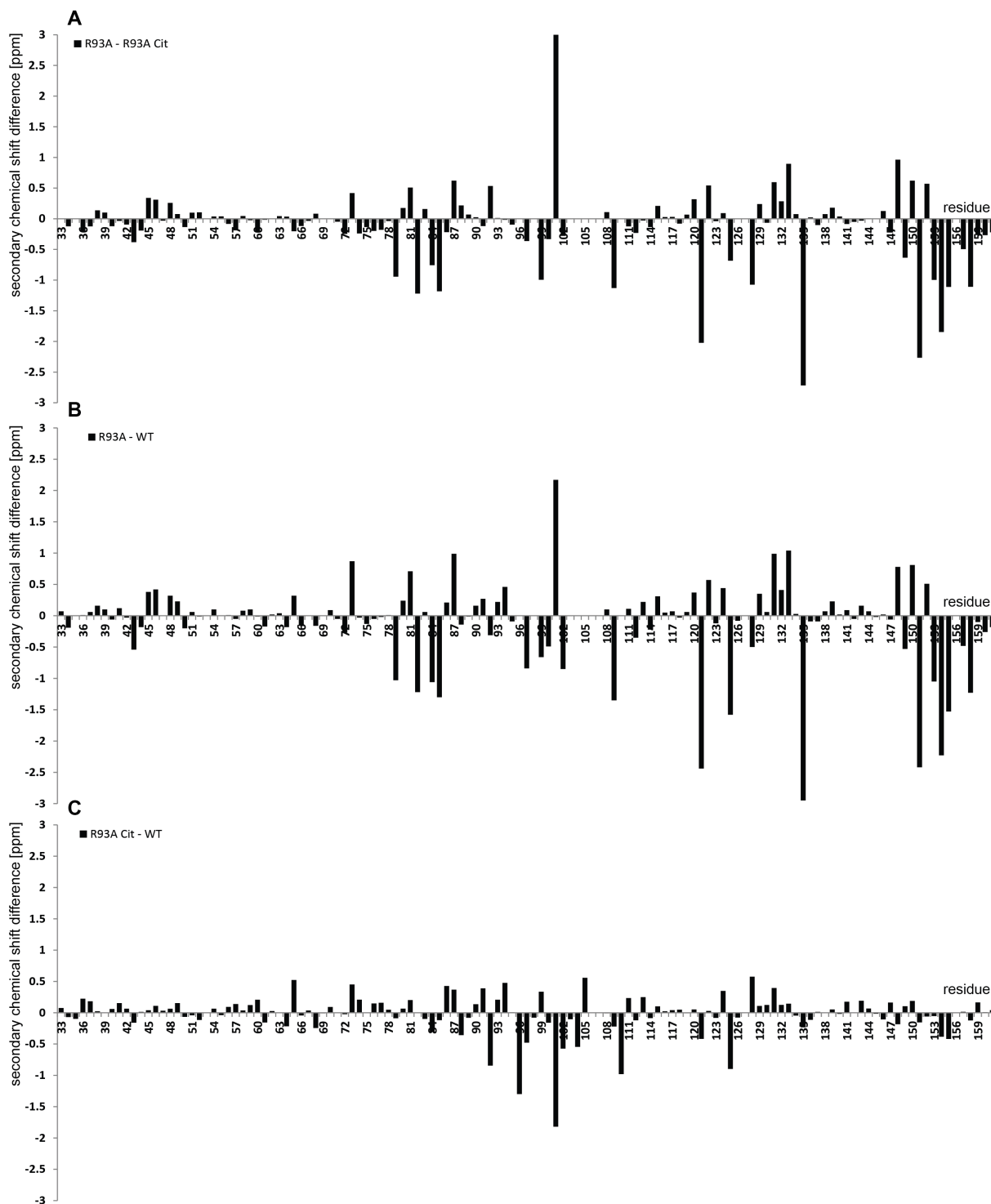


Figure 3.6: $C\alpha$ - $C\beta$ -secondary chemical shift differences between PAsp constructs. A: Secondary chemical shift difference between citrate-free and citrate-bound CitA PAsp R93A. B: Difference between citrate-free PAsp R93A and wild-type PAsp. C: Comparison of wild-type PAsp and PAsp R93A (citrate-bound).

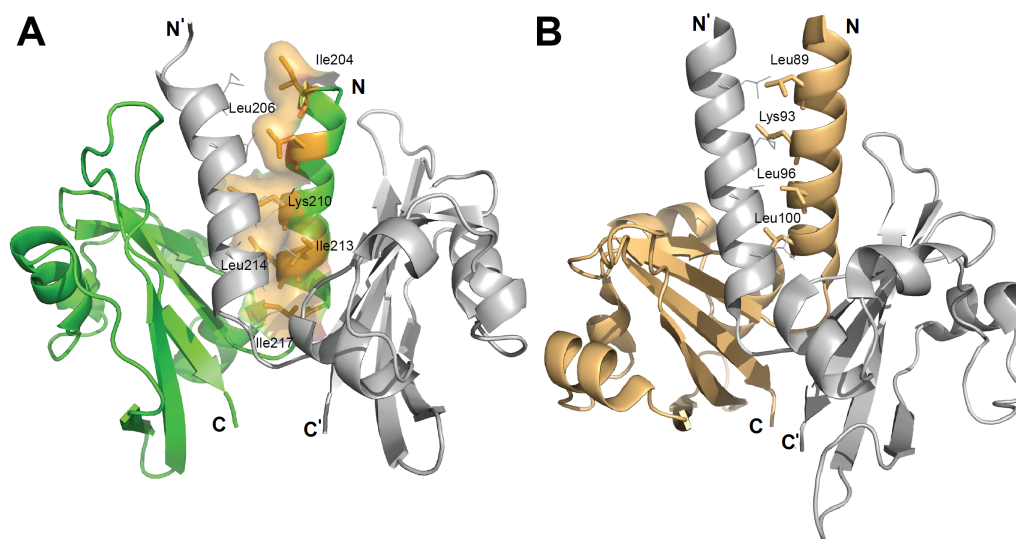


Figure 3.7: Crystal structure of CitA PASc. A: Crystal structure of PASc. Monomers are coloured green and grey. The hydrophobic zipper contacts in the N-terminal helix are shown as sticks for one monomer and as lines in the second monomer. The hydrophobic surface between the N-terminal helices is shown in light orange. B: The PAS-domain preceding the kinase core of the VicK crystal structure (PDB accession code:4I5S). Like for CitA PASc, hydrophobic contacts between the N-terminal helices are shown as sticks and lines.

3.2 The cytosolic PAS domain (PASc)

G. thermodenitrificans CitA PASc was purified in the same way as PASp. In contrast to PASp, PASc is a dimer in solution based on the gel filtration elution profile (see figure 3.1). Crystallisation of PASc yielded crystals which diffracted up to 1.78 Å. To solve the phase problem, PASc was also produced using selenomethionine labelling. The crystal structure was solved by Dr. Stefan Becker (Department of NMR-based Structural Biology, Max-Planck-Institute for Biophysical Chemistry, Göttingen, GER) using multi-wavelength anomalous dispersion (see tables 8.1 and 8.2) and reveals a canonical PAS-fold with five β -strands sandwiched between an N-terminal α -helix and four shorter helices (see figure 3.7 A). The dimer found in the asymmetric unit reflects the dimeric state seen in solution and reveals an exchange of N-terminal helices between monomers. The interaction between N-terminal helices from different monomers is supported by a hydrophobic zipper motif similar to the PAS domain of VicK, the first HK with a PAS domain adjacent to the kinase core (Wang *et al.*, 2013).

	200	210	220	230	240
<i>G. thermodenitrificans</i> CitA	<u>peEIGLLYQE</u>	<u>KQAILEAI</u> RE	<u>GIVAINQEGT</u>	<u>ITMVNQTALK</u>	<u>LLgydnernv</u>
<i>E. coli</i> DcuS	<u>pyEISTLFEQ</u>	<u>RQAMLQSI</u> KE	<u>GVVAVDDRGE</u>	<u>VTLINDAAQE</u>	<u>LLnyrksqdd</u>
	214	224	234	244	254
	250	260	270	278	288
<i>G. thermodenitrificans</i> CitA	<u>lgtpilqlip</u>	<u>hsrlpevirt</u>	<u>ggaey--DDE</u>	<u>MVLGGETVIA</u>	<u>NR</u> IPIKnkqG
<i>E. coli</i> DcuS	<u>eklstlshsw</u>	<u>sqvvdvsevl</u>	<u>rdgtprrrDEE</u>	<u>ITIKDRL</u> LI	<u>N</u> TVPVRsn-G
	264	274	284	294	304
	298	308			
<i>G. thermodenitrificans</i> CitA	<u>RVIGAVSTFR</u>	NK			
<i>E. coli</i> DcuS	<u>VIIGAISTFR</u>	DK			
	313	323			

Figure 3.8: Alignment of *Geobacillus thermodenitrificans* CitA PASc and *Escherichia coli* DcuS PASc. Functional mutants in PASc of *E. coli* DcuS were transferred to *G. thermodenitrificans* CitA based on a sequence alignment. Transferred ON-mutants in DcuS are highlighted green, OFF-mutants are shown in red. For DcuS N304D, R289 neighbouring the aligned N288 in CitA was selected as a second potential candidate for mutation. Capital letters indicate high sequence homology.

In DcuS, another HK of the CitA family, PASc mutants were tested for effects on the activity and dimerisation state of full-length DcuS (Monzel *et al.*, 2013). The PASc mutants associated with alterations in DcuS signalling can be divided into ON-mutants leaving the HK in a constitutive kinase-competent state and OFF-mutants which trap the DcuS kinase in the inactive state. The ON-mutants trigger signalling even without dicarboxylate ligands while OFF-mutant DcuS variants cannot be activated by adding dicarboxylates. While OFF-mutants conserve the dimeric HK state and binding capability to DctA, a DcuS co-receptor, ON-mutants can be subdivided further. The ON I-subtype destroys the HK dimer, which most likely does not correspond to biologically relevant states. ON II-subtype mutants on the other hand retain the dimeric state; ON IIB-mutants also still bind DctA while this interaction is lacking in ON IIA-mutants.

Based on the mutation analysis carried out *in vivo* on the PASc domain of homologous *E. coli* DcuS (Monzel *et al.*, 2013), mutants of *G. thermodenitrificans* CitA PASc were generated. Conserved residues in *G. thermodenitrificans* CitA PASc that were mutated in DcuS PASc were identified based on a sequence alignment of *E. coli* DcuS PASc and *G. thermodenitrificans* CitA PASc (see figure 3.8) generated with Dialign (Morgenstern, 2004). While selection of OFF-mutants was not restrained, ON-mutants were chosen from the ON IIB-subtype. In contrast to ON I- and ON IIA-mutants, DcuS dimer formation

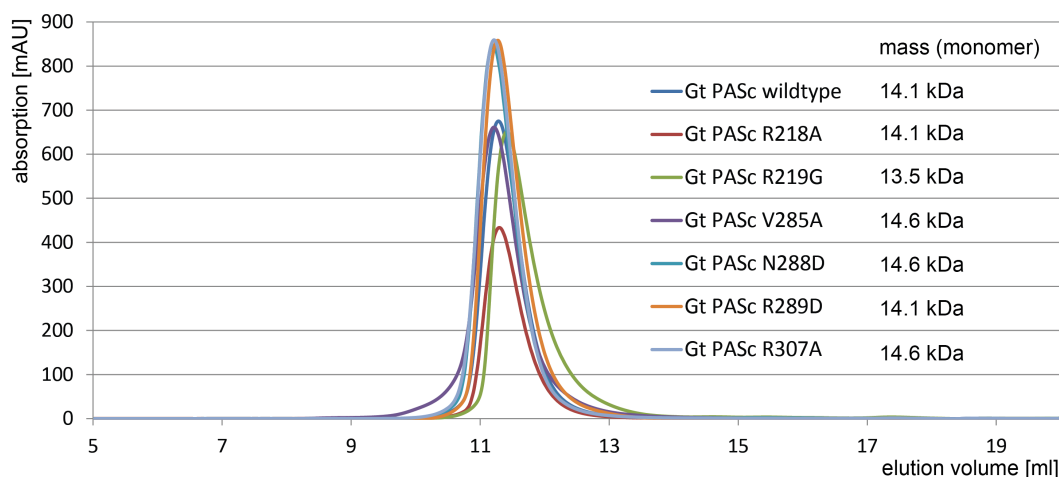


Figure 3.9: SEC profiles of CitA PASC mutants. Like for wild-type PASC and PASC, the molecular weight can be calculated from a calibration and is depicted for PASC mutant monomers, assuming dimers in solution. The SEC profile of wild-type PASC is shown as a reference.

and DctA interaction is intact in ON IIB-mutants, which therefore most likely correspond to the ligand induced wild-type conformation of DcuS.

In the case of N288 in *G. thermodenitrificans* CitA PASC the neighbouring R289, being a polar residue as well, was chosen as a second possible mutant to rule out errors in the sequence alignment. Like wild-type PASC, all selected point mutants are dimeric in solution based on SEC profiles (see figure 3.9). The dimer is stable in solution; SEC was run at concentrations of 1.5 mM, 150 μ M and 15 μ M for PASC N288D. In all cases, the elution profiles corresponded to dimeric protein. As SEC is limited by UV detection sensitivity, a concentration where monomeric protein could be observed was not reached. For all *G. thermodenitrificans* CitA point mutants, crystallisation trials were carried out (see table 3.1).

Table 3.1: Crystallisation of PASC mutants

PASC mutant	Crystallisation condition
R218A (SeMet)	0.4 M MgCl ₂ , 23.5 % PEG 3350, 0.1 M Tris pH 8.5
E219G	no crystals
V285A (native)	0.8 M Na ₂ HPO ₄ , 0.8 M KH ₂ PO ₄ , 0.1 M HEPES pH 7.5
N288D (SeMet)	0.4 M MgCl ₂ , 19 % PEG 8000, 0.1 M Tris pH 8.5
R289D (SeMet)	0.2 M Li ₂ SO ₄ , 27 % PEG 1000, 0.1 M phosphate-citrate pH 4.2
R307A (native)	2.2 M NaCl, 2 % PEG 6000

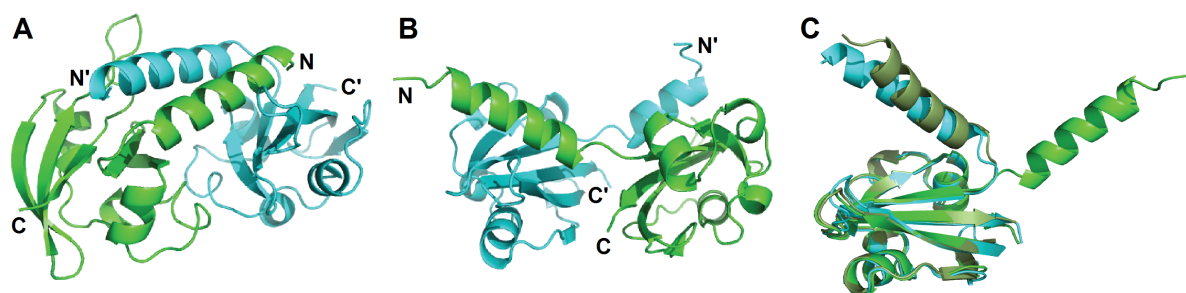


Figure 3.10: Crystal structures of proposed functional mutants of CitA PASc.

A: The structure of PASc N288D reveals an anti-parallel dimer (monomers coloured green and cyan). PASc R218A yields an identical fold. B: PASc R289D crystallises as an open dimer in which the *N*-terminal helix interaction between the monomers is missing. C: Alignment of the PAS-core of one monomer for wild-type PASc (olive), PASc N288D (cyan) and PASc R289D (green). While the overall fold is retained, the position of the *N*-terminal helix varies significantly.

Crystal structures could be solved for the proposed OFF-mutants CitA PASc R218A and V285A as well as for the proposed ON-mutants N288D, R289D and R307A (for details on structural data contact Dr. Stefan Becker, Department of NMR-based Structural Biology, Max-Planck-Institute for Biophysical Chemistry, Göttingen, GER). The PAS-fold excluding the *N*-terminal helix was conserved in all mutants with a maximum backbone rmsd of 0.42 Å compared to wild-type PASc, but the position of the *N*-terminal helix varied substantially in mutants R218A, N288D and R289D (see figure 3.10 C). PASc V285A and R307A crystal structures are identical to the wild-type structure. The re-orientation of the *N*-terminal helix in PASc R218A, N288D and R289D is related to different orientations of PASc monomers with respect to each other. In PASc R218A and N288D, the *N*-terminal helices form an anti-parallel dimer not connected to the PAS core. In PASc R289D the helices of the two monomers do not interact with each other, but are contacting the central β -sheet scaffold in *trans*, thus creating an open dimer in which the central β -scaffolds of the two monomers are anti-parallel (see figure 3.10 A, B). In contrast to DcuS, *in vivo* HK activity measurements on CitA PASc mutants carried out by the group of Prof. Uden did not show any effect over wild-type *G. thermodenitrificans* CitA for any of the PASc mutants.

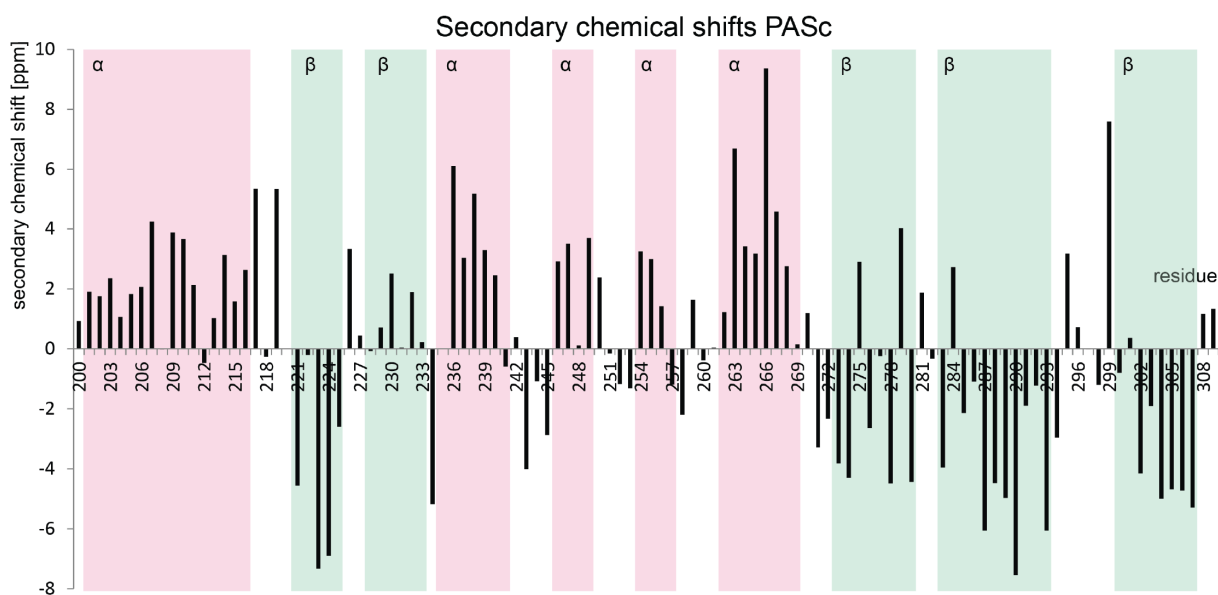


Figure 3.11: $C\alpha$ - $C\beta$ -secondary shift analysis of PASC in solution. The secondary chemical shifts reflect secondary structure propensity, with positive values indicating α -helix, negative values corresponding to β -strands. The secondary structure elements of the PASC crystal structure are superimposed (red: α -helix, green: β -strand).

Wild-type *G. thermodenitrificans* CitA PASC was assigned using liquid-state NMR experiments (see table 2.5). In total, 92 % of proton, 85 % of carbon and 69 % of nitrogen resonances were assigned. The backbone assignment reached 86 % completeness. The missing assignments are mainly clustered in the *N*-terminal helix due to very weak or non-existent peaks in ^{15}N -HSQC-based experiments (see figure 3.12). Assignment of these residues was therefore mainly based on ^{13}C -HSQC-NOESY contacts and HCCH-TOCSY correlations. The $C\alpha$ - $C\beta$ -secondary chemical shifts of assigned residues correspond well to secondary structure elements found in the crystal structure of PASC (see figure 3.11). Some residues in the second and third β -strand, expected to be negative, are found to display positive secondary shift values.

The PASC structure reveals twists in the two β -strands for which secondary shift values do not match secondary structure elements. Analysis of the backbone dihedral angles in the crystal structure demonstrates a deviation from ideal angles for anti-parallel β -strands ($\psi = -140^\circ$; $\phi = 135^\circ$). The positive secondary chemical shift values therefore correspond with strained β -strands in the crystal structure.

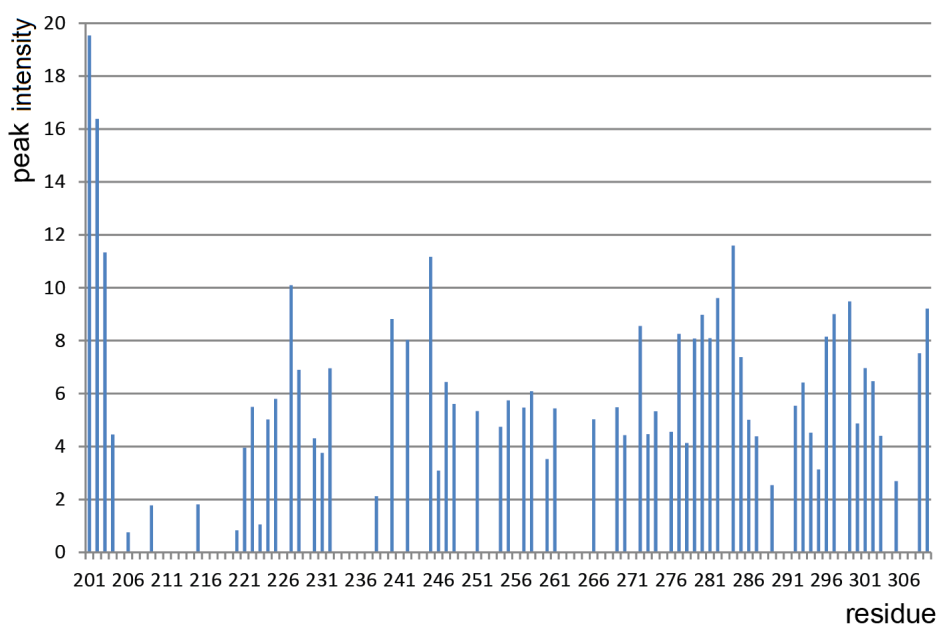


Figure 3.12: Peak intensity of PASC in a ^{15}N -HSQC. Visualisation of the intensity of well separated peaks in a ^{15}N -HSQC experiment demonstrates the generally low intensity at the N -terminus of the domain. As assignment based on amide-correlation based spectra in this region was impossible, most resonances in the N -terminal helix were assigned based on ^{13}C -HSQC-NOESY and HCCH-TOCSY experiments.

To confirm that citrate is only binding to PAsp and not to PASC, a control ^{15}N -HSQC of isolated PASC was set up with a twofold excess of citrate. As the spectrum is unchanged compared to citrate-free PASC (see figure 3.13) and no citrate was found in the crystal structure, effects on PASC in the citrate-bound form must be transmitted through binding of citrate to PAsp alone. Additionally, the residues in the citrate-binding pocket of PAsp are highly conserved (see figure 3.4) and not to be found in the sequence and structure of PASC (Gerharz *et al.*, 2003).

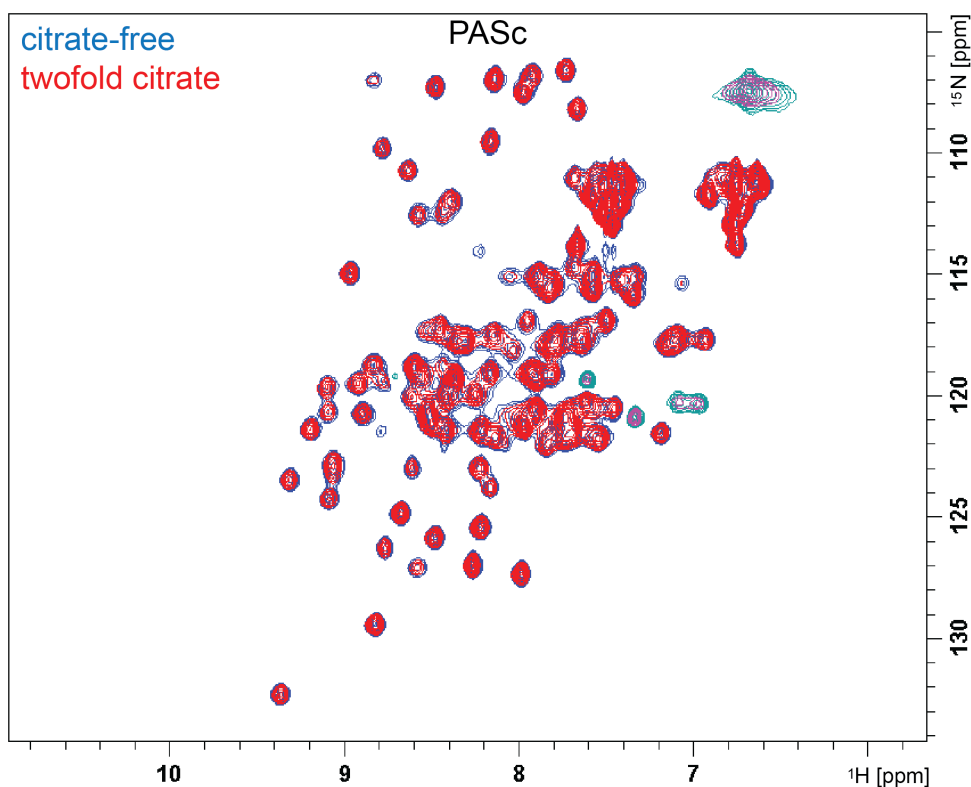


Figure 3.13: ^{15}N -HSQC of PASC with excess citrate. To exclude citrate binding capacities of CitA PASC, a spectrum of isolated PASC with twofold excess of citrate (red) was compared with the spectrum of a citrate-free sample (blue). Spectra are shown at slightly different contour levels for visibility. No citrate binding effect is observed.

3.3 Liposome-embedded CitApc

The liquid-state NMR characterisation of large membrane proteins is challenging due to the huge particle size and the corresponding anisotropy and low tumbling times (Cross and Opella, 1994). Additionally, membrane proteins have to be embedded in micelles, bicelles or lipid nanodiscs for liquid-state NMR studies. These membrane mimetic systems can influence protein structure and functionality in unexpected ways (Zhou and Cross, 2013). To overcome the liquid-state NMR limitations, *G. thermodenitrificans* CitApc was therefore studied by solid-state NMR spectroscopy of liposome-embedded protein. For forming the multi-lamellar liposomes, asolectin was chosen because of the low phase transition temperature which allowed recording of solid-state spectra at ~ 10 °C in the liquid crystalline phase. At higher temperatures, heteronuclear magnetisation transfer is

less efficient. By reducing the temperature from 25 °C to 9 °C, NCA signal intensity was increased by 70 % (see figure 3.14).

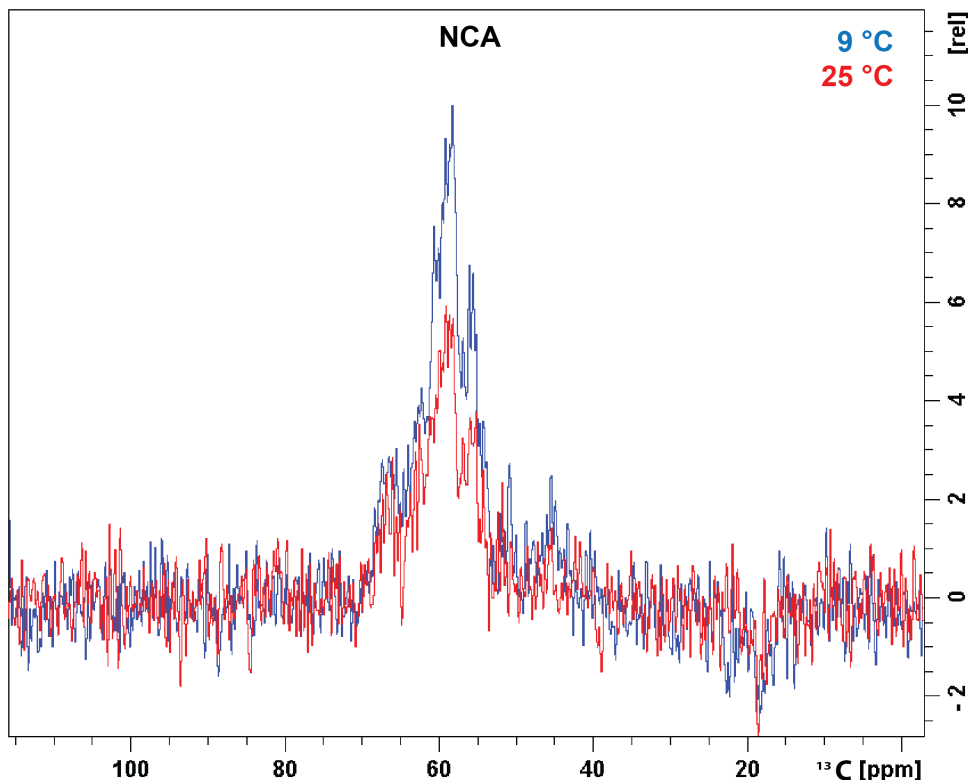


Figure 3.14: Heteronuclear cross-polarisation efficiency in CitApc at different temperatures. Upon reducing the temperature from 25 °C (red) to 9 °C (blue), peak intensity can be increased by 70 % in an NCA-experiment.

Solid-state spectra were assigned using the liquid-state assignments and the approach outlined in chapter 1.7. For the globular domains, 94 % of PASp and 40 % of PASc residues could be assigned in 20 ms PDS, NCACB, NCOCA, and NCOCACB spectra (see figure 3.15 A). In most cases, the overlap between liquid-state resonance assignments and solid-state peak positions was better than ± 0.2 ppm with the only major differences in the region of the PASp dimer interface (see figures 3.15 B and 3.16). Residues at the PASp dimer interface were assigned based on sequential assignment. As PASp is monomeric in solution, these differences can be expected for dimeric CitApc.

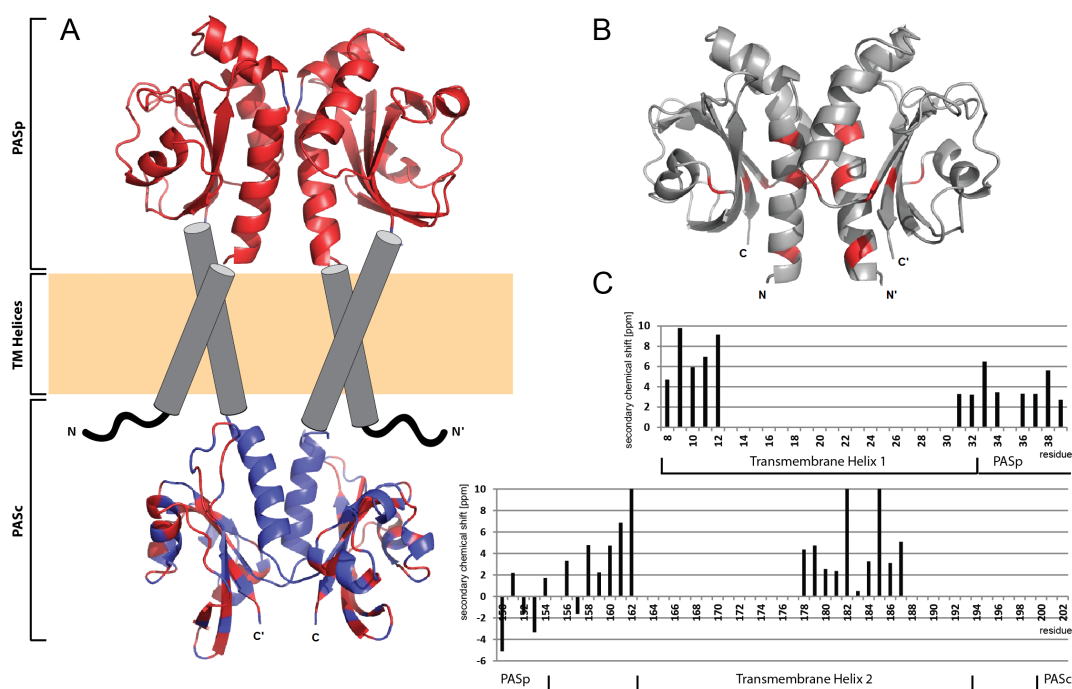


Figure 3.15: Solid-state assignments of wild-type CitApc. A: Assignments found for PASp and PASc using solid-state experiments. Assigned residues are highlighted in red, unassigned residues are shown in blue. Transmembrane helices are shown as grey cylinders due to the lack of structural information. B: Differences between liquid-state assignments of PASp and the solid-state assignments. $C\alpha$ - $C\beta$ -secondary chemical shift differences of more than 0.5 ppm are highlighted red. C: $C\alpha$ - $C\beta$ -secondary chemical shift values of assigned residues in the transmembrane helices.

Based on the existing assignments of the globular domains and spectra for sequential assignment (3D NCACB, NCOCA, NCOCACB and 2D CA(NCO)CA), a partial *de novo*-assignment of the transmembrane helices was possible. In total, 9 new residue assignments in the first and 17 assignments in the second transmembrane helix were obtained (see figure 3.15 C) and correspond to helical conformation based on secondary chemical shifts.

To access the citrate-free state, an R93A mutant was introduced in the periplasmic PAS domain. A 20 ms PDS spectrum of citrate-free CitApc R93A in asolectin revealed peak doubling around the citrate binding pocket, with one set of peaks corresponding to the citrate-free and the other set corresponding to the citrate-bound state in solution (see figure 3.17 A). In 3D spectra, only peaks matching the citrate-bound assignments were visible. Liquid-state spectra of asolectin solubilised in 10 % sodium dodecyl sulfate revealed citrate impurities in the lipid mixture (see figure 3.17 B). CitApc R93A was

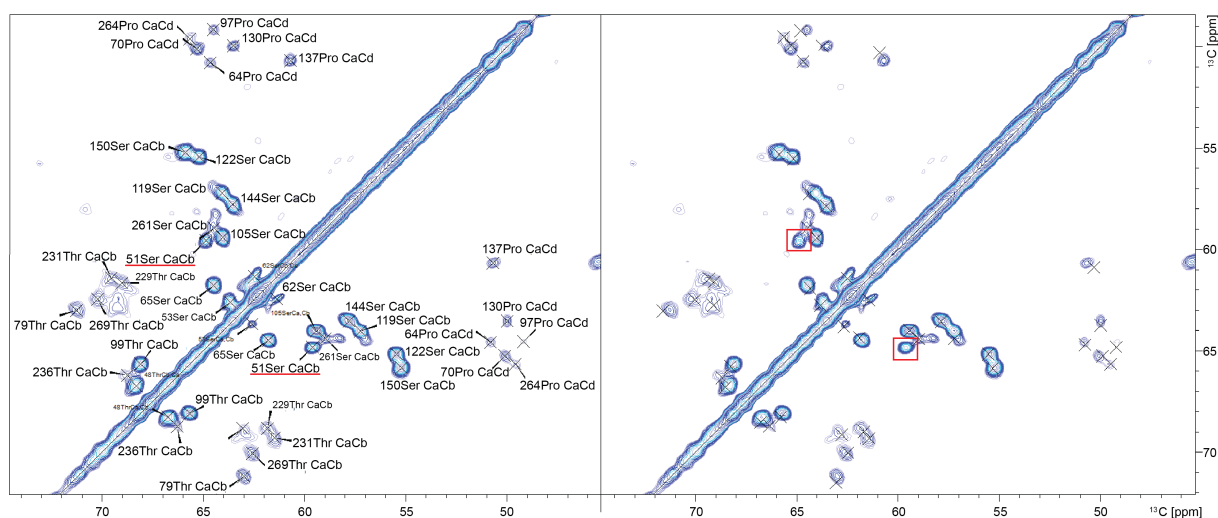


Figure 3.16: Assignment consistency between liquid- and solid-state NMR. Left: assigned peaks in the Ser/Thr $C\alpha$ - $C\beta$ region of a PDS spectrum. With exception of Ser51, all peaks presented here were assigned based on liquid-state data. Ser51, situated at the PASp dimer interface, was identified based on sequential assignment (red). Right: predicted peak positions for assigned peaks based solely on liquid-state NMR data. With few exceptions, the overlap between liquid- and solid-state peak positions is better than 0.2 ppm.

therefore not accessible in a pure citrate-free state in asolectin. The peak doubling detected in solid-state spectra suggests slow exchange between citrate and PASp on an NMR timescale, as opposed to the fast exchange observed in the isolated domain. The peak doubling was confirmed in a PDS spectrum of CitApc R93A at 20 °C, the temperature of isolated PASp R93A titration.

To reach a citrate-free state of the receptor, new samples of *G. thermodenitrificans* CitApc R93A in the pure phospholipid 1,2-dimyristoyl-*sn*-glycero-3-phosphocholine (DMPC) were produced. The assignment routine used for wild-type CitApc was repeated, yielding 81 % of PASp and 59 % of PASc residues that could directly be assigned based on liquid-state data. Additionally, a sample of CitApc R93A with excess citrate embedded in DMPC liposomes was produced to study the citrate-bound form of the R93A mutant receptor. Here, 86 % of PASp and 45 % of PASc could be assigned. The assignment of the PAS domains in the different CitApc constructs allows for a comparison between the different signalling states.

First, differences in secondary chemical shifts observed in liquid-state spectra of the

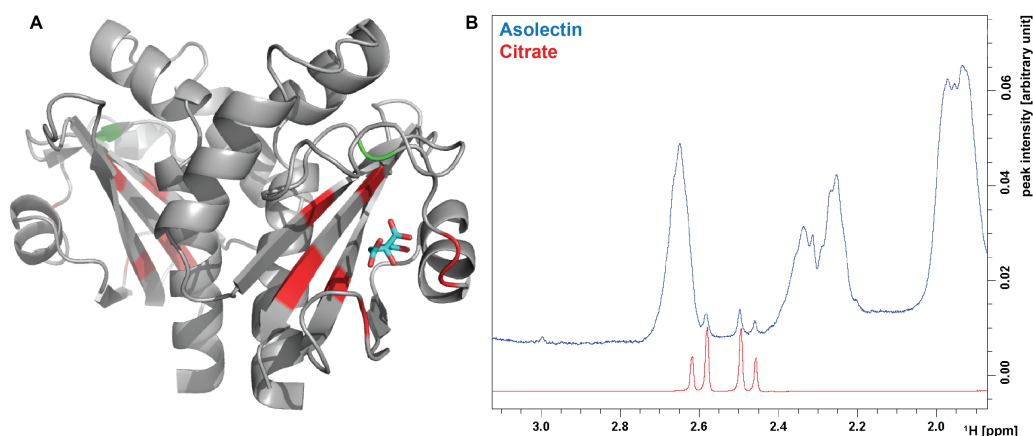


Figure 3.17: Effects of citrate impurities on PASp. A: Residues that can be assigned for both citrate-free and citrate-bound state in PDS of CitApc R93A (citrate-free) are highlighted in red. The mutation site is shown in green. B: Citrate CH₂-quartet visible in an asolectin proton spectrum (blue) solubilised in 10 % sodium dodecyl sulfate (SDS). A spectrum of pure citrate in 10 % SDS is shown in red.

isolated PASp between citrate-free and citrate-bound form can be confirmed for CitApc (see figure 3.19). Second, differences in the visibility of certain residues in PASc, mainly in the central β -scaffold, between citrate-free and citrate-bound CitApc R93A become apparent. In total, 62 residues of PASc in the citrate-free and 45 residues in the citrate-bound state could be assigned based on liquid-state chemical shifts; ambiguities in 2D PDS spectra could be resolved in 3D NCACB and NCOACB spectra for 2 residues in the citrate-free state and 5 residues in the citrate-bound state. As few PASc residues could be detected in 3D spectra due to low signal/noise (see figure 3.18), assignment of PASc relies predominantly on PDS spectra.

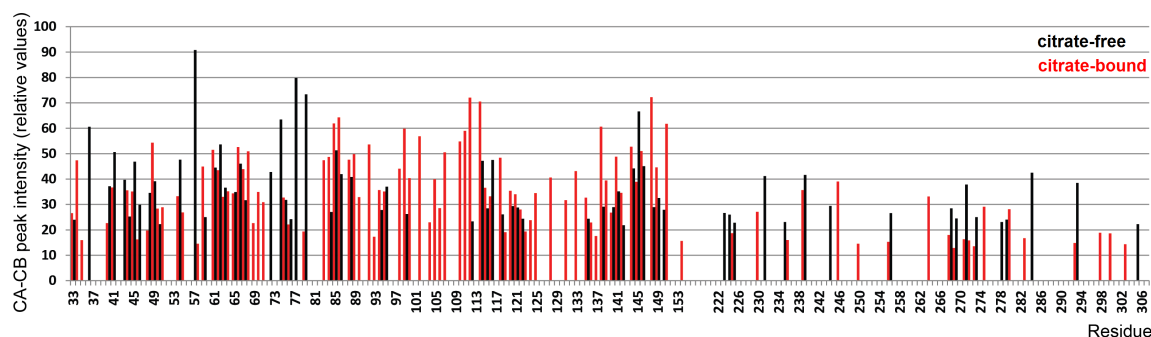


Figure 3.18: Peak intensity of PASp and PASc in solid-state spectra. The peak intensity of isolated $C\alpha$ - $C\beta$ -peaks in 3D solid-state spectra reveals a generally reduced peak height in PASc for both citrate-free (black) and citrate-bound (red) CitApc.

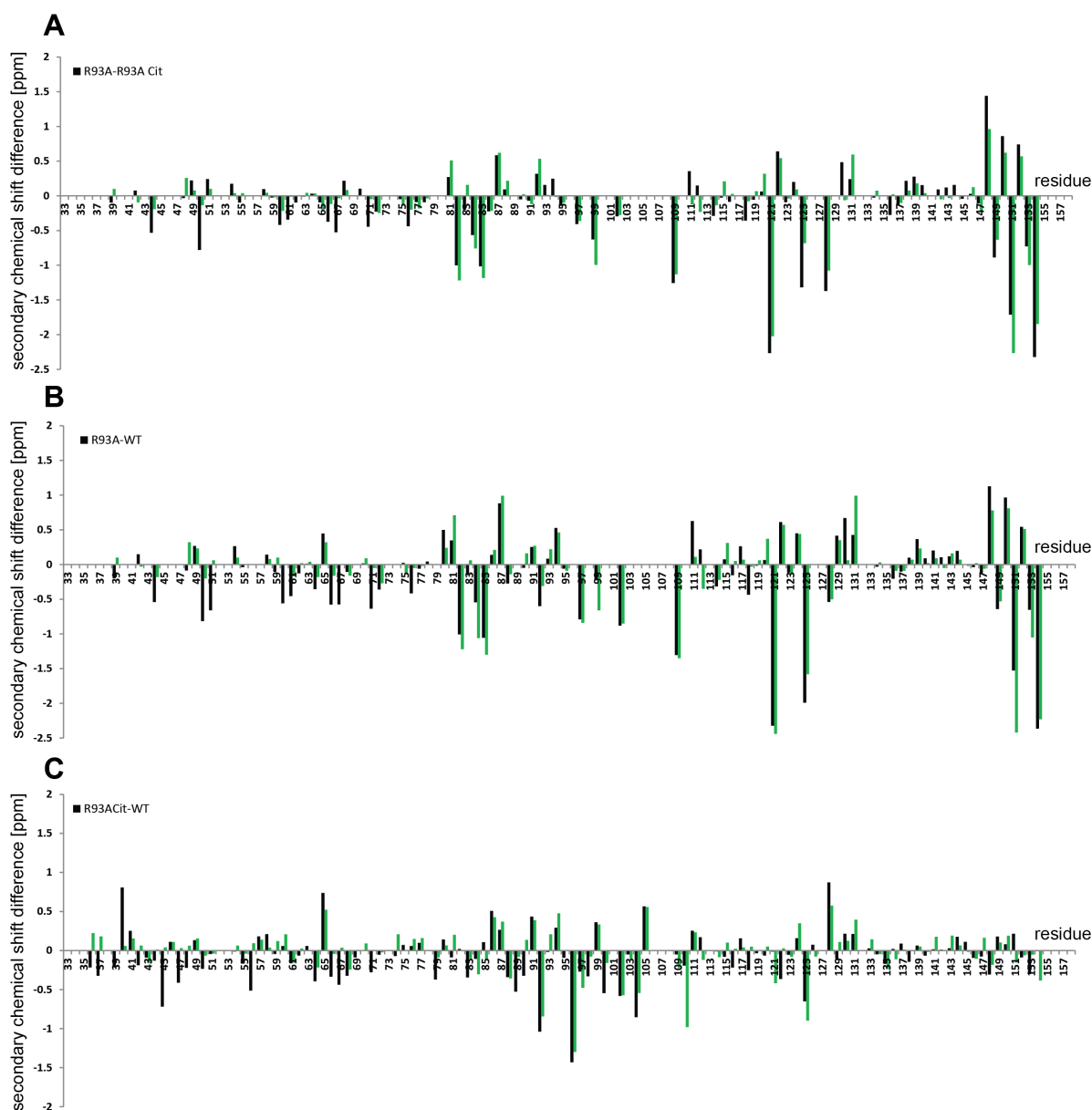


Figure 3.19: C_{α} - C_{β} -secondary chemical shift differences in PASp of membrane-embedded CitApc constructs. Secondary chemical shift differences of PASp in CitApc are shown in black; the secondary shift differences observed in isolated PASp (see figure 3.6) are shown again in green for comparison. Only secondary shift differences that are evaluated for both liquid- and solid-state spectra are shown for clarity. A: Secondary chemical shift changes between citrate-free and citrate-bound PASp R93A. B: Difference between PASp in citrate-free CitApc R93A and PASp in wild-type CitApc. C: Comparison of the citrate-bound PASp in CitApc R93A and PASp in wild-type CitApc.

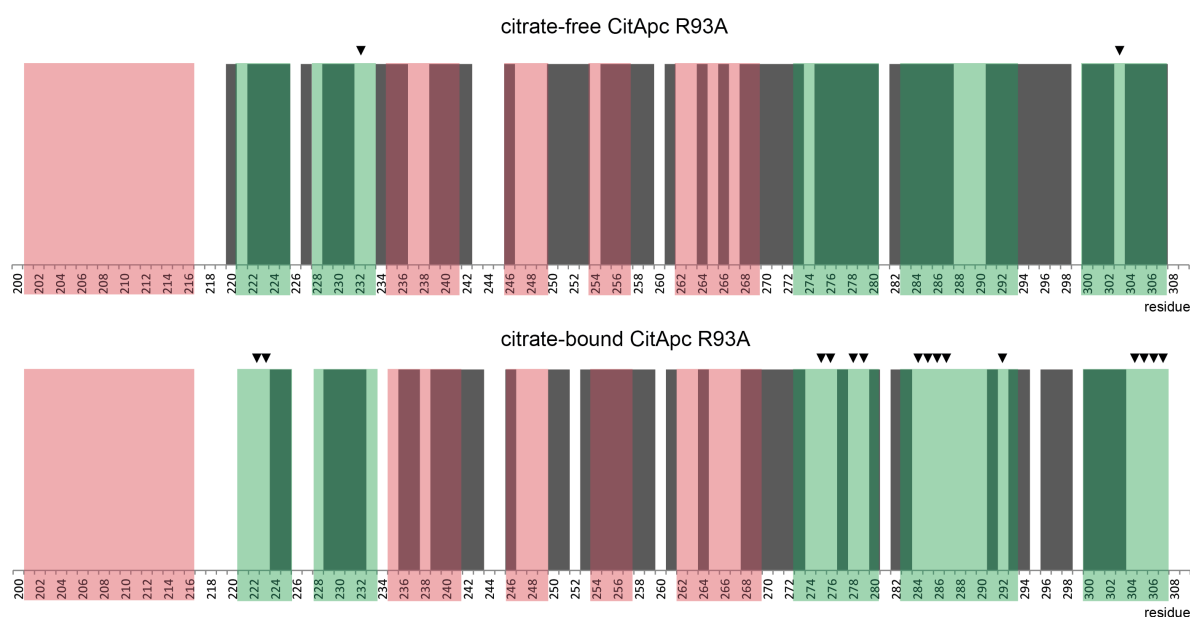


Figure 3.20: Assigned PASC residues in citrate-free and citrate-bound CitApc R93A. PASC residues assigned in citrate-free and citrate-bound CitApc R93A based on liquid-state chemical shifts are shown in grey. Secondary structure motifs of the PASC crystal structure are highlighted (α -helices red, β -strands green). Residues in β -strand conformation that are visible only in either citrate-free or citrate-bound state are marked with arrows.

Of the additional 16 residues of PASC that can be assigned in the citrate-free state, 15 are found in β -strands forming the PASC core (see figure 3.20). While the missing assignments in citrate-bound CitApc could be the result of a discrepancy of liquid-state shifts and solid-state peak positions, additional unassigned peaks would be expected in this scenario. For the case of residues in α -helical conformation, these additional peaks could either correspond to PASC or the transmembrane helices, but additional peaks for residues in β -strand conformation could only be related to PASC if helical conformation is assumed for the transmembrane regions. In few cases where peak overlap is low, the existence of additional unassigned peaks in citrate-bound CitApc R93A, reflecting different conformations of β -strand residues that were assigned in citrate-free CitApc R93A, can be ruled out (see figure 3.21). Among the residues that are visible in the citrate-free state but cannot be assigned in the citrate-bound state is arginine 307 at the *C*-terminus of PASC, leading into the DHp domain and thus the kinase core.

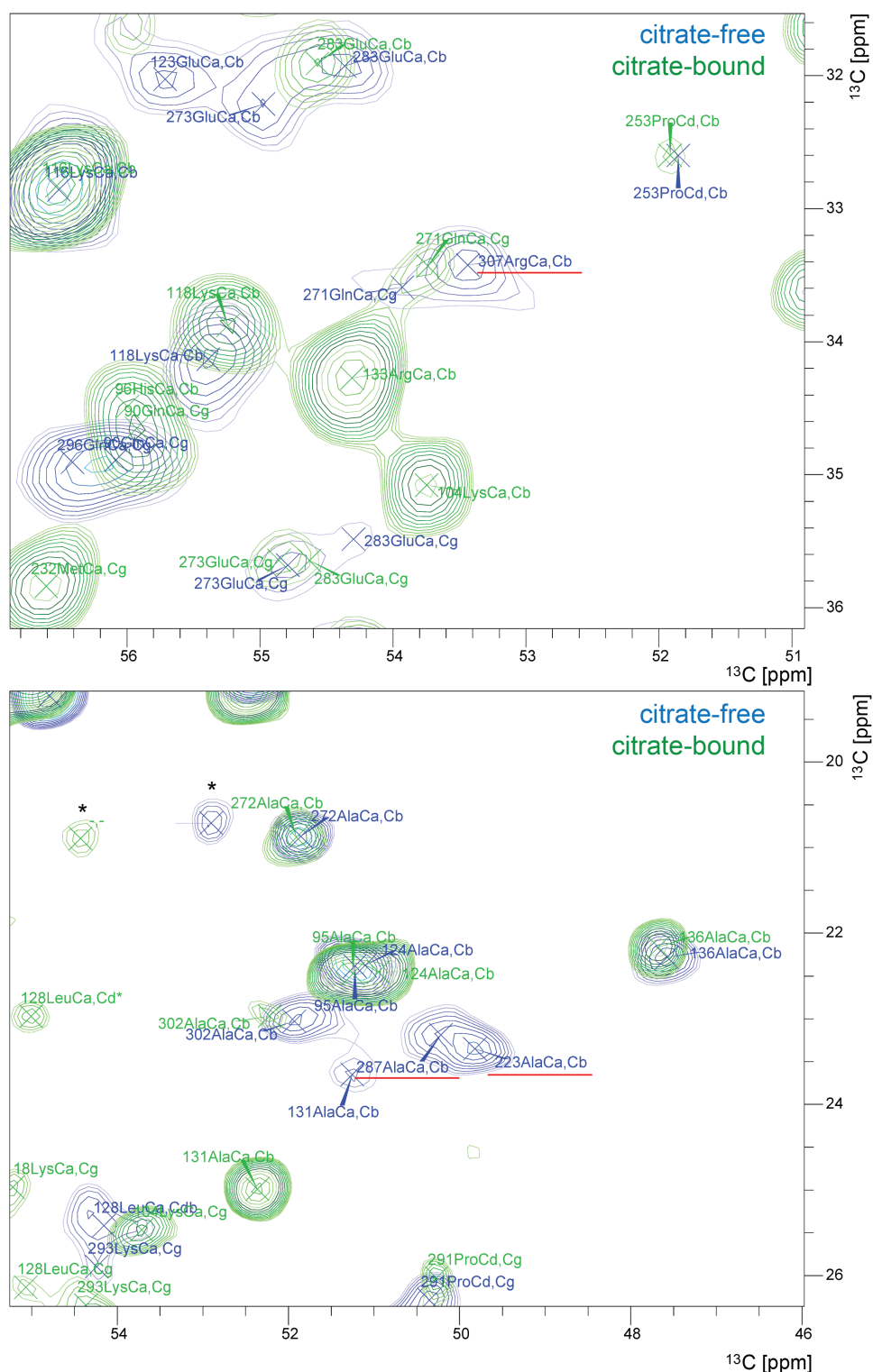


Figure 3.21: PASC visibility in PDS spectra of citrate-free and citrate-bound CitApc R93A. For the highlighted residues (red) in β -strand conformation, liquid-state assignments could be confirmed in a PDS spectrum of citrate-free CitApc R93A (blue), but not in the citrate-bound state (green). In citrate-bound CitApc R93A, no unassigned peaks in the vicinity of highlighted peak positions could be found. The peaks marked with asterisks are not assigned and correspond to an alanine in coil conformation.

4 Discussion

4.1 The periplasmic PAS domain (PASp)

The first step towards proposing a signalling model for CitA is getting structural information on the signal receptor domain PASp in both signalling states. To this end, samples of *Geobacillus thermodenitrificans* CitA PASp were purified both for liquid-state NMR studies and crystallisation trials. Based on crystal structures available for the kinase core (Marina *et al.*, 2005; Albanesi *et al.*, 2009; Vu *et al.*, 2011; Wang *et al.*, 2013) and the homologous structure of citrate-bound CitA PASp from *Klebsiella pneumoniae* (Sevvana *et al.*, 2008), a dimeric state of the kinase assembly can be assumed. Despite the proposed dimeric state in the full-length receptor, PASp of *G. thermodenitrificans* CitA appears to be a monomer in solution based on SEC profiles (see figure 3.1) and liquid-state NMR spectra. The apparent molecular weight of 17.8 kDa is above the expected 14.9 kDa, but differences between observed and theoretical molecular weight are generally observed for proteins that are not spherical (Andrews, 1964). The observed mass can thus not be attributed to PASp dimers. In addition, linewidth broadening for peaks around the dimerisation interface would be expected, but is not observed in a ^{15}N -HSQC spectrum (see figure 4.1). Interestingly, although the crystal structure of citrate-bound *K. pneumoniae* CitA PASp is dimeric, the crystal structure of citrate-free *K. pneumoniae* CitA PASp (Sevvana *et al.*, 2008) and the NMR structure of *Escherichia coli* DcuS PASp (Pappalardo *et al.*, 2003) show monomeric states of PASp domains. It therefore seems plausible that the dimerisation affinity of isolated PASp-domains is not necessarily high and that dimerisation of full-length histidine kinases is predominantly influenced by the transmembrane helix assembly and the DHp domains forming a helix bundle.

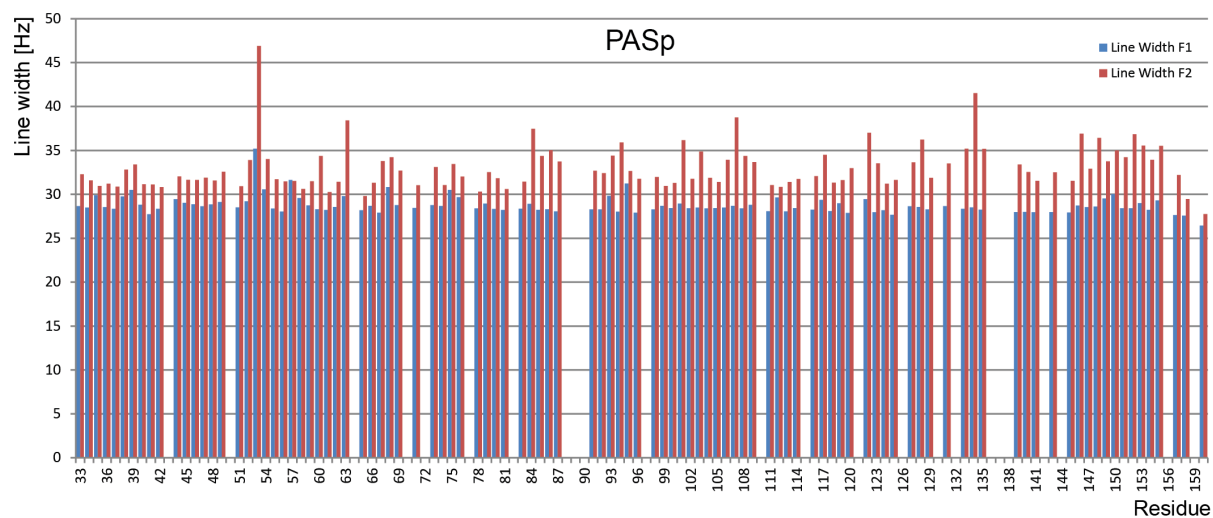


Figure 4.1: PAsp linewidth in a ^{15}N -HSQC. A ^{15}N - and ^1H -linewidth (F1 and F2, respectively) plot does not reveal regions with broadened lines indicative for a dimerisation propensity. Only isolated peaks in the ^{15}N -HSQC spectrum were analysed.

When *G. thermodenitrificans* CitA PAsp was titrated with citrate, no binding was observed. While the lack of effect on chemical shifts during the titration might be related to a non-functional isolated receptor domain, full-length *G. thermodenitrificans* CitA clearly shows activity *in vivo* (see 3.1). Additionally, although no citrate was added during set-up, the crystal structure of *E. coli* CitA PAsp contains citrate in the binding pocket. A similar behaviour was described for a ligand-binding PAS domain of HK DctB where succinate was found in the binding pocket of the crystal structure despite being absent in the purification and crystallisation protocol (Cheung and Hendrickson, 2008). It was therefore reasonable to assume that the binding of citrate to PAsp both for *E. coli* and *G. thermodenitrificans* CitA might be too strong to isolate a citrate-free state. Based on the crystal structures of citrate-bound *K. pneumoniae* CitA PAsp and *E. coli* CitA PAsp, a conserved arginine residue (Gerharz *et al.*, 2003) contacting citrate

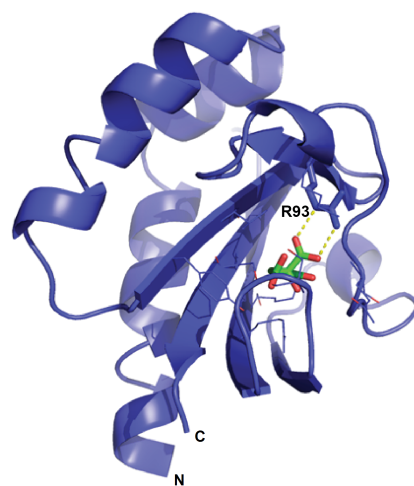


Figure 4.2: Mutation site in CitA PAsp. Arginine 93 is shown as sticks, other residues in the citrate binding pocket as lines. The R93 side-chain forms two hydrogen bonds with a citrate carboxyl group.

in the binding pocket was identified (see figure 4.2). The corresponding arginine 93 in *G. thermodenitrificans* CitA PASp was mutated to alanine to reduce binding affinity. With the R93A mutant, chemical shift differences upon citrate addition to PASp could be observed, supporting the hypothesis that recombinant wild-type PASp is citrate-bound under experimental conditions. With *G. thermodenitrificans* CitA PASp R93A it is thus possible to study the receptor in both signalling states. The determined K_D value of $624 \pm 21 \mu\text{M}$ is two orders of magnitude weaker than the ligand binding affinity of wild-type *K. pneumoniae* CitA PASp (Kaspar *et al.*, 1999), but in the same range or stronger than the affinity of *E. coli* DcuS towards its ligands (Kneuper *et al.*, 2005). *In vivo*-studies on *G. thermodenitrificans* CitA R93A carried out by the group of Prof. Uden (Johannes Gutenberg-Universität Mainz, GER) demonstrated citrate specificity and receptor activity, indicating that the R93A mutant does not alter the signalling functionality of CitA, but only reduces citrate affinity (see figure 3.3).

4.1.1 Citrate binding and activation of PASp

Liquid-state NMR assignments of PASp R93A, both citrate-free and citrate-bound, allow for a detailed analysis of the effects of citrate binding. To visualise structural rearrangements caused by ligand binding, an I-TASSER model of *G. thermodenitrificans* CitA PASp based on *K. pneumoniae* CitA PASp was used. The changes to secondary structure can be correlated with differences in $C\alpha$ - $C\beta$ -secondary chemical shifts. When $C\alpha$ - $C\beta$ -secondary shifts of citrate-free PASp R93A are compared with citrate-bound R93A, the whole central β -sheet scaffold including the *C*-terminal strand leading into the second transmembrane helix is affected (see figure 4.3 A). This suggests that citrate is indeed binding to the pocket evident from crystal structures of homologous *K. pneumoniae* CitA PASp and *E. coli* CitA PASp. As a control of the physiological relevance of the citrate-bound state generated in PASp R93A, the $C\alpha$ - $C\beta$ -secondary shifts of citrate-bound PASp R93A can be compared to wild-type PASp. The differences are all in close proximity to the mutation site, the remainder of the domain, including the central β -scaffold and the *C*-terminus, are conserved between the two constructs (see figure 4.3 B). Not only does this confirm that wild-type PASp is in a citrate-bound state, but also that

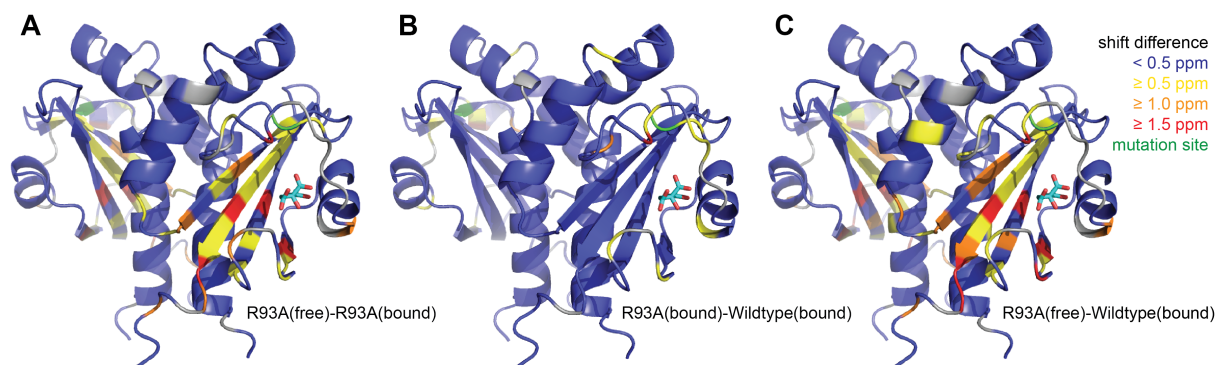


Figure 4.3: C α -C β -secondary chemical shift changes upon PASp activation in solution. A: Differences between citrate-free and citrate-bound PASp R93A. The whole binding pocket undergoes structural reorganisation. Citrate is shown as cyan sticks for citrate-bound PASp. B: Comparison of citrate-bound PASp R93A and wild-type PASp. The citrate binding pocket is structurally unperturbed, indicating the same conformation of both proteins. Differences are seen around the mutation site R93A highlighted in green. C: Comparison of citrate-free PASp R93A and citrate-bound wild-type PASp reproduces differences observed between the two signalling states of PASp R93A.

citrate binding to PASp R93A restores a conformation very similar to that of wild-type protein. As a further control, shifts of citrate-free PASp R93A can be compared to the citrate-bound wild-type PASp; the shift differences observed match those for PASp R93A with and without citrate (see figure 4.3 C). The R93A mutant can therefore be used as a valid model for investigating citrate binding to CitA, circumventing the inaccessibility of inactivated PASp in wild-type *G. thermodenitrificans* CitA.

From crystal structures and NMR data on *K. pneumoniae* CitA PASp, a contraction of the β -scaffold upon citrate binding can be deduced (see figure 4.4). This contraction results in a shortening of the last β -strand in PASp by one amino acid (Sevvana *et al.*, 2008). The same behaviour is apparent in PASp R93A of *G. thermodenitrificans* (see figure 4.5), where leucine 154 switches from negative to positive secondary chemical shift values upon citrate addition, corresponding to a transition from β -strand to α -helical conformation. In a sequence alignment of *G. thermodenitrificans* CitA and *K. pneumoniae* CitA, the affected leucine 154 can be aligned with threonine 171 in *K. pneumoniae* CitA. Interestingly, threonine 171 is the residue which in the crystal structures of *K. pneumoniae* CitA is affected by the shortening of the C-terminal β -strand. The alignment of PASp domains can be visualised in an overlay of the crystal structure of citrate-free *K.*

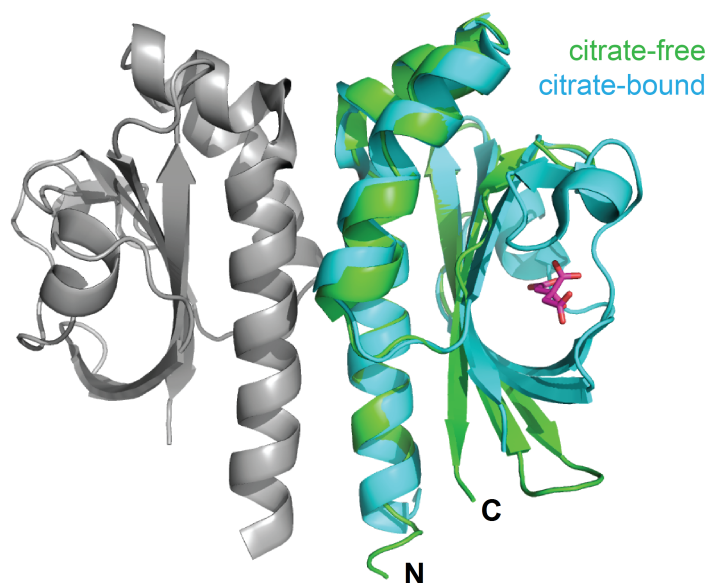


Figure 4.4: Structural reorganisation upon citrate binding in *Klebsiella pneumoniae* CitA PASp. An overlay of crystal structures of *K. pneumoniae* CitA PASp in citrate-free (green) and citrate-bound (cyan) states reveals a shortening of the *C*-terminal β -strand by one residue (Sevvana *et al.*, 2008). Citrate found in the binding pocket of the citrate-bound form is shown in pink. PDB-accession codes for citrate-free and citrate-bound PASp: 2V9A and 2J8O.

pneumoniae CitA PASp with the I-TASSER structural model of *G. thermodenitrificans* CitA PASp (see figure 4.5 right). As *K. pneumoniae* CitA threonine 171 is structurally equivalent with *G. thermodenitrificans* CitA leucine 154, it is likely that the change in $C\alpha$ - $C\beta$ -secondary chemical shift observed for leucine 154 reflects a shortening of the *C*-terminal β -strand in *G. thermodenitrificans* CitA. While the secondary chemical shifts of glutamate 156 and succeeding residues also exhibit secondary shift changes upon citrate addition, they are not part of the isolated domain and changes are most likely unspecific.

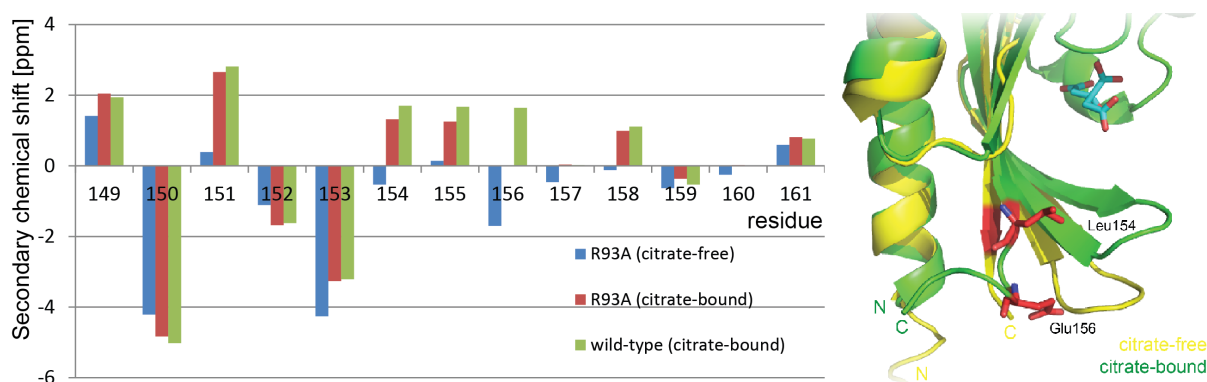


Figure 4.5: $C\alpha$ - $C\beta$ -secondary chemical shift differences between citrate-free and citrate-bound states. Left: Secondary chemical shifts indicate a secondary structure alteration at leucine 154, which switches from negative (indicative of β -strand conformation) in R93A to positive values (helical) in the citrate-bound states. Right: Comparison of the position of leucine 154 in a model of *Geobacillus thermodenitrificans* CitA PASp (green) based on citrate-bound *Klebsiella pneumoniae* CitA PASp and the corresponding residue in citrate-free *K. pneumoniae* CitA PASp (yellow). In the citrate-free state, the corresponding threonine 171 in *K. pneumoniae* CitA PASp is in β -strand conformation, while leucine 154 is at the C-terminus of the β -strand in the citrate-bound state. While the secondary chemical shift of glutamate 156 is also affected by citrate binding, it is not part of the domain and changes are most likely unspecific.

4.2 The cytosolic PAS domain (PASc)

Like PASp, samples of *G. thermodenitrificans* CitA PASc were produced both for crystallography and liquid-state NMR spectroscopy. As opposed to PASp, CitA PASc appears to be a dimer in solution based on the apparent molecular weight of 28.3 kDa in SEC profiles, corresponding to a 14.1 kDa monomer (see figure 3.1). As for PASp, the difference of 1.2 kDa to the theoretical mass of PASc (12.9 kDa) can be explained by taking into account deviations from ideal spheres in the overall PASc structure. In contrast to PASp, the N-terminal region of PASc appears to be affected by line broadening which likely reflects the dimerisation (see figure 4.6).

The dimeric state is retained in the crystal structure that could be solved for PASc (see figure 3.7 A). This structure corresponds well with the PAS domain (see figure 3.7 B) found in the cytoplasmic assembly of VicK (Wang *et al.*, 2013), the first structure of a histidine kinase with adjacent PAS domain, with a backbone rmsd for one PAS-monomer of 1.63 Å. As the PASc structure is comparable to the VicK cytosolic PAS domain in

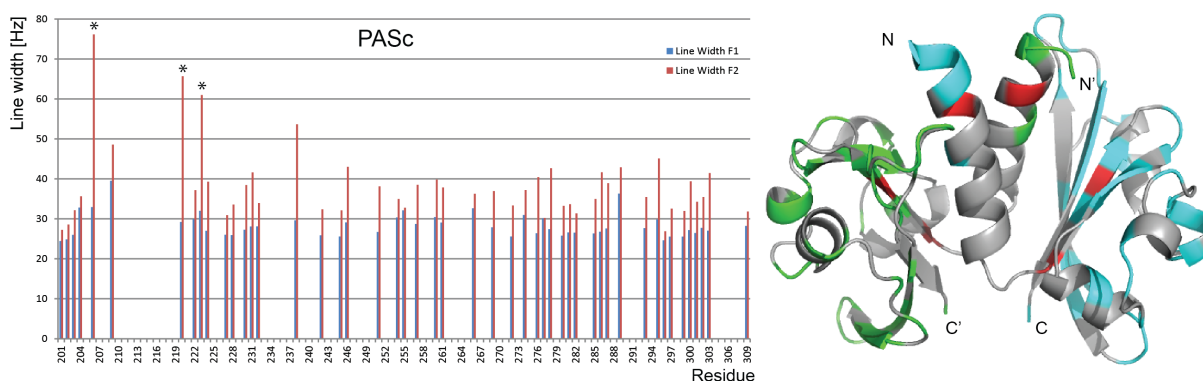


Figure 4.6: PASc linewidth in a ^{15}N -HSQC. Left: A ^{15}N - and ^1H -linewidth (F1 and F2, respectively) plot demonstrates broadened lines at the N -terminus of PASc indicative for a dimerisation propensity. Only isolated peaks in the ^{15}N -HSQC spectrum were analysed. Right: Peaks with increased line widths (marked with asterisks) are plotted on the PASc crystal structure (red). The affected residues are close to the dimerisation interface. Overlapped or unassigned residues are greyed out.

context of the kinase core, the crystal structure of CitA PASc most likely represents a biologically relevant conformation. The liquid-state NMR assignments correspond well with structural features found in the crystal, the only major difference being residues in the second and third β -strand of the crystal structure which display positive secondary shifts in solution. However, these β -strands are twisted in the crystal structure and display unfavourable dihedral angles for extended conformations, thus reflecting unusual shifts for β -strands in solution. Chemical shift prediction based on the crystal structure (Han *et al.*, 2011) did not yield satisfying results for comparison with liquid-state data as deviations of calculated chemical shifts from experimental values was in the range of 1-2 ppm.

As in VicK, the N -terminal helix bundle of *G. thermodenitrificans* CitA PASc is stabilised by a hydrophobic zipper motif (see figure 3.7). The hydrophobic interface between the helices covers 869 \AA^2 , the interface between one helix and the β -scaffold of the second monomer spans 1067 \AA^2 (calculated using Pymol), suggesting a rigid binding of the PASc monomers. It is therefore quite surprising that crystal structures of PASc mutants based on functionally relevant mutants in DcuS (Monzel *et al.*, 2013) yield very different structures (see figure 3.10). Of the proposed OFF-mutants, PASc V285A crystallised like wild-type, while PASc R218A, the second suggested OFF-mutant, forms an asymmetrical dimer like the proposed ON-mutant PASc N288D. On the other hand, the

putative ON-mutant PASC R307A is structurally equivalent to wild-type PASC and the OFF-mutant V285A. In addition, *in vivo* activation studies on full-length *G. thermodenitrificans* CitA constructs with the mutations in PASC carried out by the group of Prof. Uden did not show any effect over wild-type CitA. All tested ON- and OFF-mutants were inactive without citrate and could be triggered by addition of 20 mM citrate like wild-type protein. The expected effects on CitA functionality could not be confirmed for *G. thermodenitrificans* CitA PASC mutants. As there is structurally no consistent discrimination between ON- and OFF-mutants and no mutation effect on the full-length receptor, our results demonstrate that functional mutations in PASC cannot simply be transferred from homologous DcuS PASC.

Also, the biological relevance of mutant crystal structures (see figure 3.10) differing from wild-type PASC is questionable as the orientation of the *N*- and *C*-termini is not compatible with a dimeric full-length receptor where the transmembrane helices should traverse the membrane in parallel orientation (see figure 4.7). The absence of any mutation effect *in vivo* also supports an identical PASC assembly between mutants and wild-type CitA. As a second state of PASC reflecting a second functional state most likely exists, the crystal structures obtained for PASC mutants might still contain information on functional roles. Although a complete reorganisation of the transmembrane helix bundle seems unlikely, helix tilts leading to an anti-parallel assembly of PASC monomers cannot be completely ruled out. Nonetheless, the vastly different orientations of the *N*-terminal helix in the PASC mutant crystal structures suggests that a high degree of structural flexibility around the *N*-terminal helix-pair might be possible. In such a scenario, the hydrophobic interfaces around the *N*-terminal helices could act as a lubricant to enable motions around the dimer core.

4.3 Liposome-embedded CitApc

4.3.1 CitApc in Asolectin

Mutation studies on PASC were inconclusive regarding differences between the ON- and OFF-state as shown in section 4.2. To analyse the role of PASC in CitA activity, solid-

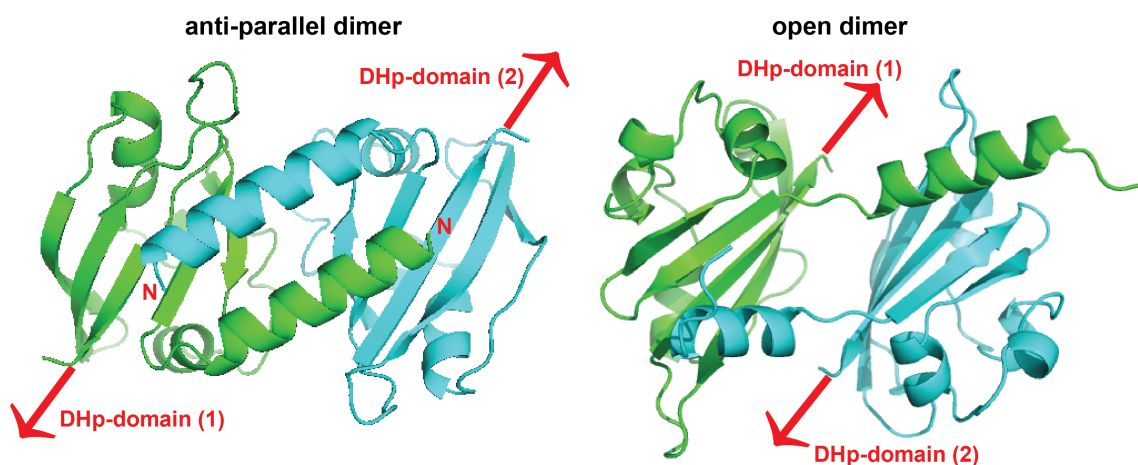


Figure 4.7: Orientation of monomers in PASc mutant crystal structures. For both crystal forms differing from wild-type found in PASc mutants, monomers are shown in green and cyan. The positions of the *C*-termini, which in full-length protein would be followed by the DHp domain, are highlighted in red. As DHp needs to be dimeric in functional receptors, physiological relevance of the crystal structures differing from wild-type is unlikely. In addition, the *N*-termini (N) in the anti-parallel crystal form are on opposite sides of the protein making attachment to the membrane impossible.

state NMR can be employed to characterise the different signalling states in context of the transmembrane helices. Citrate-bound wild-type CitApc reconstituted in asolectin was assigned based on liquid-state resonances for PASp and PASc. This left only a comparably small number of unassigned peaks which in part could be assigned to the two transmembrane helices (see figure 3.15). Since wild-type CitApc was purified in the citrate-bound state, the R93A mutant was introduced in the citrate binding pocket, allowing for study of both signalling states by reducing citrate affinity.

CitApc R93A samples were initially reconstituted in asolectin to compare with wild-type CitApc. In the citrate-free sample of *G. thermodenitrificans* CitApc R93A, peak doubling in PDS spectra was observed for residues around the citrate binding pocket (see figure 3.17 A). The two resonance sets for affected residues corresponded to liquid-state assignments of the citrate-free and citrate-bound state, respectively. In the 3D spectra, only the citrate-bound state was visible. As peaks in 2D spectra are generally less intense for the citrate-free state (see figure 4.8), the signal/noise ratio is probably not sufficient for detection of the citrate-free state in 3D spectra. Subsequently, asolectin was identified

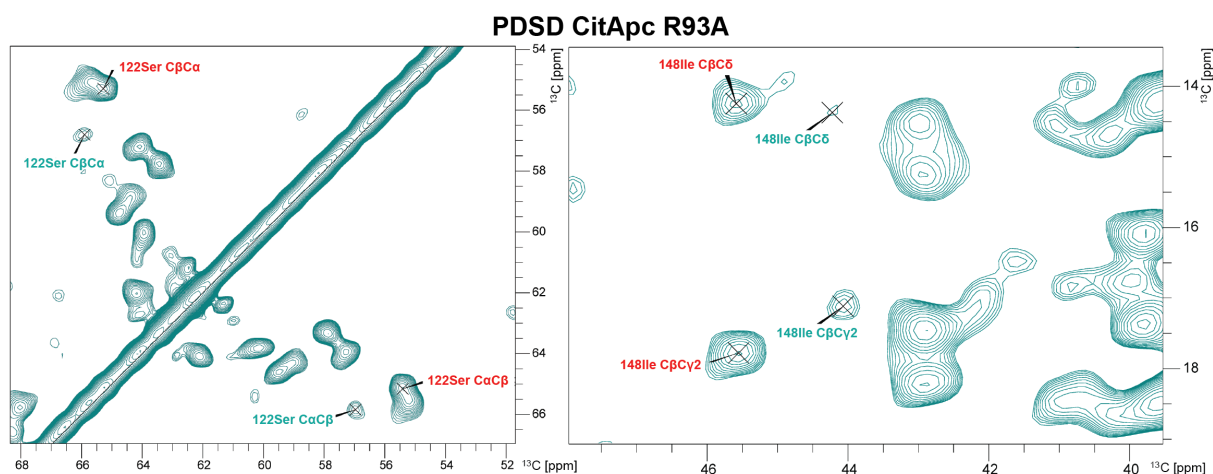


Figure 4.8: Peak doubling of PASp in a PDS-spectrum of citrate-free CitApc R93A. For the citrate-free sample of CitApc R93A in asolectin, peak doubling for several residues around the citrate binding pocket was observed. One set of peaks corresponds to liquid-state assignments of citrate-free PASp R93A while the second signal set reflects citrate-bound PASp R93A. Examples for peak doublings are shown with serine 122 (left) and isoleucine 148 (right). In most cases, peaks corresponding to the citrate-free state (teal) are much weaker than peaks of citrate-bound PASp R93A (red).

as a possible source for citrate impurities in the sample. 1D proton spectra of asolectin in 10 % SDS confirmed the presence of citrate in asolectin used for sample preparation (see figure 3.17 B). To generate a citrate-free state of CitApc R93A, new samples were prepared in 1,2-dimyristoyl-*sn*-glycero-3-phosphocholine (DMPC) instead of asolectin. The peak doubling suggests slow exchange between CitApc R93A and citrate as opposed to the fast exchange observed for isolated PASp R93A. It can be concluded that citrate binding kinetics of PASp are dependent on structural context. Possibly, domain dynamics of PASp are reduced in context of the transmembrane helices, allowing for detection of both receptor states.

4.3.2 CitApc R93A in DMPC

As the phase transition point for DMPC is at 24 °C compared to the melting temperature of asolectin membranes below 0 °C, initial experiments on DMPC-embedded CitApc R93A were carried out at 25 °C. At these high temperatures the N-C-magnetisation transfer was very inefficient, thus later spectra were recorded at temperatures between 6 °C and 10 °C, increasing the magnetisation transfer by 70 % (see figure 3.14). Overall, spectra above

and below the melting point of DMPC are comparable; the isolated domains are readily assignable based on liquid-state data in both cases (see figure 4.9).

As discussed in section 3.3, the percentage of transferable assignments from liquid- to solid-state spectra is higher for PAsp than for PAsc in all cases. This is in part caused by a generally lower signal/noise ratio for PAsc, as can be visualised for isolated $C\alpha$ - $C\beta$ -peaks in 3D-NCACB and NCOACB spectra (see figure 3.18). In total, 25 PAsc residues in citrate-free and 26 PAsc residues in citrate-bound CitApc R93A could be assigned in 3D spectra. The number of unassigned peaks in 3D spectra does not account for the missing assignments based on liquid-state data (see table 4.1), especially if the missing assignments of transmembrane helices, which likely also contribute to unassigned peaks, are taken into account.

Table 4.1: Assignments of PAS domains in CitApc R93A.

citrate-free CitApc R93A				
PAsp	spectrum	residues assigned	residues missing	unassigned peaks*
	PDS	93	35	-
	NCACB	70	58	14
	NCOACB	23	105	14
PAsc	spectrum	residues assigned	residues missing	
	PDS	59	50	
	NCACB	24	85	
	NCOACB	2	108	
citrate-bound CitApc R93A				
PAsp	spectrum	residues assigned	residues missing	unassigned peaks
	PDS	106	22	-
	NCACB	101	27	26
	NCOACB	90	38	8
PAsc	spectrum	residues assigned	residues missing	
	PDS	40	69	
	NCACB	21	88	
	NCOACB	5	104	

* due to spectral crowding, it is impossible to specify a number of

* unassigned peaks for PDS spectra.

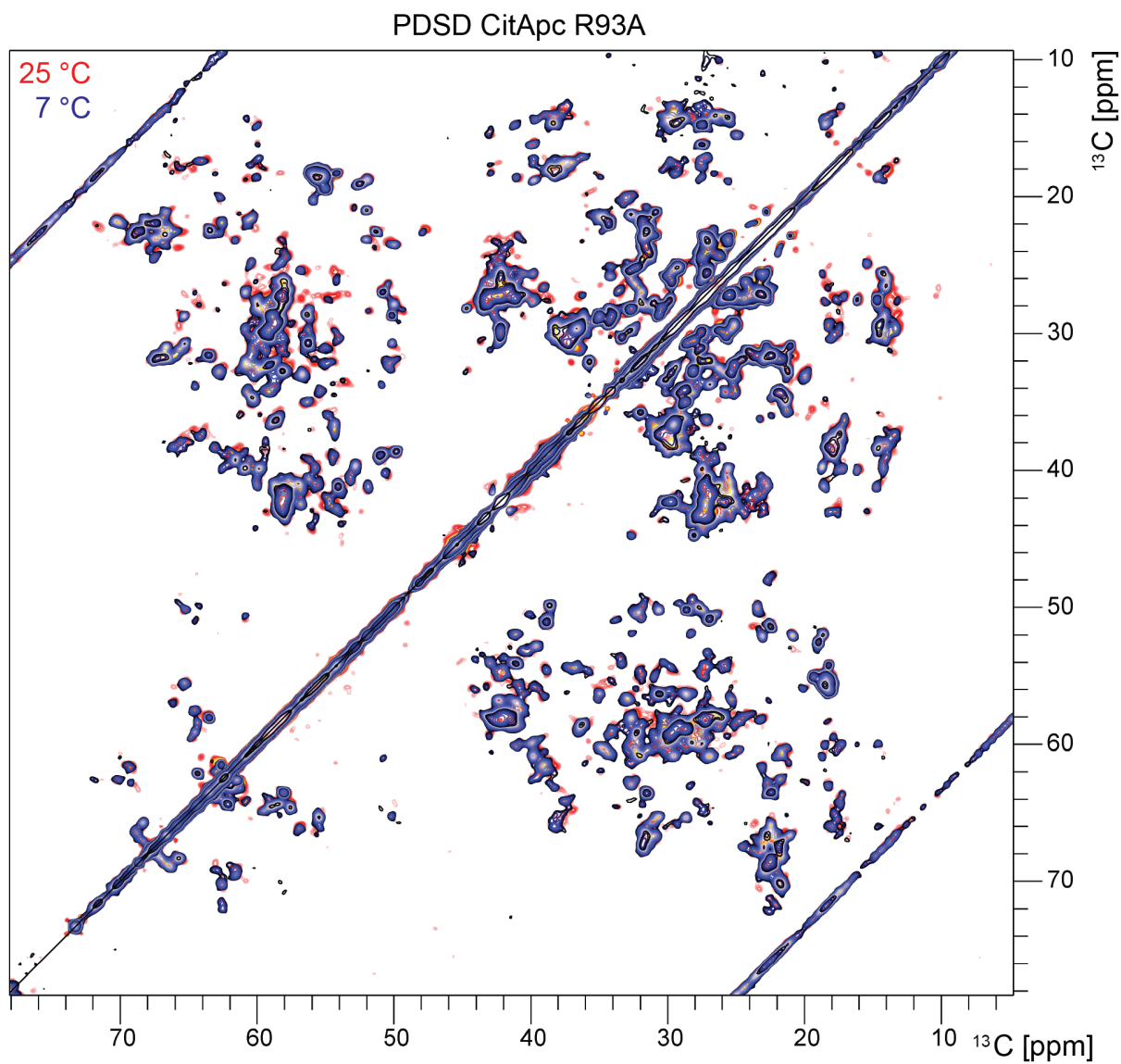


Figure 4.9: Spectra of CitApc R93A at different temperatures. PDS D-spectra of CitApc R93A were recorded above and below the phase transition temperature of DMPC. Proton 1D spectra were used for discrimination between the liquid crystalline and solid phases of DMPC.

It is therefore likely that the discrepancy between liquid-state assignments and solid-state peak positions for certain parts of the PAS domains, most notably PASc (59 % and 45 % assigned in citrate-free and citrate-bound state, respectively), is related to increased mobility of the invisible regions. INEPT spectra of CitApc R93A in both signalling states only contain peaks of lipid headgroups, so rapid exchange of unstructured protein regions can be ruled out. Also, no additional peaks appear in INEPT-spectra of the citrate-bound state. The non-assignable parts of PASp and PASc are therefore likely undergoing dynamic motions on a time scale that is not detectable with the acquired solid-state experiments.

The available assignments of PASp and PASc can be utilised to identify structural rearrangements in the two signalling states. Structural differences can be easily tracked in PASp by analysing C α -C β -secondary chemical shift changes upon citrate binding to CitApc R93A (see figure 4.10). The secondary structure reorganisation observed in liquid state (see section 4.1.1) can be reproduced in membrane-embedded solid state samples. It can thus be assumed that the changes observed for the individual PASp domain are comparable to the structural switching in context of the transmembrane helices.

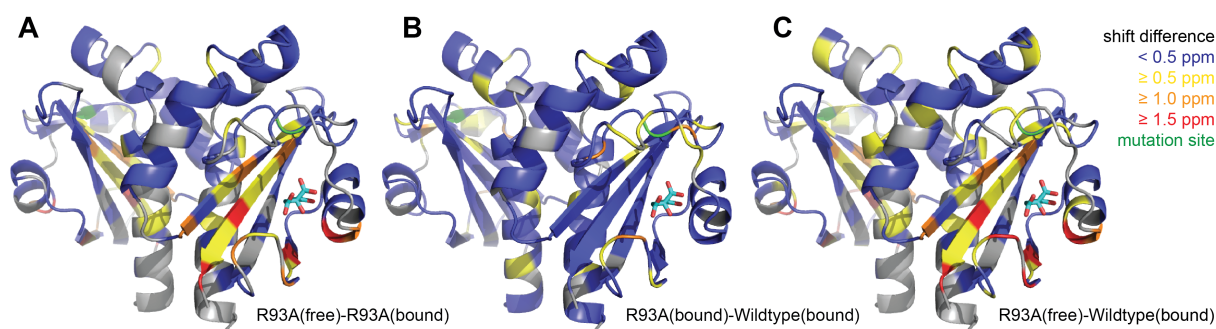


Figure 4.10: $C\alpha$ - $C\beta$ -secondary chemical shift differences of PASp in membrane-embedded CitApc between the ON- and OFF-state. A: Differences between citrate-free and citrate-bound PASp R93A. Like in the isolated domains, the whole binding pocket undergoes structural reorganisation. Citrate is shown as cyan sticks for citrate-bound PASp. B: Comparison of citrate-bound PASp R93A and citrate-bound wild-type PASp. The citrate binding pocket is structurally conserved, indicating the same conformation of both citrate-bound states. Differences are seen around the mutation site R93A highlighted in green. C: Comparison of citrate-free PASp R93A and citrate-bound wild-type PASp reproduces differences observed between the ON- and OFF-states of PASp R93A.

Of note is the secondary chemical shift change of leucine 154 at the end of the C -terminal β -strand in PASp, which switches from extended conformation in citrate-free CitApc R93A to helical in citrate-bound samples of both CitApc wild-type and R93A (see figure 4.11). As solid-state assignments of residues succeeding leucine 154 are missing, other potential structural changes at the PASp - transmembrane helix interface remain to be elucidated. It can be concluded that the C -terminal β -strand is shortened by one amino acid upon citrate binding. This finding is in agreement with observations in crystal structures of citrate-free and citrate-bound CitA PASp in *K. pneumoniae* (Sevvana *et al.*, 2008). Just like in *G. thermodenitrificans* CitA PASp, the C -terminal β -strand is one amino acid shorter in the citrate-bound state due to the contraction of the domain upon citrate binding (Sevvana *et al.*, 2008).

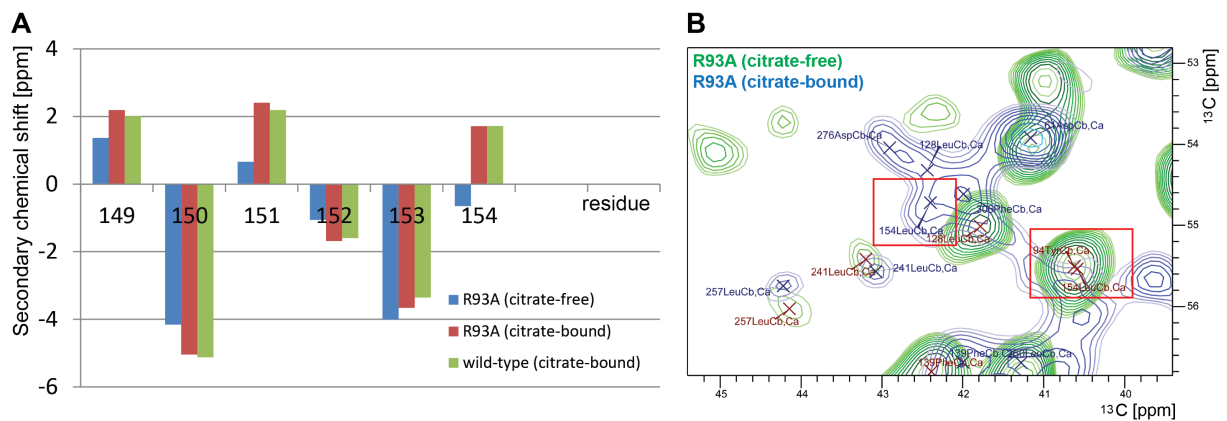


Figure 4.11: Spectral differences between the two signalling states at the PASp-TM2-interface. A: $C\alpha$ - $C\beta$ -secondary chemical shifts indicate a secondary structure alteration at leucine 154, which switches between extended conformation in citrate-free CitApc R93A and helical conformation in citrate-bound CitApc R93A. In citrate-bound wild-type CitApc, L154 is also found in helical conformation. Upon citrate binding, the C -terminal β -strand of PASp is thus shortened by one amino acid. B: Section of PDSN spectra of CitApc R93A in both citrate-free (blue) and citrate-bound (green) states. The $C\alpha$ - $C\beta$ -crosspeak of leucine 154 is shifted upon citrate binding. Residues succeeding leucine 154 are not assigned in solid-state spectra.

Transmembrane signalling is conceivable with four principle mechanistic models: translation, piston-type displacement, pivot movement parallel to the membrane or rotation perpendicular to the membrane (Hulko *et al.*, 2006; Matthews *et al.*, 2006). Although other mechanisms cannot easily be excluded, the shortening of the C -terminal β -strand in CitA is consistent with a piston-model for transmembrane signalling (Ottemann *et al.*, 1999). In this model, the second transmembrane helix is pulled out of the membrane upon signal recognition. This piston-like movement could be triggered by the contraction of PASp in CitA coupled with a shortening of the C -terminal β -strand (see figure 4.12) exerting a pull on the second transmembrane helix. In addition to the piston movement, a slight helix tilt or rotation could also contribute to net helix motion.

4.3.3 Citrate affinity of PASp

The tight binding of wild-type *G. thermodenitrificans* PASp to citrate is striking, as a sensor that cannot be switched off through releasing its ligand does not allow for regulation based on citrate availability. One reason for the tight ligand binding could be that both

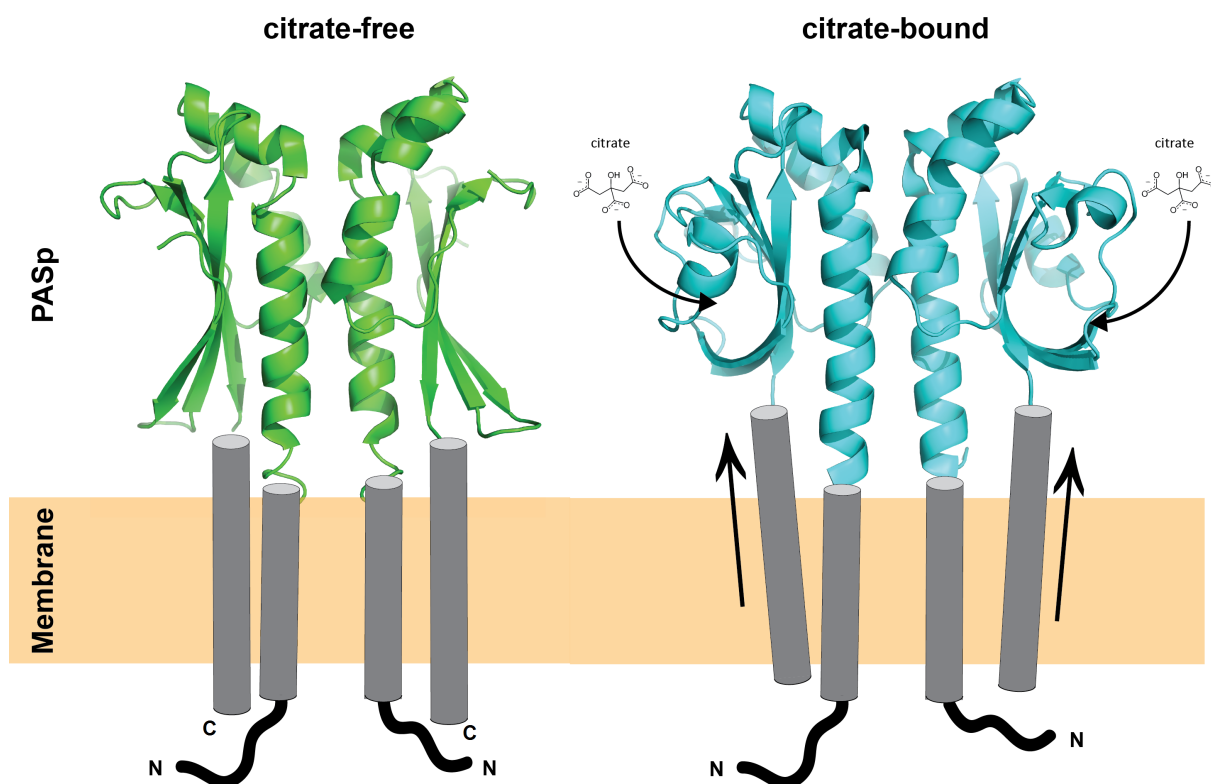


Figure 4.12: Piston-model for transmembrane signalling. Based on the crystal structures of *Klebsiella pneumoniae* CitA PASp, a signal transduction model has been proposed in which a citrate-binding induced pull on the terminal β -strand in PASp triggers a piston movement of the second transmembrane helix. PDB-accession codes for citrate-free and citrate-bound PASp (Sevvana *et al.*, 2008): 2V9A and 2J8O.

copies of PASp in the full-length receptor dimer need to bind citrate for signalling to occur, which would be facilitated by the low off-rate of binding. It has been suggested that a symmetry/asymmetry switch in the signal receiving domains could play a role in signal transduction (Neiditch *et al.*, 2006; Moore and Hendrickson, 2012). However, this seems not to be the case in *G. thermodenitrificans* CitA as solid-state spectra reveal changes on the cytosolic part of CitApc R93A upon citrate addition and only one set of resonances for a CitA monomer is visible. It can therefore be assumed that citrate is bound to both PASp domains in the dimer. As no asymmetric species can be observed, activation of CitA through symmetric citrate binding seems plausible.

The release of citrate from PASp *in vivo* might be possible at the higher temperatures of *G. thermodenitrificans* habitats, reported at an optimum of 60-65 °C (Feng *et al.*, 2007; Cihan *et al.*, 2011). However, the tight ligand binding observed in *G. thermodenitrificans*

CitA (see section 3.1) was observed for the mesophile *E. coli* CitA PASp as well. It is therefore likely that citrate is released from PASp by a mechanism yet to be understood. One potential mechanism of citrate release is by binding of a co-receptor of the TctC-family. Tct is a tripartite tricarboxylate transporter, with TctC being a periplasmic tricarboxylate receptor (Ashton *et al.*, 1980). Tct proteins are found in almost all bacteria, but the absence of TctA, TctB or TctC in several organisms led to the assumption that the individual components might have other roles than just tricarboxylate transport. In some instances, TctC is the only Tct component present in a genome. For *Bacillus subtilis* it has been postulated that this lone copy of TctC could interact with a HK with effects on switching of the sensor (Winnen *et al.*, 2003) analogous to *vir*-operon activation in *Agrobacterium tumefaciens* (Cangelosi *et al.*, 1990). As TctC homologues can be found in both *G. thermodenitrificans* and *E. coli* it is possible that it plays a role in signal recognition and deactivation of CitA PASp.

4.3.4 Signalling effects in the cytosolic PAS domain

For CitA PASp, analysing differences between the ON- and OFF-state of the receptor is straightforward due to the availability of both signalling states through addition of citrate to PASp R93A. For PASc however, it is impossible to predict which signalling state the crystal structure and the liquid-state NMR assignments correspond to. Therefore, tracking differences in the solid-state spectra for the first time opens up the possibility to study effects of citrate binding on the cytosolic PAS-domain. Parts of PASc are visible in all three samples, but sequential assignment is impossible due to the scarcity of PASc-peaks in 3D spectra. This lack of coverage could be caused by generally higher domain dynamics of PASc compared to PASp. While PASp is anchored to the transmembrane helix bundle both at the *N*- and *C*-terminus, PASc is only linked to the central helical scaffold by the *N*-terminal helices, potentially allowing for increased mobility around the central coiled coil formed by the transmembrane helices. However, it is striking that large portions of PASc are not visible upon citrate binding in CitApc R93A while appearing in spectra of citrate-free CitApc R93A (see figure 4.13 and tables 4.1 and 8.9).

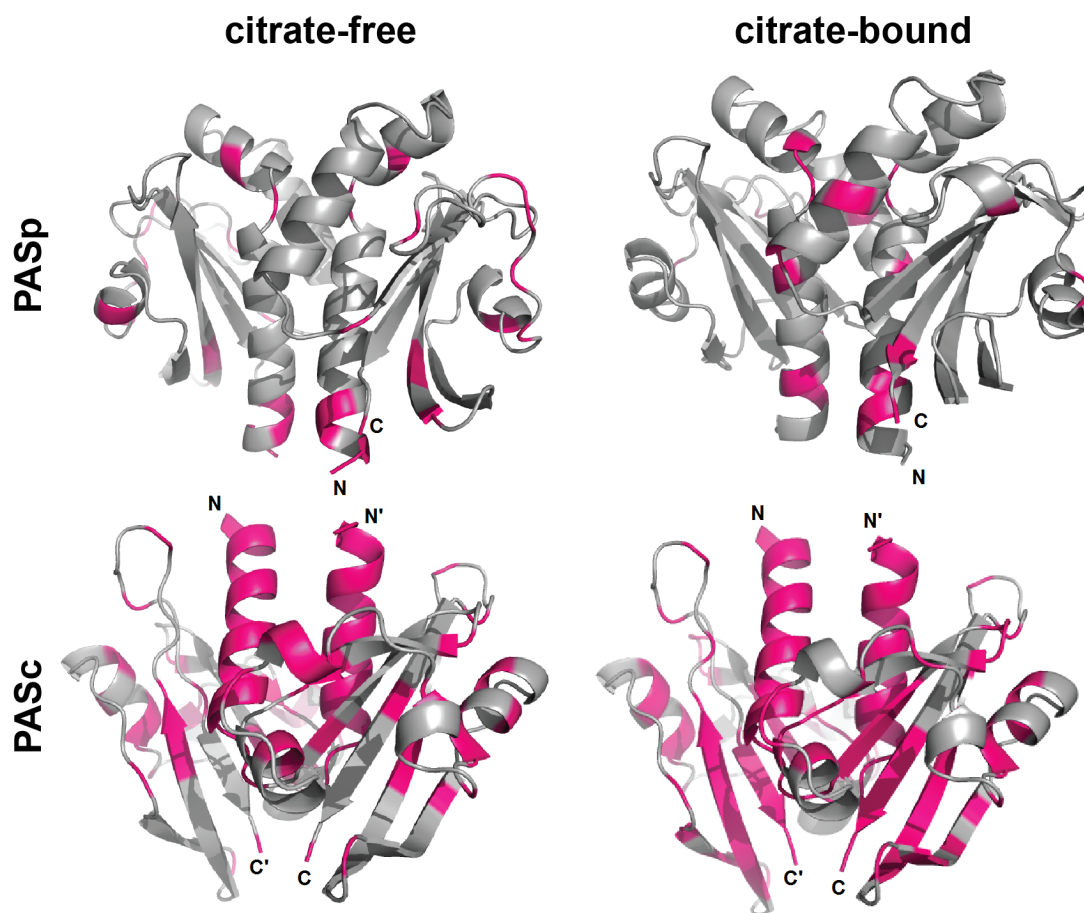


Figure 4.13: Visibility of PASp and PASc in solid-state spectra of CitApc R93A. In citrate-free PASp, almost the whole domain can be assigned in solid-state spectra. Unassigned residues are mostly found in a loop closing the citrate binding pocket and in one of the β -strands facing the C -terminus (unassigned residues highlighted in pink). In citrate-bound PASp, this loop and the whole β -scaffold can be assigned. While the N -terminal helix of PASc could not be assigned for both signalling states, large parts of the β -sheet core of PASc including the C -terminus are only visible in the citrate-free state and disappear in the citrate-bound state (unassigned residues highlighted in pink).

As additional peaks in 3D spectra that could be assigned to shifted PASc residues do not appear and INEPT spectra are also devoid of protein peaks, it is very likely that the decrease in PASc visibility upon citrate binding corresponds to increased flexibility in the citrate-bound state. The increased dynamics of the C -terminus in PASc could result in triggering the HK in full-length CitA. This assumption is backed by functional studies on the HK ArcB, where formation of disulfide bridges and therefore reduction of flexibility between two PAS-monomers preceding the DHp domain switches off the kinase

activity (Malpica *et al.*, 2004). In addition, increased PASC flexibility was proposed as the activity switch for *E. coli* DcuS (Etzkorn *et al.*, 2008). Functional mutants in DcuS PASC (Monzel *et al.*, 2013) were employed to generate a constitutively active functional state of DcuSpc constructs (analogous to CitApc and consisting of both PAS domains and the transmembrane helices without the kinase core). Solid-state NMR spectra of precipitated DcuS PASC and kinase-competent DcuSpc in liposomes suggest disorder at the PASC dimer interface in the active receptor state. Based on dimeric crystal structures of homologous PAS domains, it was therefore postulated that PASC in inactive DcuS is more ordered and that the active state is characterised by increased flexibility. The similar effects observed for *G. thermodenitrificans* CitApc further support the role of PASC plasticity in signalling.

The proposition that changes in protein mobility at the interface of PASC and DHP could be the key for activating the kinase is in line with observations on crystal structures of the kinase core. In HK853, a HK of unknown function, the *N*-termini of the α 1-helices in the DHP domains are unstructured in the active state of the kinase, while being in helical conformation in the inactive state (Marina *et al.*, 2005; Casino *et al.*, 2010). The same is true for the temperature sensor DesKC, where the crystal structure of the kinase-competent state DesKC $_{\Delta 174}$ has a shortened *N*-terminal helix compared to DesKC $_{H188V}$, the phosphatase-competent state (Albanesi *et al.*, 2009). This suggests that the *N*-terminal region of the helix bundle in DHP is intrinsically strained and activation of the kinase could either be triggered by the cogwheel rotation of a HAMP domain, a signal transducing domain found *C*-terminal of transmembrane helices in many HKs, as suggested by (Casino *et al.*, 2010), or by reducing structural constraints like in PASC of CitA as shown here.

4.3.5 PASC in context of full-length CitA

The dimeric assembly of the *G. thermodenitrificans* CitA PASC crystal structure is easily superimposed with the structure solved for VicK, suggesting a similar mode of structural assembly for the two HKs (see figure 4.14 A and B). The backbone rmsd between individual PAS domains of 1.63 Å can be reduced to 1.44 Å by omitting the *N*-

terminal helix which is rotated by 14 degrees between the two crystal structures. The low coordinate deviation of the PAS core suggests that cytosolic PAS domains are structurally highly conserved between CitA and VicK. The sequence identity of 30 % is comparable to the values found for periplasmic, citrate binding PAS domains.

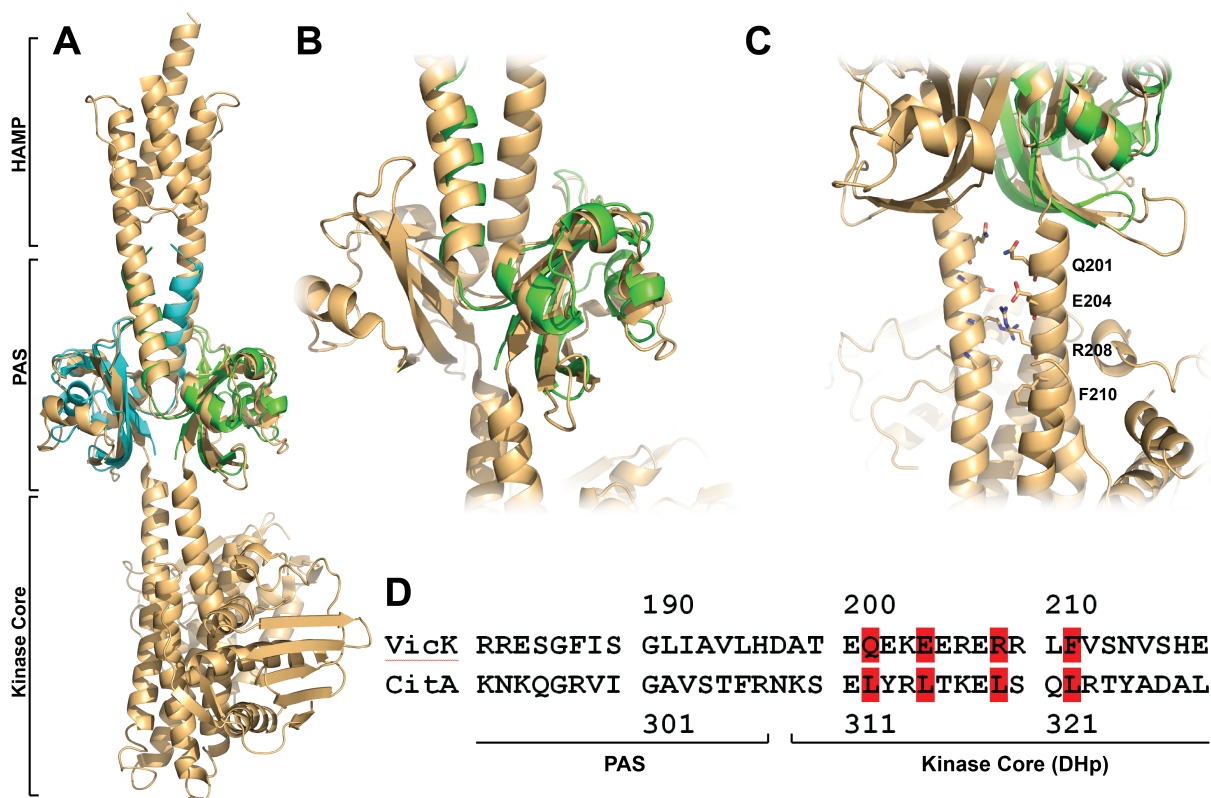


Figure 4.14: Comparison of VicK and CitA PASc crystal structures. A: The crystal structure of CitA PASc (green and cyan monomers) is easily superimposed with the structure of VicK (light orange, PDB accession code: 4I5S), a cytosolic HK containing HAMP and PAS domains preceding the kinase core. B: Close-up of one CitA PASc monomer aligned to VicK PAS with a backbone rmsd of 1.44 Å for the PAS core. C: The *N*-terminal helix bundle interface of VicK DHp is characterised by a cluster of charged residues. D: a Dialign (Morgenstern, 2004) alignment of VicK and CitA reveals a leucine zipper at the CitA DHp interface in contrast to the charged interface in VicK DHp.

The different position of the *N*-terminal helix in CitA PASc is possibly caused by the lack of context. As *N*-terminal helices of the PAS-domain in VicK are extended to form a four-helix bundle, it can be assumed that a similar orientation is found in *G. thermodenitrificans* CitA PASc if the four-helix bundle of the transmembrane helices is taken into consideration. The predicted second transmembrane helix of *G. thermodenitrificans*

CitA (residues 169-188) is followed by 26 residues in helical conformation, including the *N*-terminal helix of the PASC crystal structure. In VicK, 22 residues are needed to bridge the gap between the HAMP four-helix bundle and the PAS core. Therefore, a similar protein architecture in CitA is conceivable.

Differences between VicK and CitA can be found at the *C*-terminus of the PAS-domain leading into the DHp-domain. In VicK, the *N*-terminus of DHp is highly charged, leading to stabilising salt bridges between E205 and R208 of different monomers (see figure 4.14 C), whereas the CitA sequence reveals a leucine zipper motif at the *N*-terminus of DHp (see figure 4.14 D). Consequently, the rigidity of the two different DHp domains might be fine-tuned to the different functional roles. In VicK, the PAS domain is believed to receive stimuli, whereas in CitA, the stimulus is received in the periplasm and transferred to the kinase *via* PASC.

4.3.6 Signal transduction model

One major question that still remains unanswered is concerning the role of the transmembrane helices during signalling. The combined data collected on *K. pneumoniae* CitA and *G. thermodenitrificans* CitA suggest a piston model, in which the contraction of the β -scaffold of PASp upon citrate binding leads to a shortening of the *C*-terminal β -strand and as a consequence a pull on the second transmembrane helix. For a piston movement to occur, different residues around the second transmembrane helix will come in contact with the membrane. Therefore, two different positions of the second transmembrane helix have to be accessible: in the citrate-bound state, residues inside the membrane would have to be displaced towards the *C*-terminus when compared with the citrate-free state due to the pull on the *N*-terminus of the helix (see figure 4.15).

Transmembrane helix prediction software (Hofmann and Stoffel, 1993; Cserzo *et al.*, 1997; Sonnhammer *et al.*, 1998; Tusnády and Simon, 2001) gives accurate positions for helix one (residues 7-26) and helix two (residues 169-188). Interestingly, six residues before the predicted *N*-terminus of the second transmembrane helix a tryptophane residue (W163) is situated. A similar arrangement is found in *E. coli* CitA, where a tryptophane is positioned four residues *N*-terminal of the second transmembrane helix and a second

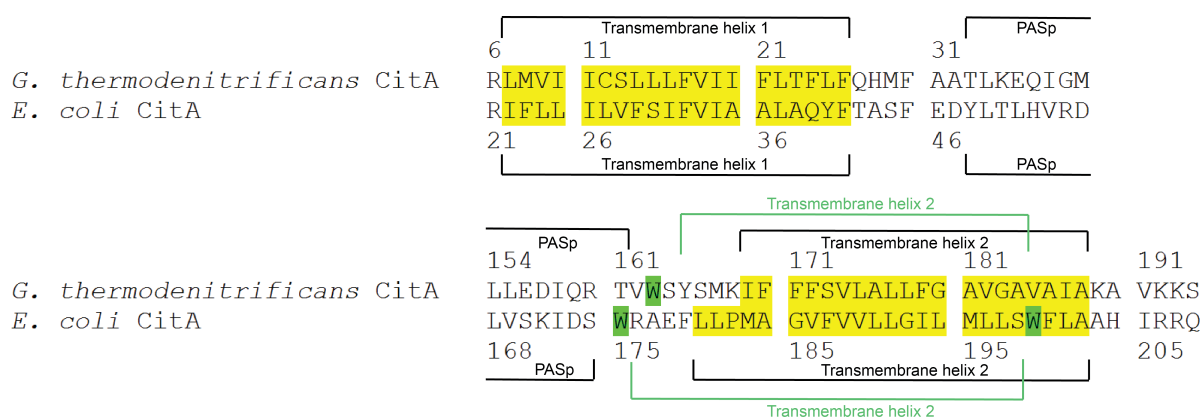


Figure 4.15: Transmembrane helices in CitA. In an alignment of *Geobacillus thermodenitrificans* CitA with *Escherichia coli* CitA, the position of transmembrane segments can be predicted (yellow). Both in *G. thermodenitrificans* CitA and *E. coli* CitA, tryptophane residues (green) are positioned in proximity of transmembrane regions. If the predicted position of the second transmembrane helix is assumed to correspond to the citrate-bound state, a second position of the helix closer to the *N*-terminus (green brackets) would bring the tryptophane residues close to the membrane interfaces and could reflect the citrate-free state.

tryptophane four residues before the predicted *C*-terminus of the transmembrane helix (see figure 4.15). As tryptophane residues are often found at transmembrane helix surfaces and the databases for transmembrane helix prediction are based on static helices, one could speculate that the predicted position of the second transmembrane helix corresponds to the citrate-bound state and a second position of the helix with the tryptophane closer to the lipid interface reflects the citrate-free state (see figure 4.16). According to the piston model, the position of the *N*-terminus of the second transmembrane helix would be closer to the membrane surface in the citrate-free state. The position of tryptophane 163 in CitA suggests that a second orientation of the *C*-terminal transmembrane helix and thus a piston movement pulling the *N*-terminal residues out of the membrane is possible. In addition to a piston movement, helix rotation is conceivable and cannot be excluded.

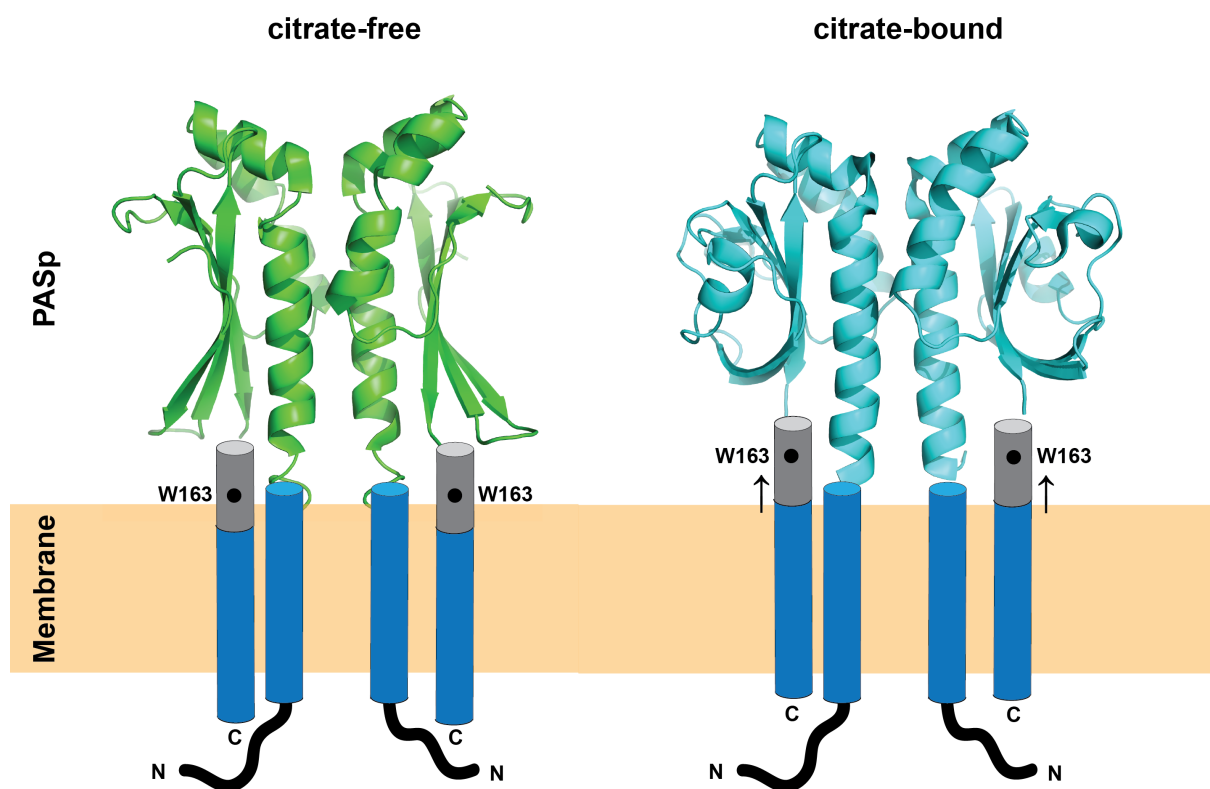


Figure 4.16: Transmembrane helix piston model. Transmembrane section predictions yield well defined regions for both the first and the second transmembrane helix (blue). A hypothetical helix displacement according to the piston model would bring tryptophane 163, predicted to be six residues away from the second transmembrane helix, closer to the membrane interface and could represent a citrate-free state. The citrate-bound state would in this case be reflected by the predicted position for the second transmembrane helix, with the pull originating in citrate-bound PASp dragging tryptophane 163 towards the periplasm. *Klebsiella pneumoniae* CitA PASp structures were utilised to display both signalling states.

4.4 Outlook

In this work, the shortening of the *C*-terminal β -strand found in *K. pneumoniae* CitA PASp could be confirmed in context of the transmembrane helices. Unfortunately, the scarcity of NMR data on the transmembrane regions does not allow for a detailed analysis of helix reorientations during the signalling process. To overcome this blind spot, a variety of approaches could be used. First, the solid-state assignment is at the moment limited by signal/noise ratio for the transmembrane sections. The most complete assignment was obtained for wild-type CitApc in asolectin; CitApc R93A constructs in DMPC yielded

less peaks that could be related to the transmembrane helices. Therefore, the membrane environment could be a limiting factor to spectral quality. Since it is not guaranteed that a lipid composition resembling native *G. thermodenitrificans* membranes will produce optimal spectra at the low temperatures needed for solid-state NMR experiments, a variety of different lipid environments for CitApc could be tested and optimised.

Second, assignment of the transmembrane helices could be facilitated by using selective labelling approaches to simplify spectra so that distance information could be obtained from 2D experiments. For example, alanine forward labelling (LeMaster and Cronan, 1982; LeMaster and Richards, 1982) could be used to obtain distance information based on known alanine residues in the transmembrane helices. Furthermore, leucine forward labelling could reveal and identify leucine pairs and triplets found in the transmembrane helices. Leucine labelling could also be utilised to obtain information on the leucine 154 - leucine 155 residue pair at the second transmembrane helix interface.

Third, the use of proton-detected solid-state NMR experiments might result in new assignment possibilities for the transmembrane helices. Finally, solid-state assignments of transmembrane helix residues could be employed to obtain distance restraints to correlate helix contacts with potential signalling models.

With scanning cysteine accessibility mutagenesis (SCAM) (Zhu and Casey, 2007), an alternative strategy could be employed to test the piston-movement hypothesis of transmembrane signalling. With SCAM, the solvent accessibility of residues around the membrane interfaces can be determined. Assuming a piston model, different residues of the second transmembrane helix would be expected to be buried in the membrane and could be identified.

Another point that needs to be clarified is the fate of PASC in the citrate-bound state. As the liquid-state NMR data on wild-type PASC best match the citrate-free CitApc R93A, it likely represents the OFF-state. To achieve a more favourable state of PASC for NMR studies, low-temperature experiments could be carried out to reduce domain dynamics. Alternatively, electron paramagnetic resonance (EPR) spectroscopy (Perozo *et al.*, 1999) could be employed to determine distances between selected residues of PASC from different monomers in the citrate-free and citrate-bound state. If residues at the

C-terminus of PASc are selected, the inter-domain distance could be probed for increased flexibility in the citrate-bound state. These experiments could also be carried out in full-length CitA and thus in context of the DHp domain. The dimer assembly of PASc mutants differing from the wild-type crystal structure should be further investigated. Although *in vivo* data suggest wild-type like assemblies of PASc for all point mutants, the dimerisation propensity of isolated PASc mutants suggests that the anti-parallel orientation of monomers might also exist in solution. This could be tested with liquid-state NMR spectroscopy by identifying inter-monomer NOE contacts. Anti-parallel orientations would also easily be identifiable with EPR-spectroscopy.

In addition to optimising solid-state NMR sample conditions, the structure of CitA PASp R93A still needs to be solved. Although the model based on homologous domains is close to experimental structures for the citrate-bound state, the model of the citrate-free state does not represent the experimental results demonstrating an extended last β -strand in comparison with citrate-bound PASp. As NMR assignments are available, it should be possible to obtain structures based on NOEs and RDCs. These structures will very likely reproduce previous findings on *K. pneumoniae* CitA PASp and might even deepen the understanding on transitions in the PASp-transmembrane helix 2-interface. As citrate binding kinetics seem to be affected by structural context, a ligand titration of CitApc R93A might be employed to determine the dissociation constant for PASp R93A in its native state for comparison with the results obtained on the isolated domain.

Ideally, structural information should be gathered on full-length CitA reconstituted in liposomes, as the lack of context at the *C*-terminus of PASc might still affect functional states in CitApc studied so far. Solid-state NMR of full-length CitA will most likely be challenging because of the increased protein size leading to crowded spectra. However, due to the flexibility observed in crystal structures of the kinase core, CA-domains will likely not be observable, thus adding only the DHp domain to be assigned in addition to the PAS domains and transmembrane helices. To facilitate assignment, further liquid-state constructs of DHp or the kinase core could be produced for transfer of liquid-state assignments to solid-state spectra. In addition to the R93A mutant in PASp, different PASc mutants yielding anti-parallel crystal structures could also be studied in context

of full-length CitA to identify potential different orientations. By characterising full-length CitA R93A in both signalling states, it might be possible to formulate a final, consistent model for the function of each individual domain and their interactions in CitA transmembrane signalling.

5 Abstract

Bacteria utilise two component systems (TCS) consisting of a homodimeric receptor histidine kinase (HK) and a response regulator (RR) as a prevalent mechanism of stimulus perception and signal transduction. TCSs are key players in the regulation of metabolism, motility and development, and in addition are crucial for virulence in a number of pathogenic species. The study of TCSs is therefore motivated by their importance as a fundamental and widely used signalling system.

In this study, the *Geobacillus thermodenitrificans* Citrate receptor A (CitA) is used as a model system for HKs. Free citrate is recognised by a periplasmic PAS (Per-Arnt-Sim) domain (PASp) and the input signal is then relayed to a second, cytosolic PAS domain (PASc) before leading to auto-phosphorylation in the conserved kinase core. Even though the phosphate transfer mechanism of the kinase has been described in depth, signal transduction across the membrane remains poorly understood. The aim of this PhD project therefore is to elucidate the signalling mechanism of CitA by means of combining liquid- and solid-state-NMR spectroscopy with X-ray crystallography.

Our results show a shortening of the *C*-terminal β -strand of CitA PASp by one residue upon citrate binding, potentially exerting a pull on the second transmembrane helix. The restructuring of the *C*-terminus of PASp is in agreement with previously published results on an isolated citrate-binding PAS domain and a piston model for transmembrane helix motion. Additionally, liposome-embedded CitA constructs for the first time allow monitoring changes in the cytosol upon periplasmic citrate binding. In the citrate-bound state, PASc mobility increases, suggesting a constraining role of PASc keeping the kinase domain in an inactive conformation until CitA is triggered.

Bibliography

- C. Aaij and P. Borst. The gel electrophoresis of DNA. *Biochim. Biophys. Acta*, **1972**. 10(269(2)); 192–200.
- A. E. Abo-Amer, J. Munn, K. Jackson, M. Aktas, P. Golby, D. J. Kelly and S. C. Andrews. DNA interaction and phosphotransfer of the C4-dicarboxylate-responsive DcuS-DcuR two-component regulatory system from *Escherichia coli*. *J. Bacteriol.*, **2003**. 186(6); 1879–1889.
- A. Adiguzel, H. Ozkan, O. Baris, K. Inan, M. Gulluce and F. Sahin. Identification and characterization of thermophilic bacteria isolated from hot springs in Turkey. *J. Microbiol. Methods*, **2009**. 79; 321–328.
- D. Albanesi, M. Martín, F. Trajtenberg, M. C. Mansilla, A. Haouz, P. M. Alzari, D. de Mendoza and A. Buschiazzo. Structural plasticity and catalysis regulation of a thermosensor histidine kinase. *Proc. Natl. Acad. Sci. U. S. A.*, **2009**. 106(38); 16185–16190.
- S. F. Altschul, W. Gish, W. Miller, E. W. Myers and D. J. Lipman. Basic local alignment search tool. *J. Mol. Biol.*, **1990**. 215; 403–410.
- A. Ambroz. *Denitrobacterium thermophilus* spec. nov. Ein Beitrag zur Biologie der thermophilen Bakterien. *Zbl. Bakt. Parasit.*, **1913**. 2; 3–16.
- P. Andrews. Estimation of the molecular weights of proteins by Sephadex gel-filtration. *Biochem. J.*, **1964**. 91; 222–233.

O. Ashenberg, A. E. Keating and M. T. Laub. Helix bundle loops determine whether histidine kinases autophosphorylate in cis or in trans. *J. Mol. Biol.*, **2013**. 425; 1198–1209.

D. M. Ashton, G. D. Sweet, J. M. Somers and W. W. Kay. Citrate transport in salmonella typhimurium: Studies with 2-fluoro-L-erythrocytrate as a substrate. *Can. J. Biochem.*, **1980**. 58; 797–803.

D. Auguin, P. Barthe, C. Royer, M.-H. Stern, M. Noguchi, S. T. Arold and C. Roume-stand. Structural basis for the co-activation of protein kinase B by T-cell Leukemia-1 (TCL1) family proto-oncoproteins. *J. Biol. Chem.*, **2004**. 279(34); 35890–35902.

A. Bax, M. Clore and A. M. Gronenborn. 1H-1H correlation via isotropic mixing of 13C magnetization, a new three-dimensional approach for assigning 1H and 13C spectra of 13C-enriched proteins. *J. Magn. Reson.*, **1990**. 88(2); 425–431.

K. A. Borkovich and M. I. Simon. Coupling of receptor function to phosphate-transfer reactions in bacterial chemotaxis. *Methods Enzymol.*, **1991**. 200; 205–214.

M. Bott, M. Meyer and P. Dimroth. Regulation of anaerobic citrate metabolism in *Klebsiella pneumoniae*. *Mol. Microbiol.*, **1995**. 18(3); 533–546.

P. D. Boyer, M. DeLuca, K. E. Ebner, D. E. Hultquist and J. B. Peter. Identification of phosphohistidine in digests from a probable intermediate of oxidative phosphorylation. *J. Biol. Chem.*, **1962**. 237; 3306.

D. Bray. Protein molecules as computational elements in living cells. *Nature*, **1995**. 376(6538); 307–312.

A. T. Brünger. Free R value: a novel statistical quantity for assessing the accuracy of crystal structures. *Nature*, **1992**. 355; 472–475.

G. A. Cangelosi, R. G. Ankenbauer and E. W. Nester. Sugars induce the *Agrobacterium* virulence genes through a periplasmic binding protein and a transmembrane signal protein. *Proc. Natl. Acad. Sci. U. S. A.*, **1990**. 87; 6708–6712.

- P. Casino, L. Miguel-Romero and A. Marina. Visualizing autophosphorylation in histidine kinases. *Nature Communications*, **2014**. 5; 1–12.
- P. Casino, V. Rubio and A. Marina. Structural insight into partner specificity and phosphoryl transfer in two-component signal transduction. *Cell*, **2009**. 139; 325–336.
- P. Casino, V. Rubio and A. Marina. The mechanism of signal transduction by two-component systems. *Curr. Opin. Struct. Biol.*, **2010**. 20; 763–771.
- M. Chamkha, S. Mnif and S. Sayadi. Isolation of a thermophilic and halophilic tyrosol-degrading *Geobacillus* from a Tunisian high-temperature oilfield. *FEMS Microbiol. Lett.*, **2008**. 283; 23–29.
- J. Cheung, C. A. Bingman, M. Reyngold, W. A. Hendrickson and C. D. Waldburger. Crystal structure of a functional dimer of the PhoQ sensor domain. *J. Biol. Chem.*, **2008**. 283(20); 13762–13770.
- J. Cheung and W. A. Hendrickson. Crystal structures of C4-dicarboxylate ligand complexes with sensor domains of histidine kinases DcuS and DctB. *J. Biol. Chem.*, **2008**. 283(44); 30256–30265.
- V. Chevelkov, K. Giller, S. Becker and A. Lange. Efficient CO-CA transfer in highly deuterated proteins by band-selective homonuclear cross-polarization. *J. Magn. Reson.*, **2013a**. 230; 205–211.
- V. Chevelkov, C. Shi, H. K. Fasshuber, S. Becker and A. Lange. Efficient band-selective homonuclear CO-CA cross-polarization in protonated proteins. *J. Biomol. NMR*, **2013b**. 56; 303–311.
- U. S. Cho, M. W. Bader, M. F. Amaya, M. E. Daley, R. E. Klevit, S. I. Miller and W. Xu. Metal bridges between the PhoQ sensor domain and the membrane regulate transmembrane signaling. *J. Mol. Biol.*, **2006**. 356(5); 1193–1206.
- A. C. Cihan, B. Ozcan, N. tekin and C. Cokmus. *Geobacillus thermodenitrificans* subsp. *calidus*, subsp. nov., a thermophilic and α -glucosidase producing bacterium isolated from Kizilcahamam, Turkey. *J. Gen. Appl. Microbiol.*, **2011**. 57; 83–92.

P. J. Cock and D. E. Whitworth. Evolution of prokaryotic two-component system signaling pathways: gene fusions and fissions. *Mol Biol. Evol.*, **2007**. 24; 2355–2357.

N. Coudeville, P. Montaville, A. Leonov, M. Zweckstetter and S. Becker. Structural determinants for Ca²⁺ and phosphatidylinositol 4,5-bisphosphate binding by the C2A domain of Rabphilin-3A. *J. Biol. Chem.*, **2008**. 283(51); 35918–35928.

T. A. Cross and S. J. Opella. Solid-state NMR structural studies of peptides and proteins in membranes. *Curr. Opin. Struct. Biol.*, **1994**. 4; 574–581.

M. Cserzo, E. Wallin, I. Simon, G. von Heijne and A. Elofsson. Prediction of trans-membrane alpha-helices in prokaryotic membrane proteins: the Dense Alignment Surface method. *Protein Eng.*, **1997**. 10(6); 673–676.

F. Delaglio, S. Grzesiek, G. W. Vuister, G. Zhu, J. Pfeifer and A. Bax. NMRPipe: a multidimensional spectral processing system based on UNIX pipes. *J. Biomol. NMR*, **1995**. 6; 277–293.

J.-N. Dumez, M. E. Halse, M. C. Butler and L. Emsley. A first-principles description of proton-driven spin diffusion. *Phys. Chem. Chem. Phys.*, **2011**. 14; 86–89.

R. Dutta and M. Inouye. GHKL, an emergent ATPase/kinase superfamily. *Trends Biochem. Sci.*, **2001**. 25; 24–29.

M. Etzkorn, H. Kneuper, P. Dünwald, V. Vijayan, J. Krämer, C. Griesinger, S. Becker, G. Unden and M. Baldus. Plasticity of the PAS domain and a potential role for signal transduction in the histidine kinase DcuS. *Nat. Struct. Mol. Biol.*, **2008**. 15(10); 1031–1039.

L. Feng, W. Wang, J. Cheng, Y. Ren, G. Zhao, C. Gao, Y. Tang, X. Liu, W. Han, X. Peng, R. Liu and L. Wang. Genome and proteome of long-chain alkane degrading *Geobacillus thermodenitrificans* NG80-2 isolated from a deep-surface oil reservoir. *Proc. Natl. Acad. Sci. U. S. A.*, **2007**. 104(13); 5602–5607.

- H. U. Ferris, S. Dunin-Horkawicz, N. Hornig, M. Hulko, J. Martin, J. E. Schultz, K. Zeth, A. N. Lupas and M. Coles. Mechanism of regulation of receptor histidine kinases. *Structure*, **2012**. 20; 56–66.
- D. P. Frueh. Practical aspects of NMR signal assignment in larger and challenging proteins. *Proc. Nucl. Magn. Reson. Spectrosc.*, **2014**. 78; 47–75.
- C. A. Fyfe, K. C. Wong-Moon, Y. Huang and H. Grondey. INEPT experiments in solid-state NMR. *J. Am. Chem. Soc.*, **1995**. 117(41); 10397–10398.
- R. Gao and A. M. Stock. Biological insights from structures of two-component proteins. *Annu. Rev. Microbiol.*, **2009**. 63; 133–154.
- T. Gerharz, S. Reinelt, S. Kaspar, L. Scapozza and M. Bott. Identification of basic amino acid residues important for citrate binding by the periplasmic receptor domain of the sensor kinase CitA. *Biochemistry*, **2003**. 42; 5917–5924.
- P. Golby, S. Davies, D. J. Kelly, J. R. Guest and S. C. Andrews. Identification and characterization of a two-component sensor-kinase and response-regulator system (DcuS-DcuR) controlling gene expression in response to C4-dicarboxylates in *Escherichia coli*. *J. Bacteriol.*, **1999**. 181(4); 1238–1248.
- W. Gong, B. Hao and M. K. Chan. New mechanistic insights from structural studies of the oxygen-sensing domain of *Bradyrhizobium japonicum* FixL. *Biochemistry*, **2000**. 39(14); 3955–3962.
- M. Goujon, H. McWilliam, W. Li, F. Valentin, S. Squizzato, J. Paern and R. Lopez. A new informatics analysis tools framework at EMBL-EBI (2010). *Nucleic Acids Res.*, **2010**. 38(2); 695–699.
- T. W. Grebe and J. B. Stock. The histidine protein kinase superfamily. *Adv. Microb. Physiol.*, **1999**. 41; 139–227.
- B. Han, Y. Liu, S. Ginzinger and D. Wishart. SHIFTX2: significantly improved protein chemical shift prediction. *J. Biomol. NMR*, **2011**. 50(1); 43–57.

P. I. Hanson and H. Schulman. Neuronal Ca²⁺ / Calmodulin-dependent protein kinases. *Annu. Rev. Biochem.*, **1992**. 61; 559–601.

W. A. Hendrickson, J. R. Horton and D. M. LeMaster. Selenomethionyl proteins produced for analysis by multiwavelength anomalous diffraction (MAD): a vehicle for direct determination of three-dimensional structure. *EMBO J.*, **1990**. 9(5); 1665–1672.

J. F. Hess, R. B. Bourret and M. I. Simon. Histidine phosphorylation and phosphoryl group transfer in bacterial chemotaxis. *Nature*, **1988**. 336; 139–143.

K. Hofmann and W. Stoffel. TMbase - a database of membrane spanning proteins segments. *Biol. Chem.*, **1993**. 374; 166.

W. Hsing, F. D. Russo, K. K. Bernd and T. J. Silhavy. Mutations that alter the kinase and phosphatase activities of the two-component sensor EnvZ. *J. Bacteriol.*, **1998**. 180(17); 4538–4546.

M. Hulko, F. Berndt, M. Gruber, J. U. Linder, V. Truffault, A. Schultz, J. Martin, J. E. Schultz, A. N. Lupas and M. Coles. The HAMP domain structure implies helix rotation in transmembrane signaling. *Cell*, **2006**. 126; 929–940.

M. Ikura, L. E. Kay and A. Bax. A novel approach for sequential assignment of ¹H, ¹³C and ¹⁵N spectra of larger proteins: Heteronuclear triple-resonance three-dimensional NMR spectroscopy. *Biochemistry*, **1990**. 29; 4659–4667.

I. G. Janausch, I. Garcia-Moreno and G. Unden. Function of DcuS from Escherichia coli as a fumarate-stimulated histidine protein kinase in vitro. *J. Biol. Chem.*, **2002**. 277(42); 39809–39814.

S. Kaspar and M. Bott. The sensor kinase CitA (DpiB) of Escherichia coli functions as a high-affinity citrate receptor. *Arch. Microbiol.*, **2002**. 177; 313–321.

S. Kaspar, R. Perozzo, S. Reinelt, M. Meyer, K. Pfister, L. Scapozza and M. Bott. The periplasmic domain of the histidine autokinase CitA functions as a highly specific citrate receptor. *Mol. Microbiol.*, **1999**. 33(4); 858–872.

- L. A. Kelley and M. J. E. Sternberg. Protein structure prediction on the web: A case study using the Phyre server. *Nat. Methods*, **2009**. 4; 363–371.
- J. Key, M. Hefti, E. B. Purcell and K. Moffat. Structure of the redox sensor domain of *Azotobacter vinelandii* NifL at atomic resolution: signaling, dimerization, and mechanism. *Biochemistry*, **2007**. 46(12); 3614–3623.
- H. Kneuper, I. G. Janausch, V. Vijayan, M. Zweckstetter, V. Bock, C. Griesinger and G. Unden. The nature of the stimulus and of the fumarate binding site of the fumarate sensor DcuS of *Escherichia coli*. *J. Biol. Chem.*, **2005**. 280(21); 20596–20603.
- K. K. Koretke, A. N. Lupas, P. V. Warren, M. Rosenberg and J. R. Brown. Evolution of two-component signal transduction. *Mol. Biol. Evol.*, **2000**. 17; 1956–1970.
- T. Krell, J. Lacal, A. Busch, H. Silva-Jiménez, M.-E. Guazzaroni and J. L. Ramos. Bacterial sensor kinases: diversity in the recognition of environmental signals. *Annu. Rev. Microbiol.*, **2010**. 64; 539–559.
- J. Lacal, A. Busch, M. E. Guazzaroni, T. Krell and J. L. Ramos. The TodS-TodT two-component regulatory system recognizes a wide range of effectors and works with DNA-bending proteins. *Proc. Natl. Acad. Sci. U. S. A.*, **2006**. 103(21); 8191–8196.
- D. M. LeMaster and J. E. Cronan. Biosynthetic production of ¹³C-labeled amino acids with site-specific enrichment. *J. Biol. Chem.*, **1982**. 257(3); 1224–1230.
- D. M. LeMaster and F. M. Richards. Preparative-scale isolation of isotopically labeled amino acids. *Anal. Biochem.*, **1982**. 122(2); 238–247.
- R. Malpica, B. Franco, C. Rodriguez, O. Kwon and D. Georgellis. Identification of a quinone-sensitive redox switch in the ArcB sensor kinase. *Proc. Natl. Acad. Sci. U. S. A.*, **2004**. 101(36); 13318–13323.
- A. Marina, C. D. Waldburger and W. A. Hendrickson. Structure of the entire cytoplasmic portion of a sensor histidine-kinase protein. *EMBO J.*, **2005**. 24; 4247–4259.

- E. E. Matthews, M. Zoonens and D. M. Engelman. Dynamic helix interactions in transmembrane signaling. *Cell*, **2006**. 127; 447–450.
- T. L. Maugeri, C. Gugliandolo, D. Caccamo and E. Stackebrandt. Three novel halotolerant and thermophilic *Geobacillus* strains from shallow marine vents. *System. Appl. Microbiol.*, **2002**. 25; 450–455.
- L. P. McIntosh and F. W. Dahlquist. Biosynthetic incorporation of ^{15}N and ^{13}C for assignment and interpretation of nuclear magnetic resonance spectra of proteins. *Q. Rev. Biophys.*, **1990**. 23(1); 1–38.
- W. J. Metzler, K. L. Constantine, M. S. Friedrichs, A. J. Bell, E. G. Ernst, T. B. Lavoie and L. Mueller. Characterization of the three-dimensional solution structure of human profilin: ^1H , ^{13}C , and ^{15}N NMR assignments and global folding pattern. *Biochemistry*, **1993**. 32(50); 13818–13829.
- C. Monzel, P. Degreif-Dünnwald, C. Gröpper, C. Griesinger and G. Udden. The cytoplasmic PASC domain of the sensor kinase DcuS of *Escherichia coli*: role in signal transduction, dimer formation, and DctA interaction. *Microbiology*, **2013**. 2(6); 912–927.
- J. O. Moore and W. A. Hendrickson. An asymmetry-to-symmetry switch in signal transmission by the histidine kinase receptor for TMAO. *Structure*, **2012**. 20; 729–741.
- B. Morgenstern. DIALIGN: Multiple DNA and protein sequence alignment at BiBiServ. *Nucleic Acids Res.*, **2004**. 32(2); 33–36.
- G. Mosqueda, M. I. Ramos-González and J. L. Ramos. Toluene metabolism by the solvent-tolerant *Pseudomonas putida* DOT-T1 strain, and its role in solvent impermeabilization. *Gene*, **1999**. 232(1); 69–76.
- K. Nath and B. A. Azzolina. Cleavage properties of site-specific restriction endonucleases. *Gene Amplif. Anal.*, **1981**. 1; 113–130.
- M. B. Neiditch, M. J. Federle, A. J. Pompeani, R. C. Kelly, D. L. Swem, P. D. Jeffrey, B. L. Bassler and F. M. Hughson. Ligand-induced asymmetry in histidine sensor kinase complex regulates quorum sensing. *Cell*, **2006**. 126(6); 1095–1108.

- A. J. Ninfa, E. G. Ninfa, A. N. Lupas, A. Stock, B. Magasanik and J. Stock. Crosstalk between bacterial chemotaxis signal transduction proteins and regulators of transcription of the Ntr regulon: evidence that nitrogen assimilation and chemotaxis are controlled by a common phosphotransfer mechanism. *Proc. Natl. Acad. Sci. U. S. A.*, **1988**. 85; 5492–5496.
- T. Ogino, M. Matsubara, N. Kato, Y. Nakamura and T. Mizuno. An *Escherichia coli* protein that exhibits phosphohistidine phosphatase activity towards the HPt domain of the ArcB sensor involved in the multistep His-Asp phosphorelay. *Mol. Microbiol.*, **1998**. 27; 573–585.
- K. M. Ottemann, W. Xiao, Y. K. Shin and D. E. Koshland. A piston model for transmembrane signaling of the Aspartate Receptor. *Science*, **1999**. 285; 1751–1754.
- L. Pappalardo, I. G. Janausch, V. Vijayan, E. Zientz, J. Junker, W. Peti, M. Zweckstetter, G. Unden and C. Griesinger. The NMR structure of the sensory domain of the membranous two-component fumarate sensor (histidine protein kinase) DcuS of *Escherichia coli*. *J. Biol. Chem.*, **2003**. 278(40); 39185–39188.
- M. Perego. Kinase-phosphatase competition regulates *Bacillus subtilis* development. *Trends Microbiol.*, **1998**. 6; 366–370.
- M. Perego and J. A. Hoch. Protein aspartate phosphatases control the output of two-component signal transduction systems. *Trends Genet.*, **1996**. 12(3); 97–101.
- E. Perozo, D. M. Cortez and L. G. Cuello. Structural rearrangements underlying K⁺-channel activation gating. *Science*, **1999**. 285(5424); 73–78.
- M. M. Pierce, C. S. Raman and B. T. Nall. Isothermal titration calorimetry of protein-protein interactions. *Methods*, **1999**. 19(2); 213–221.
- A. I. Podgornaia, P. Casino, A. Marina and M. T. Laub. Structural basis of a rationally rewired protein-protein interface critical to bacterial signaling. *Structure*, **2013**. 21; 1636–1647.

A. Razvi and M. J. Scholtz. Lessons in stability from thermophilic proteins. *Protein Sci.*, **2006**. 15(7); 1569–1587.

S. Reinelt, E. Hofmann, T. Gerharz, M. Bott and D. R. Madden. The structure of the periplasmic ligand-binding domain of the sensor kinase CitA reveals the first extracellular PAS domain. *J. Biol. Chem.*, **2003**. 278(40); 39189–39196.

M. Ryan T, B. P. Tripet, J. R. Pearlstone, L. B. Smillie and B. D. Sykes. Defining the region of Troponin-I that binds to Troponin-C. *Biochemistry*, **1999**. 38; 5478–5489.

R. K. Saiki, D. H. Gelfand, S. Stoffel, S. J. Scharf, R. Higuchi, G. T. Horn, K. B. Mullis and H. A. Erlich. Primer-directed enzymatic amplification of DNA with a thermostable DNA polymerase. *Science*, **1988**. 239(4839); 487–491.

F. Sanger and A. R. Coulson. A rapid method for determining sequences in DNA by primed synthesis with DNA polymerase. *J. Mol. Biol.*, **1975**. 94; 441–448.

M. Sevana, V. Vijayan, M. Zweckstetter, S. Reinelt, D. R. Madden, R. Herbst-Irmer, G. M. Sheldrick, M. Bott, C. Griesinger and S. Becker. A ligand-induced switch in the periplasmic domain of sensor histidine kinase CitA. *J. Mol. Biol.*, **2008**. 377; 512–523.

C. Shi, H. K. Fasshuber, V. Chevelkov, S. K. Vasa, S. Becker and A. Lange. BSH-CP based 3D solid-state NMR experiments for protein resonance assignment. *J. Biomol. NMR*, **2014**. 59(1); 15–22.

E. L. L. Sonnhammer, G. von Heijne and A. Krogh. A hidden Markov model for predicting transmembrane helices in protein sequences. *Proc. of Sixth Int. Conf. on Intelligent Systems for Molecular Biology*, **1998**. pp. 175–182.

O. Soubias, V. Réat, O. Saurel and A. Milon. High resolution 2D ¹H-¹³C correlation of cholesterol in model membrane. *J. Magn. Reson.*, **2002**. 158(1); 143–148.

P. A. Steinmetz, S. Wörner and G. Unden. Differentiation of DctA and DcuS function in the DctA/DcuS sensor complex of *Escherichia coli*: function of DctA as an activity switch and of DcuS as the C4-dicarboxylate sensor. *Mol. Microbiol.*, **2014**. 94(1); 218–229.

- T. J. Stevens, R. H. Fogh, W. Boucher, V. A. Higman, F. Eisenmenger, B. Bardiaux, B. J. van Rossum, H. Oschkinat and E. D. Laue. A software framework for analysing solid-state MAS NMR data. *J. Biomol. NMR*, **2011**. 51(4); 437–447.
- A. Sugino, H. M. Goodman, H. L. Heyneker, J. Shine, H. W. Boyer and N. R. Cozzarelli. Interaction of bacteriophage T4 RNA and DNA ligases in joining of duplex DNA at base-paired ends. *J. Biol. Chem.*, **1977**. 252; 3987–3994.
- D. Suter and R. R. Ernst. Spin diffusion in resolved solid-state NMR spectra. *Phys. Rev. B*, **1985**. 32(9); 5608–5627.
- H. Szurmant, R. A. White and J. A. Hoch. Sensor complexes regulating two-component signal transduction. *Curr. Opin. Microbiol.*, **2007**. 17; 706–715.
- B. L. Taylor and I. B. Zhulin. PAS domains: Internal sensors of oxygen, redox potential and light. *Microbiol. Mol. Biol. Rev.*, **1999**. 63(2); 479–506.
- P. Thomason and R. Kay. Eukaryotic signal transduction via histidine-aspartate phosphorelay. *J. Cell Sci.*, **2000**. 113(3); 3141–3150.
- G. E. Tusnády and I. Simon. The HMMTOP transmembrane topology prediction server. *Bioinformatics*, **2001**. 17; 849–850.
- W. F. Vranken, W. Boucher, T. J. Stevens, R. H. Fogh, A. Pajon, M. Llinas, E. L. Ulrich, J. L. Markley, J. Ionides and E. D. Laue. The CCPN data model for NMR spectroscopy: development of a software pipeline. *Proteins*, **2005**. 59(4); 687–696.
- J. Vreede, M. A. van der Horst, K. J. Hellingwerf, W. Crielaard and D. M. van Aalten. PAS domains. Common structure and common flexibility. *J. Biol. Chem.*, **2003**. 278(20); 18434–18439.
- A. Vu, D. J. Hamel, H. Zhou and F. W. Dahlquist. The structure and dynamic properties of the complete histidine phosphotransfer domain of the chemotaxis specific histidine autokinase CheA from *Thermotoga maritima*. *J. Biomol. NMR*, **2011**. 51; 49–55.

C. Wang, J. Sang, J. Wang, M. Su, J. S. Downey, Q. Wu, S. Wang, Y. Cai, X. Xu, J. Wu, D. B. Senadheera, D. G. Cvitkovitch, L. Chen, S. D. Goodman and A. Han. Mechanistic insights revealed by the crystal structure of a histidine kinase with signal transducer and sensor domains. *PLoS Biol.*, **2013**. 11(2); 1–14.

Y. Wang and O. Jardetzky. Probability-based protein secondary structure identification using combined NMR chemical-shift data. *Protein Sci.*, **2002**. 11(4); 852–861.

F. H. Westheimer. Why nature chose phosphates. *Science*, **1987**. 235(4793); 1173–1178.

D. White, R. J. Sharp and F. G. Priest. A polyphasic taxonomic study of thermophilic bacilli from a wide geographical area. *Antonie van Leeuwenhoek*, **1993**. 64; 357–386.

B. Winnen, R. N. Hvorup and M. H. S. Jr. The Tripartite Tricarboxylate Transporter (TTT) family. *Res. Microbiol.*, **2003**. 154; 457–465.

P. M. Wolanin, P. a. Thomason and J. B. Stock. Histidine protein kinases: key signal transducers outside the animal kingdom. *Genome Biol.*, **2002**. 3(10); 3013.1–3013.8.

S. Yamada, H. Sugimoto, M. Kobayashi, A. Ohno, H. Nakamura and Y. Shiro. Structure of PAS-linked histidine kinase and the response regulator complex. *Structure*, **2009**. 17(10); 1333–1344.

N. Yao, Y. Ren and W. Wang. Genome Sequence of a Thermophilic Bacillus, *Geobacillus thermodenitrificans* DSM465. *Genome Announc.*, **2013**. 1(6); 1–2.

J. Zapf, U. Sen, Madhusudan, J. A. Hoch and K. I. Varughese. A transient interaction between two phosphorelay proteins trapped in a crystal lattice reveals the mechanism of molecular recognition and phosphotransfer in signal transduction. *Structure*, **2000**. 8; 851–862.

E. M. Zdobnov and R. Apweiler. InterProScan - an Integration Platform for the Signature-Recognition Methods in InterPro. *Bioinformatics*, **2001**. 17(9); 847–848.

Y. Zhang. I-TASSER Server for Protein 3D Structure Prediction. *Bioinformatics*, **2008**. 9(40); 1–8.

H.-X. Zhou and T. A. Cross. Modeling the membrane environment has implications for membrane protein structure and function: Influenza A M2 protein. *Protein Sci.*, **2013**. 22; 381–394.

Q. Zhu and J. R. Casey. Topology of transmembrane proteins by scanning cysteine accessibility mutagenesis methodology. *Methods*, **2007**. 41(4); 439–450.

E. Zientz, J. Bongaerts and G. Uden. Fumarate Regulation of Gene Expression in *Escherichia coli* by the DcuSR (dcuSR Genes) Two-Component Regulatory System. *J. Bacteriol.*, **1998**. 180(20); 5421–5425.

6 Acknowledgements

First, I would like to thank Prof. Christian Griesinger for giving me the opportunity to conduct my doctoral thesis in his department. I am very grateful for the excellent supervision from Prof. Griesinger, Prof. Adam Lange and Dr. Stefan Becker over the course of my thesis project. I would also like to thank Prof. Gottfried Unden from the University of Mainz and his co-workers for the fruitful collaboration and helpful discussions. I am indebted to all people involved in the project for guidance, constructive criticism, support and advice throughout the last four years.

I would like to express my gratitude to the members of my thesis committee, Prof. Claudia Steinem and Prof. Blanche Schwappach for the productive meetings and invaluable input regarding difficulties faced during experiments. I thank Prof. Patrick Cramer, Prof. Michael Meinecke and Dr. Martin Kollmar for their participation in my oral examination.

Furthermore, I would like to express my appreciation to Karin Giller for providing excellent protein samples for solid-state NMR spectroscopy. I also thank Kerstin Overkamp and Gerhard Wolf for mass spectrometry of protein samples. A special thanks to the current and previous members of the biochemistry lab staff for the superb working atmosphere and fun times in and around the lab.

I would like to acknowledge Dr. Luigi Russo, Dr. Venita Daebel and Dr. Chaowei Shi for sharing their knowledge on various aspects of NMR spectroscopy with me. I am also indebted to Dr. Dirk Bockelmann for support with the computers and software. I thank the whole NMR II staff for the outstanding atmosphere and would especially like to thank Sebastian Täubert, Dr. Florian Siepel, Dr. Manuel Schmidt, Christian Schmidt, Dr. Ann-Christin Pöppler, Eibe Dücker, Dr. Philip Lottmann and Dr. Saskia Villinger for their help and insightful discussions.

I am very grateful for the huge amounts of measurement time taken from Dr. Rasmus Linser and for sharing his ideas for further solid-state NMR experiments with me. I appreciate the proof-reading of Dr. Peggy Findeisen and Christian Schmidt, who impressed me with the most thorough proof-reading possible.

Thanks for being the greatest bands in the world to Selling Illusions, Solid Salad and Castle Green T, hope you will all continue to play one way or another. I would also like to thank all my friends for all the great times we had over the years, whether in Göttingen, Bielefeld, Löhne or St. Andrews.

I express my deepest thanks to my family and most of all my parents for being there for me all my life and their ceaseless trust and support, without which I would never have come so far. Finally, I thank Tina Huskobla with all my heart for her love, for finding me and being the one for me.

7 List of abbreviations

APS	Ammonium persulfate
ArcB	Anoxic redox control protein B
Arnt	Aryl hydrocarbon receptor nuclear translocator
Asp	Aspartate
ATP	Adenosine triphosphate
BSH-CP	Band-selective homonuclear cross-polarisation
CA	Catalytic and ATP-binding domain
CheA	Chemotaxis kinase A
CitA/CitB	Citrate receptor protein A/B
CitApc	CitA construct containing PASp and PASc
DctA	Dicarboxylate transporter protein A
DcuB/DcuR/DcuS	Dicarboxylate uptake protein B/R/S
DesK	Desaturase regulating kinase
DHp	Dimerisation and histidine phosphorylation domain
DMPC	1,2-Dimyristoyl- <i>sn</i> -glycero-3-phosphocholine
DNA	Desoxyribonucleic acid
dNTP	Desoxyribonucleotide triphosphate
DTT	Dithiothreitol
EDTA	Ethylenediaminetetraacetate
EnvZ	Envelope stress response protein Z
EPR	Electron paramagnetic resonance
GHL ATPase	GyrB, Hsp90, MutL ATPase
GyrB	Gyrase B

H-box	Homology box containing phosphorylated His
HAMP	Histidine kinase, adenylate cyclase, methyl accepting protein and phosphatase domain
His	Histidine
HK	Histidine kinase
HPt	Histidine phosphotransfer domain
Hsp90	Heat shock protein 90
HSQC	Heteronuclear single-quantum coherence
INEPT	Insensitive nuclei enhanced by polarisation transfer
IPTG	isopropyl β -D-1-thiogalactopyranoside
LB	Luria-Bertani broth
LDAO	Lauryldimethylamine N-oxide
LuxQ	Bioluminescence protein Q
MAS	Magic-angle spinning
MutL	Mutationally inactivated protein L
NMR	Nuclear magnetic resonance
NOE	Nuclear overhauser effect
NOESY	NOE-spectroscopy
NTA	Nitrilotriacetic acid
NtrB	Nitrogen regulatory protein B
OD	Optical density
PAGE	polyacrylamide gel electrophoresis
PAS	Per-Arnt-Sim domain
PASc	cytosolic PAS domain
PASp	periplasmic PAS domain
PCR	Polymerase chain reaction
PDSD	Proton driven spin diffusion
PER	Period clock protein
PhoQ	Nonspecific acid phosphatase protein Q
PMSF	Phenylmethanesulfonyl fluoride

RDC	Residual dipolar couplings
REC	Receiver domain
RNA	Ribonucleic acid
RR	Response regulator
SCAM	Scanning cysteine accessibility mutagenesis
SEC	Size exclusion chromatography
SeMet	Selenomethionine
Ser	Serine
SIM	Single-minded protein
SDS	Sodium dodecylsulfate
TAE	Tris-Acetic acid-EDTA buffer
TCS	Two-component system
TetA/TctB/TctC	Tricarboxylate transporter A/B/C
TEMED	Tetramethylethylenediamine
TEV	Tobacco etch virus
Thr	Threonine
TOCSY	Total correlation spectroscopy
TodS	Toluene dioxygenase pathway protein S
Tyr	Tyrosine
UV	ultraviolet
VicK	Virulence competence Kinase
YT	Yeast tryptone medium

8 Appendix

8.1 Expression vectors

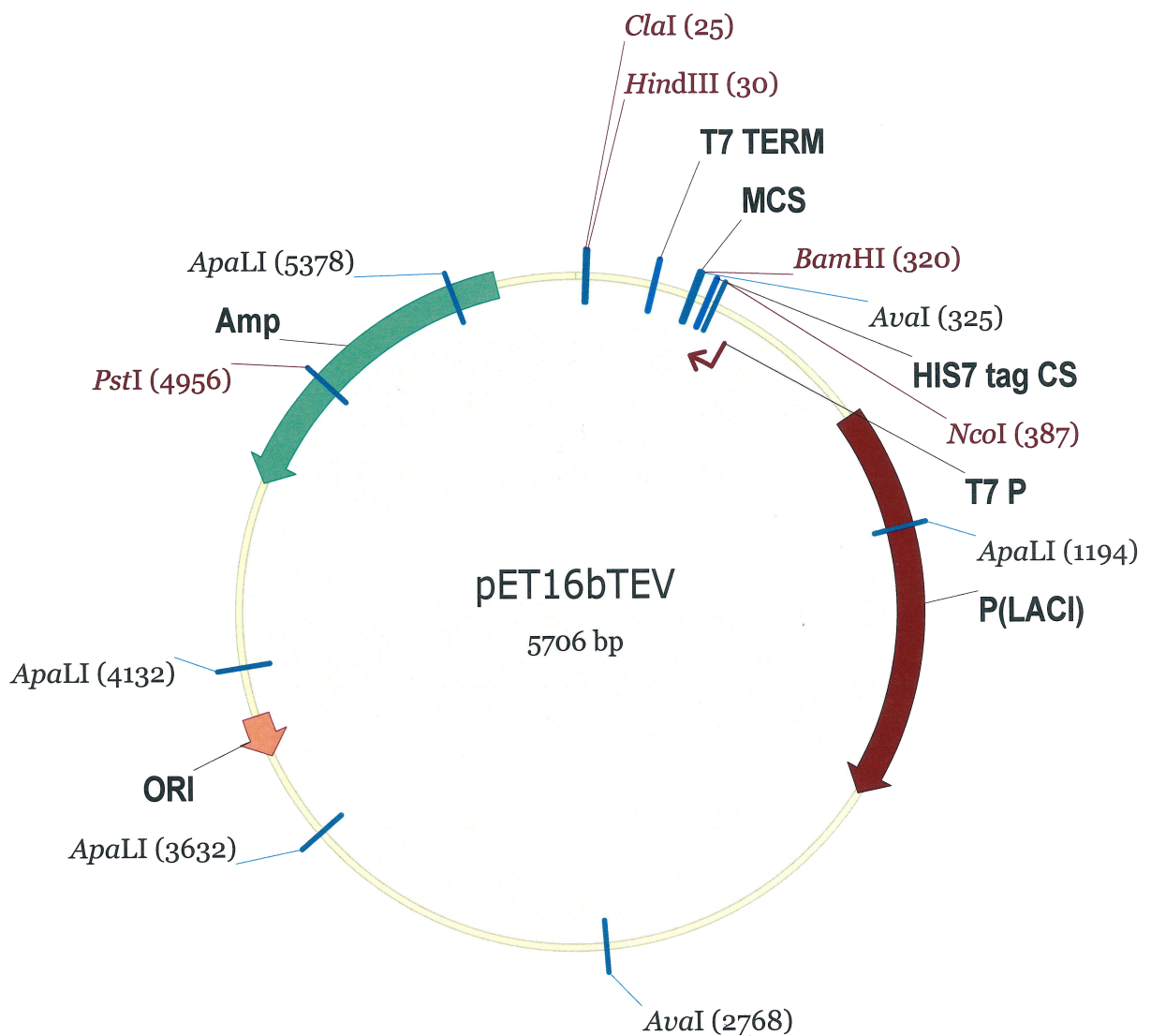


Figure 8.1: Plasmid map of pET16bTEV.

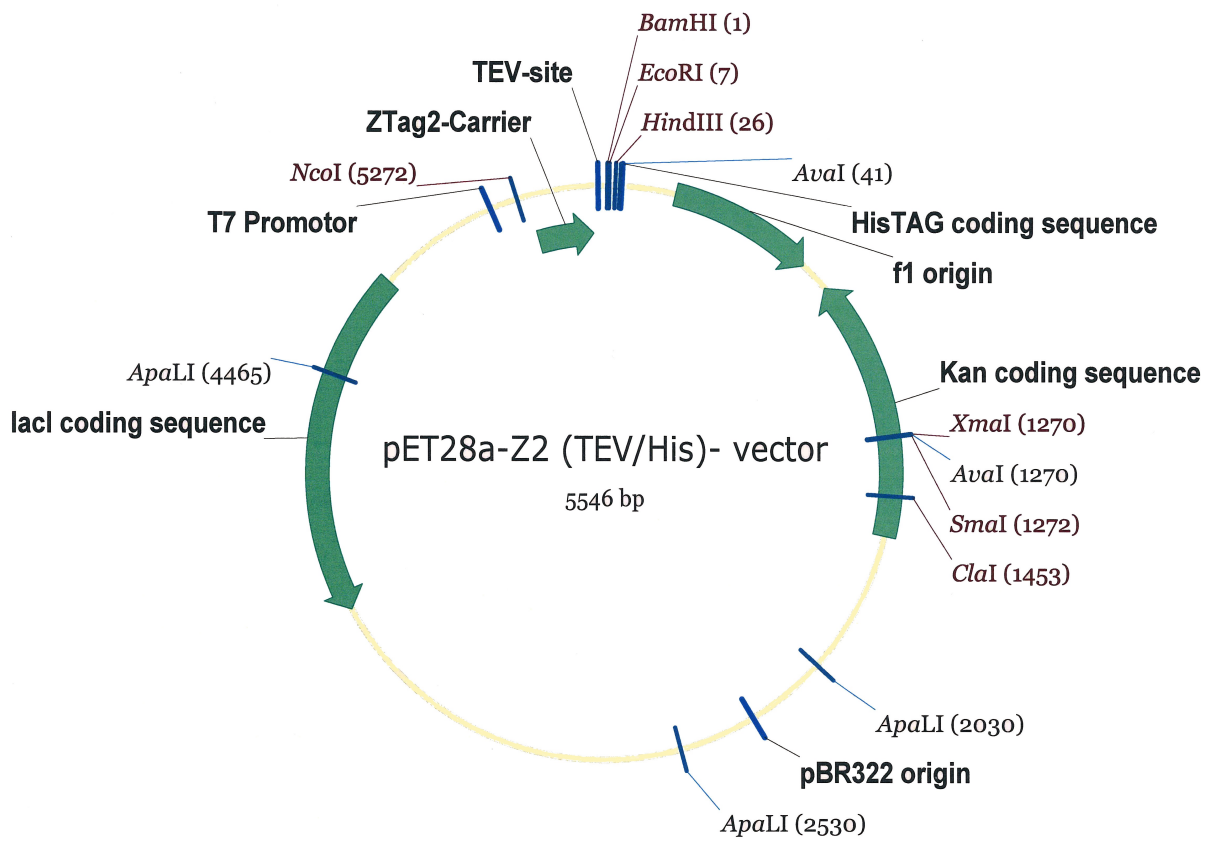


Figure 8.2: Plasmid map of pET28a-Z2.

8.2 PASC crystal data collection, phasing and refinement statistics

Table 8.1: Data collection and phasing for CitA PASC

	Peak	Inflection	High-energy remote
Data collection statistics			
Wavelength [Å]	0.97929	0.97976	0.97163
X-ray source	X10SA, Swiss light source		
Detector	Pilatus 6M		
Space group	P2 ₁ 2 ₁ 2 ₁		
Unit cell parameters ^a	a = 34.45 Å	a = 34.52 Å	a = 34.51 Å
	b = 74.03 Å	b = 74.28 Å	b = 74.20 Å
	c = 75.08 Å	c = 75.35 Å	c = 75.26 Å
	$\alpha=\beta=\gamma=90^\circ$	$\alpha=\beta=\gamma=90^\circ$	$\alpha=\beta=\gamma=90^\circ$
Resolution [Å]	1.78 (1.88-1.78)	1.99 (2.09-1.99)	1.97 (2.07-1.97)
No. of reflections (unique)	18,999	26,252	14,181
Completeness [%]	99.3 (96.5)	99.5 (96.7)	99.6 (97.6)
Mean I/[σ I]	10.78 (2.4)	12.97 (2.65)	13.18 (3.82)
R _{Int} [%] ^b	8.97 (50.64)	11.0 (51.46)	7.86 (38.04)
Substructure solution (SHELX)			
CC _{HREM/PEAK}	31.8 % at 2.4 - 2.2 Å		
CC _{HREM/INFL}	32.3 % at 3.0 - 2.6 Å		
CC _{PEAK/INFL}	35.9 % at 3.5 - 3.0 Å		
No. of sites	4		
CC _{ALL/WEAK}	42.2 / 37.6		

^a Values in parentheses are outer-resolution shells

^b $R_{int} = |F_0^2 - F_0^2(\text{mean})| / \Sigma[F_0^2]$

Table 8.2: Refinement statistics for CitA PASC

	Refinement statistics
Final R-factor [%]	
Working set	18.37
Working set + test set	18.53
Final R_{free}^a	21.76
Twin fraction	0.095
r.m.s.d.	
Bond lengths [\AA]	0.019
Bond angles [$^\circ$]	2.14
Mean B-value [\AA^2]	
Monomer A	
Main chain atoms	26.58
Side chain atoms	32.45
Monomer B	
Main chain atoms	26.99
Side chain atoms	33.03
Solvent [%]	38.3
No. of protein residues	221
No. of glycerol molecules	4
No. of phosphate molecules	3
No. of water molecules	52
Ramachandran plot (% of residues in)	
most favoured regions	98.52
additionally allowed regions	1.48
disallowed regions	-

^a 5 % of reflections in thin shells were taken as the R_{free} set (Brünger, 1992)

8.3 NMR assignments

Table 8.3: Chemical shift assignments of isolated PAsp and PAsc

	H	N	HA	HB	HG	HD	HE	C	CA	CB	CG	CD	CE
33 Thr	8.43	115.63	4.34	4.43	1.23	-	-	175.23	61.83	70.63	21.72	-	-
34 Leu	8.47	123.25	4.04	1.57,1.57	-	0.82	-	178.63	58	41.57	29.11	27.02,24.59	-
35 Lys	8.28	117.69	3.63	1.68,1.65	1.35,1.17	1.61	2.79,2.81	178.38	60.68	32.05	25.65	29.56	41.64
36 Glu	7.75	118.2	3.87	1.96,2.12	2.19	-	-	179.08	59.31	29.68	37.14	-	-
37 Glu	8.02	119	3.95	2.06	2.39,2.27	-	7.18,6.72	179.38	58.88	28.59	34.04	-	111.48:Ne2
38 Ile	8.35	121.64	3.4	1.61	0.81,0.21,1.27	0.4	-	177.78	64.06	36.89	17.49,28.57	12.31	-
39 Gly	8.27	107.56	3.42,3.71	-	-	-	-	174.55	48.03	-	-	-	-
40 Met	7.83	118.79	4.08	2.50,2.63	2.02,2.06	-	-	178.84	58.57	32.38	32.34	-	-
41 Arg	7.72	121.63	4.05	-	1.68	3.00,3.08	-	178.42	59.28	30.07	27.18	43.94	-
42 Ala	8.67	121.58	3.89	1.67	-	-	-	179.4	55.75	17.97	-	-	-
43 Leu	8.46	117.83	3.92	1.92,1.43	1.48	0.86,0.81	-	177.54	57.88	41.02	26.85	25.14,23.38	-
44 Asn	8.01	117.53	4.47	2.83,2.95	-	7.61,6.86	-	178.89	56.92	38.96	-	-	112.10:Nd2
45 Val	8.12	120.66	3.6	2.23	1.10,0.81	-	-	177.66	66.8	31.53	21.89,22.48	-	-
46 Ala	8.65	123.39	3.75	1.37	-	-	-	179.59	56	17.99	-	-	-
47 Glu	8.8	115.53	3.75	2.09	2.56,2.09	-	-	180.05	59.67	29.73	37.81	-	-
48 Thr	7.98	118.05	3.88	4.39	1.18	-	-	177.73	66.78	68.55	21.12	-	-
49 Val	8.68	123.85	3.6	2.26	1.01,0.95	-	-	177.83	67.44	31.64	22.84,24.20	-	-
50 Ala	8.54	118.95	3.74	1.31	-	-	-	178.04	55.27	18.88	-	-	-
51 Ser	7.32	109.09	-	-	-	-	-	174.74	58.2	-	-	-	-
51 Ser	-	-	4.49	4.08,4.01	-	-	-	-	-	64.19	-	-	-
52 Thr	7.71	119.88	4.18	4.45	1.33	-	-	176.36	63.86	69.34	21.55	-	-
53 Ser	9.28	126.61	4.71	4.19	-	-	-	175.65	62.73	63.8	-	-	-
54 Leu	7.77	119.93	3.83	1.58,0.89	1.25	0.54,0.37	-	177.28	58.32	42.18	27.02	24.65,24.33	-
55 Val	6.77	116.45	3.38	2.16	0.81,0.68	-	-	176.18	65.67	30.87	21.90,23.84	-	-
56 Arg	6.85	115.69	3.67	1.85,1.79	1.60,1.54	-	-	180	59.84	29.87	27.51	43.52	-
57 Glu	8.26	118.1	3.85	1.95	2.16,2.31	-	-	179.63	59.14	29.4	36.45	-	-
58 Ala	8.38	122.07	4.13	1.38	-	-	-	179.33	54.12	17.94	-	-	-
59 Phe	7.58	115.64	3.79	3.04,3.27	-	7.66	-	177.03	61.62	39.09	-	131.52	-
60 Arg	7.68	116.69	4.35	2	1.63,1.73	3.21	-	176.74	56.24	30.28	28.04	43.56	-
61 Asp	7.41	121.28	4.42	2.59,2.48	-	-	-	175.97	54.06	40.83	-	-	-
62 Ser	8.62	116.29	4.04	3.82,3.82	-	-	-	175.51	61.44	62.51	-	-	-
63 Asn	8.01	114.21	4.97	2.61,2.99	-	7.60,6.91	-	-	49.76	38.5	-	-	-
64 Pro	-	-	4.01	1.25,-0.08	1.03,1.77	3.06,3.43	-	175.85	64.69	33.3	26.8	50.75	-
65 Ser	7.45	107.04	4.12	3.92	-	-	-	175.93	61.92	64.33	-	-	-
66 Val	7.21	119.36	3.51	2.15	0.86,1.00	-	-	178.71	66.82	30.55	20.82,22.60	-	-
67 Arg	8.25	114.33	4.4	1.79,1.56	1.55,1.79	3.04,3.19	-	179.33	58.25	32.63	27.95	44.69	-
68 Leu	8.03	117.06	4.12	1.67,1.15	0.53	0.84,1.65	-	177.24	57.83	42.77	27.51	23.83,26.04	-
69 Glu	8.69	119.83	4.85	2.37,2.17	2.48,2.20	-	7.08,7.13	-	60.4	24.67	31.32	-	106.40:Ne2
70 Pro	-	-	4.34	2.27,1.85	2.06,2.13	3.55,3.63	-	179.85	65.26	30.44	28.44	49.9	-

Table 8.3: Chemical shift assignments of isolated PAsp and PASC

	H	N	HA	HB	HG	HD	HE	C	CA	CB	CG	CD	CE
71 Phe	6.6	117.92	4.19	3.21,2.96	-	7.21	7.03	176.05	61.08	39.63	-	131.65	131.27
72 Ala	8.86	122.66	3.43	1.47	-	-	-	179.5	55.67	18.27	-	-	-
73 Glu	8.06	115.78	4.2	2.08	2.19	-	-	178.83	57.92	30.25	36.89	-	-
74 Arg	7.55	120.82	3.99	1.84,1.87	1.51	3.07	-	179.41	59.34	29.65	27.3	43.8	-
75 Ile	7.62	119.11	3.53	1.78	0.65,0.99,0.59	0.33	-	179.52	62.06	35.03	26.64,18.12	8.33	-
76 Arg	8.97	125.4	3.3	1.97,1.70	1.35,1.03	3.13,2.83	-	178.06	61.02	29.48	27.21	42.63	-
77 Glu	7.94	116.68	3.88	2.05	2.48,2.28	-	6.73,7.33	178.59	58.83	28.52	34.02	-	111.24:Ne2
78 Lys	7.81	117.63	4.05	1.80,1.86	1.44	1.56	2.87	178.27	58.57	33	24.77	29.18	41.92
79 Thr	7.84	106.9	4.19	4.07	1.25	-	-	176.02	63.05	71.76	22.12	-	-
80 Gly	7.86	110	3.75,4.08	-	-	-	-	173.52	45.65	-	-	-	-
81 Ala	6.91	120.85	2.96	0.57	-	-	-	175.68	51.24	18.66	-	-	-
82 Glu	7.7	120.79	3.76	2.02,1.29	2.16,2.25	-	-	176.66	58.09	28.94	-	-	-
83 Tyr	6.36	104.81	3.95	2.61,2.27	-	-	-	172.55	55.02	38.98	35.87	-	-
84 Val	7.84	121.1	4.35	2.04	0.61,0.63	-	-	174.17	62.54	32.04	19.76,19.78	-	-
85 Val	9.71	126.83	4.41	2.1	1.28,1.18	-	-	175.6	61.06	34.38	19.63,23.96	-	-
86 Ile	7.15	124.08	5.27	1.6	1.13,1.67,1.09	0.92	-	175.11	59.6	40.75	18.52,27.78	14.69	-
87 Gly	9.59	116.39	3.59,5.01	-	-	-	-	172.64	43.88	-	-	-	109.63:Nd2
88 Asn	7.92	116.61	5.25	2.68,3.84	-	6.79,7.00	-	176.33	50.99	38.4	-	-	-
89 Arg	7.35	115.51	3.64	1.57,1.71	-	3.37	7.46,6.77	176.27	58.84	30.02	27.43	43.21	-
90 Gln	-	-	-	-	-	-	-	-	-	-	-	-	111.58:Ne2
90 Gln	7.37	115.55	4.2	1.97,2.20	2.25,2.36	-	-	175.89	55.95	28.62	34.75	-	-
91 Gly	8.14	108.21	4.01,3.35	-	-	-	-	172.63	45.14	-	-	-	-
92 Ile	7.38	120.08	3.78	1.59	1.16,1.23,0.49	0.47	-	176.4	58.37	35.23	26.64,16.94	9.13	-
93 Arg	8.14	122.07	4.11	1.44	1.34	2.64	-	177.52	57.65	32.36	29.53	43.49	-
94 Tyr	9.79	121.12	4.91	2.31,2.86	-	6.58	6.3	174.3	55.06	40.56	-	130.96	118.52
95 Ala	7.65	119.47	5.16	1.28	-	-	-	175.48	51.76	22.71	-	-	-
96 His	8.99	122.04	4.37	3.13,2.62	-	6.97	7.02	-	56.67	33.81	-	120.86	135.56
97 Pro	-	-	4.35	2.13,1.85	2.04,1.76	3.37,1.77	-	177.51	64.88	31.43	27.74	49.22	-
98 Leu	10.97	123.16	4.71	1.33,1.87	1.71	0.85,0.83	-	177.19	53.43	41.11	27.3	25.46,23.56	-
99 Thr	8.33	118.58	3.73	4.16	1.27	-	-	177.68	65.78	68.27	22.23	-	-
100 Glu	9.29	121.27	4.1	1.83,1.99	2.06,2.14	-	-	176.8	58.4	28.56	35.92	-	-
101 Arg	-	-	-	-	-	-	-	178.04	-	-	-	-	-
101 Arg	7.75	116.67	3.68	0.91,1.41	1.23,0.39	2.38	-	-	55.48	29.73	28.81	42.05	-
102 Ile	7.43	123	3.25	1.92	0.53,0.88,1.68	0.87	-	176.77	64.58	36.99	17.03,29.73	12.82	-
103 Gly	9.02	114.6	4.30,3.55	-	-	-	2.91	173.41	45.12	-	-	-	-
104 Lys	7.38	119.27	4.64	1.29,2.02	1.25,1.25	-	-	175.57	54.35	34.83	25.8	29.24	42.39
105 Ser	8.14	115.85	4.54	3.61,3.71	-	-	-	174.16	59.42	64	-	-	-
106 Met	8.64	122.41	3.98	1.31,2.76	2.53,2.27	-	-	176.14	57.52	36.44	34.46	-	-
107 Ile	9.42	126.9	4.13	1.67	0.76,1.14,1.48	0.66	-	174.95	60.26	40.83	27.03,16.37	11.95	-

Table 8.3: Chemical shift assignments of isolated PAsp and PAsc

	H	N	HA	HB	HG	HD	HE	C	CA	CB	CG	CD	CE
108 Gly	8.33	113.46	3.49,4.14	-	-	-	-	175.83	45.09	-	-	-	-
109 Gly	8.78	108.48	3.95,3.82	-	-	-	-	174.78	46.68	-	-	-	-
110 Asp	8.13	116.47	4.75	2.23,2.88	-	-	-	176.47	52.19	38.16	-	-	-
111 Asn	8.24	115.21	4.77	2.73,2.39	-	6.19,7.84	-	177.57	54.02	39.11	-	-	111.80;Nd2
112 Lys	7.81	120.23	3.72	1.70,1.85	1.43,1.27	1.63	2.93	178.95	61.26	32.59	24.79	29.29	-
113 Glu	8.95	115.94	3.98	1.92,1.82	2.14,2.28	-	-	178.85	58.63	29.34	36.39	-	-
114 Val	6.99	119.84	4.66	1.88	0.85,0.65	-	-	180.35	63.55	31.03	22.48,22.43	-	-
115 Leu	7.47	118.21	3.89	1.42,1.73	1.52	0.66,0.76	2.79	177.95	56.89	41.21	27.28	22.56,25.12	-
116 Lys	7	116.23	4.28	2.06,1.85	1.39,1.59	1.61	-	176.8	56.55	32.56	25.15	29.45	42.04
117 Gly	8.31	107.25	4.48,3.31	-	-	-	2.9	173.43	45.4	-	-	28.98	42.23
118 Lys	7.58	122.02	4.57	1.45,1.65	1.31,1.32	1.62	-	174.13	55.04	34.08	24.66	-	-
119 Ser	8.09	116.83	5.23	3.97,3.85	-	-	-	175.17	57.25	64.44	-	-	-
120 Ile	8.97	116.84	4.79	1.75	0.94,0.69,1.18	0.83	-	173.39	59.5	43.1	17.61,25.81	14.43	-
121 Ile	8.06	121.36	4.8	1.51	0.77,0.75,1.63	0.76	-	176.29	61.09	39.4	29.22,18.10	14.02	-
122 Ser	9.46	122.37	4.82	3.43,3.43	-	-	-	173.47	55.54	65.16	-	-	-
123 Glu	8.45	129.31	5.41	1.83,1.93	1.95,2.16	-	-	175.17	54.91	30.69	36.86	-	-
124 Ala	8.57	126.65	4.54	1.04	-	-	-	174.67	50.79	22.33	-	-	-
125 Val	8.51	120.17	3.79	1.95	0.75,0.81	-	-	175.62	62.59	30.35	21.08,21.81	-	-
126 Gly	6.83	112.1	4.42,4.22	-	-	-	-	176.46	44.67	-	-	-	-
127 Ser	6.72	121.5	4.17	3.54,3.89	-	-	-	176.55	62.48	62.07	-	-	-
128 Leu	10.7	123.41	4.34	1.61,1.63	1.74	0.77,0.86	-	176.66	54.8	42.44	26.36	26.22,22.47	-
129 Gly	7.1	105.33	3.72,4.68	-	-	-	-	-	43.97	-	-	-	-
130 Pro	-	-	4.7	2.35,1.94	2.23,1.94	3.75,3.65	-	176.85	63.75	32.2	27.92	49.98	-
131 Ala	9.19	128.06	5.05	1.41	-	-	-	175.05	52.17	25.13	-	-	-
132 Ile	8.46	117.87	4.88	1.52	1.38,0.98,0.84	0.79	-	173.87	59.17	41.08	16.84,29.25	14.18	-
133 Arg	9.3	123.03	5.56	1.89	1.45	2.96,3.28	-	175.18	54.32	34.09	28.51	45.08	-
134 Gly	9.14	110.89	4.94,2.82	-	-	-	-	171.93	44.07	-	-	-	-
135 Lys	9.12	122.92	5.88	1.32,1.47	1.31	1.56,1.49	2.72,2.24	173.73	54.33	34.4	26.6	29.25	41.34
136 Ala	8.83	122.54	5.04	1.1	-	-	-	-	48.07	22.07	-	-	-
137 Pro	-	-	4.3	0.66,2.03	1.57,1.77	3.43,3.64	-	174.24	60.88	31.65	26.66	50.29	-
138 Ile	7.41	118.11	3.92	0.69	0.60,0.37,1.35	0.59	-	175.1	59.81	39.71	17.00,27.48	16.14	-
139 Phe	8.79	126.49	5.36	2.65,3.02	-	7.1	6.9	177.03	56.67	42.42	-	132.15	131.64
140 Asp	8.76	118.76	4.58	2.68,3.16	-	-	-	178.21	51.9	41.11	-	-	-
141 Glu	9.54	118.09	4.01	1.98,1.96	2.25,2.24	-	-	176.57	58.84	28.65	36.12	-	-
142 Asn	8.1	116.3	4.82	2.90,2.79	-	7.68,6.88	-	175.76	52.7	39.51	-	-	114.60;Nd2
143 Gly	7.97	108.06	3.48,4.13	-	-	-	-	174.27	45.69	-	-	-	-
144 Ser	8.55	118.48	4.63	3.74,3.80	-	-	-	173.98	57.88	63.55	-	-	-
145 Val	8.81	124.84	3.9	1.85	0.76,0.69	-	-	177.35	63.71	31.46	22.21,22.12	-	-
146 Ile	8.89	120.87	4.46	1.95	0.51,0.27,0.78	0.41	-	175.41	60.99	39.83	25.28,18.57	13.89	-

Table 8.3: Chemical shift assignments of isolated PAsp and PAsc

	H	N	HA	HB	HG	HD	HE	C	CA	CB	CG	CD	CE
147 Gly	7.29	107.27	3.84,4.15	-	-	-	-	169.82	46.04	-	-	-	-
148 Ile	8.61	118.86	4.38	1.05	0.61,1.01,0.55	0.55	-	173.95	60.62	45.2	27.26,17.83	14.22	-
149 Val	8.97	124.92	4.95	1.95	0.97,0.90	-	-	174.36	60.81	33.83	21.96,21.75	-	-
150 Ser	9.41	122.07	5.27	3.08,3.72	-	-	-	173.81	55.32	65.87	-	-	-
151 Val	9.17	129.35	4.92	2.24	0.86,0.71	-	-	174.79	60.66	32.81	20.18,20.95	-	-
152 Gly	7.05	112.45	5.38,2.73	-	-	7.1	6.92	170.84	43.72	-	-	132.28	130.69
153 Phe	8.34	117.09	4.42	2.49,2.97	-	-	-	174.97	56.88	40.58	-	-	-
154 Leu	9.16	121.18	4.48	1.87,1.64	1.55	0.72,0.88	-	178.53	55.26	42.58	27.08	25.41,22.13	-
155 Leu	8.27	122.24	4.09	1.41	1.41	0.77,0.76	-	178.67	56.43	41.78	27.23	23.05,25.42	-
156 Glu	8.51	118.28	4.1	1.95	2.17	-	-	176.48	57.94	29.93	35.98	-	-
157 Asp	7.55	117.55	4.64	2.77,2.63	-	-	-	176.77	54.92	41.57	-	-	-
158 Ile	7.59	118.51	4.02	1.84	1.50,1.08,0.78	0.72	-	176.08	62.15	38.66	27.17,17.44	13.88	-
159 Gln	8.11	121.31	4.25	1.95	2.3	-	6.79,7.47	175.46	55.96	29.22	34	-	111.99:Ne2
160 Arg	7.99	122.23	4.35	1.76,1.86	1.6	3.16	-	175.72	56.28	30.84	27.22	43.41	-
161 Thr	7.74	120.67	4.08	4.17	1.11	-	-	63.34	63.34	70.73	22.01	-	-
200 Pro	-	-	4.3	1.86,2.27	1.96,2.04	3.82,3.73	-	177.87	64.43	31.84	27.66	50.68	-
201 Glu	8.45	119.26	4.1	1.94	2.23	-	-	177.43	57.91	29.64	36.6	-	-
202 Glu	8.04	121.23	4.08	1.95	2.20,2.23	-	-	177.53	57.83	29.71	36.59	-	-
203 Ile	7.99	120.6	3.86	1.8	1.38,1.10,0.79	0.71	-	177.06	62.76	38.03	17.63,28.09	12.8	-
204 Gly	8.24	109.48	3.88,3.86	-	-	-	-	46.4	-	-	-	-	-
205 Leu	-	-	4.18	1.54	-	-	-	-	56.88	42.07	26.92	24.67,23.61	-
206 Leu	8.1	118.18	4.14	1.44	-	0.83	-	56.94	41.9	41.9	27.06	23.38,25.03	-
207 Tyr	-	-	4.13	3.03,3.03	-	-	-	61.47	38.22	38.22	-	-	-
208 Gln	-	-	4.17	-	1.96	-	-	57.2	29.95	29.95	36.28	-	-
209 Glu	8.03	116.9	3.84	1.87	2.16,2.14	-	-	58.62	28.37	28.37	33.33	-	-
210 Lys	-	-	3.74	1.7	-	-	2.86	59.46	31.97	31.97	25.7	-	42.29
211 Gln	-	-	3.83	2.14	1.99	-	-	59.51	30.12	30.12	36.79	-	-
212 Ala	7.65	121.56	4.13	1.33	-	-	-	53.48	20.31	20.31	-	-	-
213 Ile	-	-	-	1.83	1.01	0.66	-	62.82	39.42	39.42	17.44,27.25	14.15	-
214 Leu	8.69	122.86	3.78	1.89,1.39	0.7	0.78,0.71	-	57.8	41.7	41.7	27.45	24.08,25.33	-
215 Glu	7.76	114.61	4.28	2.06	2.40,2.33	-	-	57.81	29.87	29.87	36.15	-	-
216 Ala	7.64	120.41	4.03	1.33	-	-	-	54.97	18.7	18.7	-	-	-
217 Ile	7.72	117.5	3.36	1.77	1.76,0.67,0.67	0.6	-	65.91	38.18	38.18	29.48,17.64	14.08	-
218 Arg	-	-	4.58	2.29,1.05	1.6	2.88,3.42	8.79	55.92	30.76	30.76	28.02	42.59	-
219 Glu	-	-	3.9	2.20,2.11	2.44,2.44	-	-	59.85	28.14	28.14	34.16	-	-
220 Gly	8.9	106.95	4.39,2.82	-	-	-	-	172.04	45.36	-	-	-	-
221 Ile	7.91	122.08	4.87	1.14	0.53,1.43	0.64	-	173.83	60.07	42.25	27.43,17.03	14.38	-
222 Val	8.3	123.01	4.71	1.84	0.94,0.81	-	-	172.89	60.85	36.02	22.18,21.46	-	-
223 Ala	8.67	127.09	5.5	1.21	-	-	-	176.52	49.85	23.53	-	-	-

Table 8.3: Chemical shift assignments of isolated PAsp and PAsc

	H	N	HA	HB	HG	HD	HE	C	CA	CB	CG	CD	CE
224 Ile	8.71	110.71	5.51	1.67	0.61,1.37	0.61	-	176.82	58.37	42.89	18.05,24.88	15.24	-
225 Asn	7.89	119.1	5.07	3.57,2.89	-	6.92,7.63	-	177	50.91	38.79	176.51	-	110.89;Nd2
226 Gln	7.91	115.68	3.77	1.99,1.94	2.25,2.30	-	6.72,7.55	176.49	58.72	28.12	33.6	179.74	111.07;Ne2
227 Glu	7.57	116.87	4.23	2.10,1.96	2.15,2.19	-	-	176.95	56.27	29.46	36.61	-	-
228 Gly	8	106.77	3.48,4.25	-	-	-	-	177.61	45.27	-	-	-	-
229 Thr	7.85	117.65	4.18	3.71	0.88	-	-	174.23	61.61	69.06	22.68	-	-
230 Ile	8.24	123.78	4.41	1.92	0.82,0.75,1.79	0.7	-	177.5	63.05	38.16	17.98,29.26	14.6	-
231 Thr	9.18	120.65	4.31	4.15	1.08	-	-	175.41	61.5	69.62	22.74	-	-
232 Met	7.26	121.54	4.45	2.34,2.29	1.68,1.96	-	-	173.08	56.37	32.29	36.22	-	-
233 Val	8.49	121.44	5.16	2.03	0.97,0.85	-	-	175.46	60.34	35.08	20.95,21.07	-	-
234 Asn	7.81	121.72	5.13	2.50,3.68	-	8.30,7.57	-	-	50.27	40.73	-	-	114.06;Nd2
235 Gln	8.84	119.32	4.09	-	-	-	-	-	59.73	-	36.62	-	-
236 Thr	-	-	3.82	3.82	1.14	-	-	176.29	66.72	68.77	21.99	-	-
237 Ala	7.62	121.83	4	1.48	-	-	-	178.4	55.72	19.05	-	-	-
238 Leu	8.22	117.44	3.81	1.60,1.89	0.63	0.6	-	178.72	58.79	40.62	25.94	24.15	-
239 Lys	7.89	117.98	4.08	1.91,1.91	1.41,1.51	1.64,1.64	2.92	180.46	59.13	32.01	25	29.04	42.13
240 Leu	7.69	120.27	4.02	1.25,1.79	1.67	0.71,0.71	-	178.29	57.64	42.21	27.01	25.28,23.35	-
241 Leu	7.88	115.38	4.11	1.83,1.64	1.79	0.72,0.76	-	176.83	55.44	43.05	26.91	25.06,23.08	-
242 Gly	7.81	106.54	3.67,3.92	-	-	-	-	174.19	45.73	-	-	-	-
243 Tyr	8	119.01	4.62	2.41,3.01	-	-	-	174.87	57.44	42.44	-	-	-
244 Asp	8.43	117.73	4.56	2.55,2.73	-	-	-	176.07	54.23	41.98	-	-	-
245 Asn	7.66	115.6	4.72	2.75,2.72	-	7.74,6.83	-	174.92	52.92	41.08	176.59	-	113.73;Nd2
246 Glu	9.39	123.47	3.88	1.94,1.99	2.14,2.20	-	-	177.5	58.38	29.09	35.48	-	-
247 Arg	8.57	121.13	3.99	1.76,1.79	1.56,1.57	3.10,3.10	-	176.76	58.43	29.5	27.16	43.15	-
248 Asn	7.97	115.01	4.68	2.80,2.62	-	7.66,6.98	-	174.12	54.01	39.18	176.71	-	111.70;Nd2
249 Val	7.49	115.2	3.86	1.62	0.34,0.48	-	-	176.08	62.69	33.95	21.21,21.86	-	-
250 Leu	7.77	120.71	3.68	1.31,1.58	1.59	0.77,0.65	-	177.97	56.72	41.36	26.72	25.25,23.10	-
251 Gly	8.86	109.79	4.25,3.44	-	-	-	-	173.98	45.19	-	-	-	-
252 Thr	7.71	117.78	4.6	4.1	1.16	-	-	-	60.79	70.13	21.2	-	-
253 Pro	-	-	4.53	1.77,2.44	2.04,1.87	3.96,3.51	-	179.45	62.95	32.6	28.14	51.81	-
254 Ile	8.84	126.24	3.98	1.78	1.32,0.98,1.34	0.87	-	175.85	63.22	37.59	30.07,18.17	15.12	-
255 Leu	8.24	119	4.17	1.64,1.47	1.66	0.88,0.89	-	178.33	56.46	40.49	27.01	25.35,22.94	-
256 Gln	7.42	115.02	4.05	2.08,2.01	2.31,2.33	-	6.83,7.51	176.41	57.55	28.86	34.2	179.57	111.39;Ne2
257 Leu	7.01	117.66	4.44	1.64,1.57	1.6	0.79,0.77	-	176.84	55.85	44.06	27.2	25.58,24.20	-
258 Ile	8.53	117.25	4.28	1.79	1.35,0.82,0.42	0.78	-	-	58.56	38.38	17.93,26.06	13.53	-
259 Pro	-	-	4.57	2.83,1.76	1.96,1.93	3.30,3.70	-	177.21	65.17	31.87	27.23	50.14	-
260 His	8.65	112.49	4.7	3.02,3.18	-	-	-	175.08	54.48	28.7	-	-	-
261 Ser	7.66	114.9	4.2	4.02,3.50	-	-	-	-	58.99	64.48	-	-	-
262 Arg	-	-	-	1.72	1.59,1.58	2.98	7.03	-	57.06	30.4	27.01	43.11	115.30;Ne

Table 8.3: Chemical shift assignments of isolated PAsp and PAsc

	H	N	HA	HB	HG	HD	HE	C	CA	CB	CG	CD	CE
263 Leu	8.69	-	3.96	1.69,1.25	1.57	0.76,0.65	-	-	59.44	39.76	26.91	24.92,23.95	-
264 Pro	-	-	3.96	1.81,2.27	1.92,1.52	3.42	-	178.8	65.85	30.78	29.02	49.78	-
265 Glu	7.21	117.96	4.19	2.06	2.23	-	-	178.2	58.34	28.8	35.23	-	-
266 Val	7.53	120.54	3.79	2.03	0.81,0.52	-	-	178.5	65.34	30.93	22.40,21.23	-	-
267 Ile	7.17	117.62	3.6	1.98	1.36,0.76,1.04	0.43	-	176.88	63.18	36.22	17.13,28.05	12.1	-

Table 8.4: Chemical shift assignments of isolated PAsp R93A (citrate-free)

	H	N	HA	HB	HG	HD	HE	C	CA	CB	CG	CD	CE
33 Thr	8.42	115.59	4.35	4.44	1.23	-	-	175.24	61.88	70.64	21.94	-	-
34 Leu	8.49	123.43	-	-	-	-	-	178.54	57.87	41.61	-	-	-
35 Lys	8.25	117.71	-	-	-	-	-	-	60.5	32.18	-	-	-
35 Lys	-	-	-	-	-	-	-	178.99	-	-	-	-	-
36 Glu	7.81	118.98	-	-	-	-	-	179.05	59.31	29.67	-	-	-
37 Gln	8.1	119.25	3.96	2.1	2.4	-	-	179.28	58.99	28.63	34.05	-	-
37 Gln	-	-	-	-	-	-	7.16,6.70	-	-	-	-	-	-
38 Ile	8.53	121.27	3.53	1.71	1.13,1.55,0.70	-	-	177.99	64.05	36.71	18.49,28.59	12.18	-
39 Gly	8.25	108.5	3.56,3.83	-	-	-	-	174.78	48.16	-	-	-	-
40 Met	7.78	118.6	-	-	-	-	-	178.65	58.24	32.12	-	-	-
41 Arg	7.64	121.7	-	-	-	-	-	177.92	59.35	29.9	-	-	-
42 Ala	8.42	121.38	3.96	1.54	-	-	-	179.23	55.94	18.14	-	-	-
43 Leu	8.19	116.65	-	-	-	-	-	177.96	57.8	41.62	-	-	-
44 Asn	8.41	117.58	4.49	2.77,2.94	-	-	-	179.22	56.93	39.14	-	-	-
44 Asn	-	-	-	-	-	6.83,7.61	-	-	-	-	-	-	111.33;Ne2
45 Val	8.54	121.44	3.62	2.24	1.21,0.86	-	-	177.55	67.28	31.63	22.83,22.38	-	-
46 Ala	8.33	122.39	3.8	1.35	-	-	-	179.3	56.26	17.68	-	-	-
47 Glu	8.95	115.71	-	-	-	-	-	180.11	59.59	29.65	-	-	-
48 Thr	8.27	118.51	3.89	4.38	1.18	-	-	177.82	67	68.47	21.06	-	-
49 Val	8.57	123.63	3.59	2.33	1.01,0.96	-	-	177.68	67.66	31.6	22.95,24.10	-	-
50 Ala	8.43	118.65	3.75	1.35	-	-	-	178.1	55.27	19.15	-	-	-
51 Ser	7.45	109.28	4.48	-	-	-	-	174.7	58.28	64.19	-	-	-
52 Thr	7.66	119.85	4.18	4.42	1.33	-	-	176.34	63.94	69.44	21.76	-	-
53 Ser	9.26	126.31	-	-	-	-	-	175.62	-	-	-	-	-
54 Leu	7.72	119.82	3.83	0.89	1.24	0.35,0.54	-	177.29	58.44	42.22	27.07	24.44,24.89	-
55 Val	6.79	116.75	3.38	2.18	0.69,0.81	-	-	176.23	65.82	31	21.91,23.95	-	-
56 Arg	6.92	115.64	3.69	-	-	-	-	179.74	59.94	29.87	27.48	43.73	-
57 Glu	8.24	117.68	-	-	-	-	-	179.65	59.15	29.46	-	-	-

Table 8.4: Chemical shift assignments of isolated PAsp R93A (citrate-free)

	H	N	HA	HB	HG	HD	HE	C	CA	CB	CG	CD	CE
58 Ala	8.42	122.32	4.12	1.38	-	-	-	179.47	54.23	17.97	-	-	-
59 Phe	7.55	115.13	3.86	3.23,3.07	-	-	-	177.03	61.69	39.06	-	-	-
60 Arg	7.68	116.78	-	-	-	-	-	176.71	56.27	30.32	-	-	-
61 Asp	7.42	121.34	-	-	-	-	-	175.99	54.11	41.05	-	-	-
62 Ser	8.61	116.19	4.04	3.82	-	-	-	175.5	61.45	62.5	-	-	111.06:ND2
63 Asn	-	-	-	-	-	6.90,7.60	-	-	-	-	-	-	-
63 Asn	8.03	114.2	4.98	3.01,2.60	-	-	-	-	49.81	38.51	-	-	-
64 Pro	-	-	4.06	1.32,0.14	1.03,1.77	3.45,3.05	-	175.97	64.73	33.52	26.78	50.86	-
65 Ser	7.5	107.69	4.08	3.89,3.96	-	-	-	175.89	62.17	64.26	-	-	-
66 Val	7.2	119.84	3.51	2.15	1.00,0.86	-	-	178.64	66.82	30.71	22.52,20.81	-	-
67 Arg	8.22	114.15	4.4	1.56,1.77	1.56,1.79	3.19,3.05	-	179.38	58.21	32.59	27.99	44.65	-
68 Leu	7.99	116.71	4.09	1.15,1.67	0.53	1.67,0.84	-	177.3	57.86	42.96	27.39	24.10,26.08	-
69 Gln	-	-	-	-	-	-	6.99,7.19	-	-	-	-	-	107.77:Ne2
69 Gln	8.65	119.7	-	-	-	-	-	-	60.63	-	-	-	-
70 Pro	-	-	4.38	1.86,2.28	2.06,2.13	3.59	-	179.75	65.34	30.43	28.32	50.03	-
71 Phe	6.59	117.91	4.21	3.21,2.99	-	-	-	176.04	61.06	39.66	-	-	-
72 Ala	8.68	122	3.41	1.35	-	-	-	179.18	55.59	18.46	-	-	-
73 Glu	7.85	115.92	-	-	-	-	-	178.66	58.43	29.89	-	-	-
74 Arg	7.64	120.68	-	-	-	-	-	179.14	59.27	29.61	-	-	-
75 Ile	7.8	119.19	3.58	1.74	0.95,0.57,0.65	0.36	-	179.47	62.13	35.23	26.89,17.81	8.61	-
76 Arg	8.7	124.67	-	-	-	-	-	178.02	60.93	29.44	-	-	111.36:Ne2
77 Gln	-	-	-	-	-	-	7.42,6.73	-	-	-	-	-	-
77 Gln	7.97	116.54	3.92	2.08	2.49	-	-	178.77	58.9	28.61	33.92	-	-
78 Lys	8.12	117.67	4.04	1.80,1.90	1.45	1.57	2.88	178.4	58.68	33.1	24.88	29.17	42
79 Thr	7.83	105.06	4.3	4.33	1.3	-	-	176.21	62.58	72.32	22.12	-	-
80 Gly	7.74	109.9	-	-	-	-	-	174.06	45.89	-	-	-	-
81 Ala	7.25	122.39	2.98	0.68	-	-	-	176.05	51.97	18.68	-	-	-
82 Glu	8.31	121.36	3.89	1.54,1.58	2	-	-	176.91	57.9	29.97	35.38	-	-
83 Tyr	6.6	107.76	4.1	2.39,2.97	-	-	-	-	56.3	40.2	-	-	-
84 Val	-	-	4.38	1.95	0.59,0.62	-	-	173.51	62.85	33.41	20.03,20.30	-	-
85 Val	9.34	126.97	4.54	1.89	1.05,0.55	-	-	175.27	60.25	34.87	21.17,22.47	-	-
86 Ile	7.8	123.92	5.07	1.66	1.11,1.64	0.9	-	175.27	60.21	41.15	18.45,27.45	14.72	-
87 Gly	9.48	115.73	4.96,3.67	-	-	-	-	172.35	44.87	-	-	-	-
88 Asn	7.83	116.43	5.19	3.86,2.63	-	-	-	176.65	51.2	38.75	-	-	110.07:ND2
88 Asn	-	-	-	-	-	7.23,6.73	-	-	-	-	-	-	-
89 Arg	7.57	116.4	3.65	-	1.45	3.42	-	176.26	59.09	30.28	27.63	43.23	-
90 Gln	7.36	115.49	4.18	2.18	2.38,2.26	-	7.46,6.78	175.88	56.14	28.65	34.81	-	111.73:Ne2
91 Gly	7.91	107.05	-	-	-	-	-	173	45.41	-	-	-	-
92 Ile	7.45	121.01	3.84	1.52	1.25,1.12,0.49	0.53	-	175.83	59.08	36.25	16.89,27.14	10.11	-

Table 8.4: Chemical shift assignments of isolated PAsp R93A (citrate-free)

	H	N	HA	HB	HG	HD	HE	C	CA	CB	CG	CD	CE
93 Ala	8.03	126.62	4.28	1.33	-	-	-	177	52.58	18.86	-	-	-
94 Tyr	9.47	122.53	4.84	2.33,2.82	-	-	-	174.71	55.58	40.62	-	-	-
95 Ala	7.88	119.57	5.12	1.2	-	-	-	175.35	51.26	22.3	-	-	-
96 His	-	-	4.13	2.52,2.65	-	-	-	-	58.2	32.29	-	-	-
96 His	9.11	124.17	-	-	-	-	-	-	-	-	-	-	-
97 Pro	-	-	4.35	1.88,2.23	1.79	2.30,3.24	-	-	64.44	31.84	27.54	49.89	-
99 Thr	-	-	3.8	4.15	1.25	-	-	-	65.4	68.55	22.3	-	-
100 Glu	-	-	4.13	1.93	2.05	-	-	176.68	58.09	28.74	36.09	-	-
101 Arg	7.83	117.08	3.91	1.17	1.26,0.99	2.76,2.85	-	177.13	54.77	26.85	28.24	41.91	-
102 Ile	7.3	121.64	3.45	1.8	0.71,0.86,1.66	0.87	-	176.52	64.07	37.33	17.17,29.25	13.07	-
107 Ile	-	-	3.98	1.74	1.02,0.82,1.40	0.66	-	174.72	61.89	38.38	27.52,17.53	13.15	-
108 Gly	8.4	113.67	-	-	-	-	-	173.64	45.19	-	-	-	-
109 Gly	8.41	110.31	-	-	-	-	-	173.64	45.33	-	-	-	-
110 Asp	7.67	118.64	-	-	-	-	-	-	54.47	-	-	-	-
111 Asn	-	-	-	2.56	-	7.57,6.39	-	176.33	54.06	39.04	-	-	-
112 Lys	8.21	120.25	3.78	1.89	1.46	1.65	2.95	178.96	60.58	32.26	24.94	29.25	41.85
113 Glu	8.29	116.61	-	-	-	-	-	179	58.73	29.22	-	-	-
114 Val	7.18	120.75	-	-	-	-	-	180.1	63.72	31.42	-	-	-
115 Leu	7.65	118.09	3.92	1.43,1.73	1.63	0.63,0.76	-	177.8	56.96	40.97	27.23	25.08,22.60	-
116 Lys	7.1	116.61	4.3	1.87,2.05	1.62,1.41	1.63	-	176.95	56.73	32.69	25.24	29.52	42.11
117 Gly	8.32	107.12	3.36,4.54	-	-	-	-	173.41	45.47	-	-	-	-
118 Lys	7.62	122.32	4.58	1.48,1.70	1.34	1.62	2.91	174.14	55.2	34.27	24.8	29.02	42.3
119 Ser	8.09	116.37	5.2	3.96	-	-	-	174.93	57.48	64.61	-	-	-
120 Ile	8.69	119.75	4.63	1.65	0.76,1.27,1.01	0.74	-	174.32	59.58	42.81	26.75,17.66	13.44	-
121 Ile	8.31	124.59	5.13	1.59	1.56,0.82,0.88	0.75	-	176.06	59.91	40.66	18.13,28.34	13.85	-
122 Ser	9.19	120.57	4.78	3.74	-	-	-	172.62	57.04	66.09	-	-	-
123 Glu	8.66	122.52	4.88	1.88,2.05	2.19	-	-	175.41	56.01	31.91	36.83	-	-
124 Ala	8.5	124.98	4.58	1.17	-	-	-	175.81	51.36	22.46	-	-	-
125 Val	8.41	120.8	3.99	1.93	0.83,0.85	-	-	176.1	63.08	32.42	21.17,21.40	-	-
126 Gly	7.58	115.12	-	-	-	-	-	175.36	44.59	-	-	-	-
127 Ser	8.86	117.18	4.1	3.82	-	-	-	175.46	61.11	63.06	-	-	-
128 Leu	8.34	120.02	4.47	1.64	1.52	0.82,0.74	-	176.39	54.4	42.54	26.95	22.89,25.44	-
129 Gly	7.37	107.12	-	-	-	-	-	-	44.32	-	-	-	-
130 Pro	-	-	4.53	2.36,1.90	1.95,2.12	3.67,3.65	-	175.23	64.09	32.48	27.68	49.92	-
131 Ala	8.75	125.67	4.97	1.19	-	-	-	175.34	51.26	23.23	-	-	-
132 Ile	8.78	120.19	4.74	1.59	1.39,1.15,0.81	0.79	-	173.39	59.26	40.76	17.89,28.75	13.27	-
133 Arg	8.97	126.25	5.52	1.59	1.43	2.89	-	175.06	54.1	32.83	27.58	43.65	-
134 Gly	9.23	110.56	-	-	-	-	-	171.44	44.1	-	-	-	-
135 Lys	8.89	122.9	5.77	1.46,1.59	1.32	1.43,1.53	2.7	174.09	54.36	37.38	25.44	30.41	42.19

Table 8.4: Chemical shift assignments of isolated PAsp R93A (citrate-free)

	H	N	HA	HB	HG	HD	HE	C	CA	CB	CG	CD	CE
136 Ala	8.91	122.15	5.09	1.14	-	-	-	-	48.21	22.3	-	-	-
137 Pro	-	-	4.32	0.72,2.03	1.78,1.61	3.67	-	174.14	61.01	31.87	26.71	50.5	-
138 Ile	7.4	117.54	3.93	0.76	0.60,0.43,0.52	0.6	-	175.07	59.98	39.81	16.86,27.36	15.98	-
139 Phe	8.87	126.5	5.34	2.69,3.01	-	-	-	177.01	56.75	42.27	-	-	-
140 Asp	8.83	119.04	4.59	3.16,2.69	-	-	-	178.2	51.93	41.12	-	-	-
141 Glu	9.56	118.13	-	-	-	-	-	176.56	58.96	28.68	-	-	-
142 Asn	-	-	4.81	2.78,2.90	-	6.89,7.68	-	175.77	-	-	-	-	114.51:ND2
142 Asn	8.11	116.21	-	-	-	-	-	52.74	39.6	-	-	-	-
143 Gly	7.98	108.05	-	-	-	-	-	174.3	45.85	-	-	-	-
144 Ser	8.54	118.56	-	3.76	-	-	-	173.87	57.94	63.54	-	-	-
145 Val	8.81	124.64	4.03	1.87	0.86,0.67	-	-	177.55	63.71	31.48	22.14,22.29	-	-
146 Ile	8.89	121.04	4.46	1.95	0.53,0.78,0.33	0.44	-	175.27	61.04	39.86	18.58,25.42	13.94	-
147 Gly	7.28	107.15	-	-	-	-	-	169.85	45.98	-	-	-	-
148 Ile	8.38	117.6	4.62	1.26	1.13,0.62,0.60	0.6	-	173.82	60.23	44.03	27.34,17.04	14.16	-
149 Val	9.04	125.51	4.93	1.95	0.93,0.97	-	-	174.37	60.69	34.24	22.08,21.62	-	-
150 Ser	9.27	121.27	5.53	3.74,3.33	-	-	-	173.61	55.55	65.29	-	-	-
151 Val	9.15	126.47	4.75	2.07	0.78,0.85	-	-	174.27	60.41	34.98	21.60,21.46	-	-
152 Gly	7.23	112.55	-	-	-	-	-	172.31	44.23	-	-	-	-
153 Phe	8.82	120.5	4.7	3.04,2.45	-	-	-	174.77	57.56	44.31	-	-	-
154 Leu	8.56	120.95	4.37	1.6	-	0.84,0.69	-	177.16	54.81	42.36	27.24	25.30,23.32	-
155 Leu	8.04	121.97	-	-	-	-	-	176.24	55.43	42.31	-	-	-
156 Glu	7.94	120.32	4.27	1.94,1.84	2.12	-	-	175.28	55.84	31.17	36.24	-	-
157 Asp	8.3	121.76	4.58	2.51,2.66	-	-	-	176.26	54.12	41.25	-	-	-
158 Ile	7.94	120.36	4.12	1.81	1.35,0.82,1.12	0.79	-	176.04	61.2	38.94	17.67,27.25	13.26	-
159 Gln	-	-	-	-	-	-	6.75,7.54	-	-	-	-	-	-
159 Gln	8.36	123.42	4.26	2.03,1.95	2.3	-	-	175.7	55.86	29.22	33.91	-	-
160 Arg	8.25	123.2	4.36	1.71,1.85	1.58	3.14	-	175.62	56.09	30.91	27.18	43.35	-
161 Thr	7.74	120.41	4.08	4.17	1.09	-	-	-	63.21	70.78	22.04	-	-

Table 8.5: Chemical shift assignments of isolated PAsp R93A (citrate-bound)

	H	N	HA	HB	HG	HD	HE	C	CA	CB	CG	CD	CE
32 Ser	-	-	4.62	3.83	-	-	-	175.05	57.9	64.09	-	-	-
33 Thr	8.43	115.64	4.35	4.44	1.23	-	-	175.23	61.83	70.56	21.8	-	-
34 Leu	8.48	123.29	4.05	1.58	1.52	0.83	-	178.63	57.91	41.55	27.03	24.54,23.86	-
35 Lys	8.29	117.74	3.65	1.65	1.18,1.36	1.62	2.81	178.46	60.63	32.1	25.65	29.52	41.78
36 Glu	7.76	118.31	-	-	-	-	-	179.09	59.42	29.57	-	-	-

Table 8.5: Chemical shift assignments of isolated PAsp R93A (citrate-bound)

	H	N	HA	HB	HG	HD	HE	C	CA	CB	CG	CD	CJE
37 Gln	8.02	119.03	3.96	-	-	-	-	179.39	58.99	28.52	34.02	-	-
38 Ile	8.38	121.67	3.42	1.63	-	-	-	177.81	64.06	36.87	28.63,17.61	12.32	-
38 Ile	-	-	-	-	1.32,0.27,0.85	0.46	-	-	-	-	-	-	-
39 Gly	8.27	107.68	3.44,3.74	-	-	-	-	174.57	48.03	-	-	-	-
40 Met	7.81	118.71	4.09	2.06,2.04	-	-	-	178.84	58.57	32.32	-	-	-
41 Arg	7.71	121.7	-	-	-	-	-	178.35	59.32	29.95	-	-	-
42 Ala	8.64	121.61	-	-	-	-	-	179.4	55.82	17.98	-	-	-
43 Leu	8.41	117.67	3.93	1.89	-	-	-	177.62	57.78	41.08	26.79	25.05,23.54	-
44 Asn	8.05	117.58	4.47	2.84,2.96	-	-	-	178.96	56.95	38.98	-	-	-
45 Val	8.2	120.82	3.61	2.25	1.13	-	-	177.66	66.86	31.55	22.08	-	-
46 Ala	8.63	123.34	-	1.38	-	-	-	179.58	56.09	17.97	-	-	-
47 Glu	8.81	115.58	3.77	-	2.55,2.10	-	-	180.08	59.65	29.68	37.82	-	-
48 Thr	8.02	118.13	3.89	4.39	1.18	-	-	177.78	66.81	68.51	21.07	-	-
49 Val	8.7	123.95	-	-	-	-	-	177.86	67.47	31.52	-	-	-
50 Ala	8.55	119	3.76	1.32	-	-	-	178.04	55.21	18.88	-	-	-
51 Ser	7.33	109.21	4.5	4.07,4.03	-	-	-	174.73	58.13	64.16	-	-	-
52 Thr	7.71	119.74	4.18	4.46	1.34	-	-	176.33	63.8	69.39	21.56	-	-
53 Ser	9.27	126.34	-	-	-	-	-	-	62.64	-	-	-	-
54 Leu	7.77	119.96	3.83	0.89	1.26	0.37,0.53	-	177.32	58.38	42.18	27.07	24.81,24.29	-
55 Val	6.75	116.4	3.35	2.16	0.69,0.82	-	-	176.16	65.71	30.94	23.89,21.99	-	-
56 Arg	6.87	115.62	-	-	-	-	-	179.96	59.87	29.81	-	-	-
57 Glu	8.27	117.95	-	-	-	-	-	179.63	59.15	29.27	-	-	-
58 Ala	8.35	122.12	4.13	1.37	-	-	-	179.36	54.16	17.94	-	-	-
59 Phe	7.54	115.06	3.84	3.24,3.09	-	-	-	177.02	61.65	39	-	-	-
60 Arg	7.71	116.88	-	-	-	-	-	176.73	56.32	30.15	-	-	-
61 Asp	7.41	121.26	4.41	2.52	-	-	-	175.99	54.04	40.97	-	-	-
62 Ser	8.62	116.29	4.05	3.84	-	-	-	175.5	61.38	62.42	-	-	-
63 Asn	8.03	114.2	4.97	3.00,2.60	-	-	-	-	49.76	38.5	-	-	-
64 Pro	-	-	4.05	1.82,0.13	1.08	3.45,3.02	-	175.88	64.66	33.48	26.75	50.76	-
65 Ser	7.44	107.47	4.04	3.92,3.90	-	-	-	175.85	62.29	64.18	-	-	-
66 Val	7.2	119.28	3.51	2.15	0.86,1.00	-	-	178.64	66.8	30.57	22.57,20.81	-	-
67 Arg	8.27	114.4	4.4	1.56,1.77	1.78,1.57	3.19,3.05	-	179.36	58.22	32.57	27.97	44.63	-
68 Leu	8.03	116.83	4.1	1.67,1.19	0.51	0.86,1.67	-	177.31	57.84	43.02	27.29	26.04,23.77	-
69 Gln	-	-	4.78	2.33,2.16	2.24,2.50	-	7.08,7.11	-	60.56	24.84	31.36	178.5	106.88;Ne2
69 Gln	8.63	119.5	-	-	-	-	-	-	-	-	-	-	-
70 Pro	-	-	4.36	2.27,1.88	2.12,2.07	3.58,3.64	-	179.83	65.34	30.42	28.37	49.94	-
71 Phe	6.59	117.94	4.19	2.99,3.19	-	-	-	176.05	61.08	39.63	-	-	-
72 Ala	8.81	122.54	3.43	1.46	-	-	-	179.46	55.65	18.28	-	-	-
73 Glu	8	115.81	4.19	-	2.16	-	-	178.78	58.07	29.95	36.34	-	-

Table 8.5: Chemical shift assignments of isolated PAsp R93A (citrate-bound)

	H	N	HA	HB	HG	HD	HE	C	CA	CB	CG	CD	CE
74 Arg	7.55	120.66	-	-	-	-	-	179.37	59.36	29.46	-	-	-
75 Ile	7.68	119.14	3.56	1.78	0.64,0.60,0.99	0.34	-	179.56	62.08	35.05	26.69,18.11	8.36	-
76 Arg	8.9	125.26	3.33	1.73,1.95	-	3.14	-	178.05	60.97	29.28	27.07	42.67	-
77 Gln	7.92	116.73	-	-	-	-	-	178.67	58.87	28.4	-	-	-
78 Lys	7.88	117.69	4.05	1.82	1.44	1.56	2.88	178.32	58.63	33.01	24.83	29.12	41.95
79 Thr	7.85	106.67	4.22	4.12	1.26	-	-	176.02	62.97	71.77	22.29	-	-
80 Gly	7.83	110	-	-	-	-	-	173.6	45.72	-	-	-	-
81 Ala	6.98	121.29	2.94	0.59	-	-	-	175.75	51.38	18.6	-	-	-
82 Glu	7.84	120.99	3.86	-	-	-	-	176.83	58.15	29	35.8	-	-
83 Tyr	6.52	105.61	4.02	2.25	-	-	-	172.66	55.28	39.34	-	-	-
84 Val	7.81	121.07	4.38	2.03	0.64,0.61	-	-	174.08	62.53	32.34	19.84,19.94	-	-
85 Val	9.66	127.21	4.5	2.04	0.90,1.27	-	-	175.73	60.87	34.31	23.33,19.86	-	-
86 Ile	7.47	124.45	5.21	1.67	1.11,1.70,1.05	0.93	-	175.26	59.83	40.55	27.64,18.61	14.72	-
87 Gly	9.71	116	-	-	-	-	-	172.72	44.25	-	-	-	-
88 Asn	-	-	-	-	-	7.08,6.77	-	176.48	-	-	176.01	-	-
88 Asn	7.86	116.34	5.22	2.63,3.81	-	-	-	-	50.97	38.74	-	-	-
89 Arg	7.39	115.68	3.66	1.58,1.70	1.49	3.38	-	176.16	58.69	29.95	27.47	43.25	-
90 Gln	7.34	115.67	4.19	-	2.24,2.37	-	-	175.95	55.93	28.47	34.76	-	-
91 Gly	8.09	107.84	-	-	-	-	-	172.61	45.53	-	-	-	-
92 Ile	7.4	120.05	3.78	1.56	0.45,1.12,1.21	0.49	-	175.72	58.35	36.05	26.69,16.90	9.64	-
93 Ala	7.72	125.86	4.32	1.4	-	-	-	177	52.6	18.9	-	-	-
94 Tyr	9.72	122.57	4.86	2.40,2.83	-	-	-	174.73	55.45	40.48	-	-	-
95 Ala	7.81	120.05	5.14	1.25	-	-	-	175.13	51.38	22.32	-	-	-
96 His	8.96	123.8	4.41	2.78,2.69	-	-	-	-	55.97	34.41	-	-	-
97 Pro	-	-	4.34	2.17,1.86	1.97,1.78	2.11,3.33	-	177.93	64.56	31.59	27.8	49.46	-
98 Leu	10.9	123.34	4.69	1.42,1.76	1.61	0.84,0.81	-	177.24	53.18	40.94	27.1	25.38,23.37	-
99 Thr	8.39	120.46	3.77	4.12	1.26	-	-	177.66	66.02	68.18	22.32	-	-
100 Glu	9.21	119.84	-	-	-	-	-	176.52	58.24	28.55	-	-	-
101 Arg	7.87	119.55	3.8	-	-	2.82,3.00	-	178.32	53.2	29.27	26.67	39.87	-
102 Ile	7.22	121.96	3.43	1.84	1.74,0.88,0.66	0.9	-	177.38	64.08	37.06	17.12,25.35	12.94	-
103 Gly	9.47	115.42	4.26	-	-	-	-	173.65	45.02	-	-	-	-
104 Lys	7.72	118.6	4.69	1.92	1.29,1.16	1.53	2.89	176.55	53.9	34.93	25.31	28.79	42.52
105 Ser	8.26	116.96	4.31	3.55,3.73	-	-	-	173.64	59.9	63.92	-	-	-
106 Met	8.65	122.75	-	-	-	-	-	-	56.45	-	-	-	-
107 Ile	-	-	-	-	-	-	-	175.38	-	-	-	-	-
108 Gly	8.26	112.63	-	-	-	-	-	175.93	45.08	-	-	-	-
109 Gly	8.81	108.91	3.83,3.96	-	-	-	-	174.71	46.46	-	-	-	-
110 Asp	8.11	116.94	4.84	2.79,2.91	-	-	-	-	52.63	39.58	-	-	-
111 Asn	-	-	4.72	2.72,2.40	-	7.76,6.17	-	177.46	54.13	38.99	175.41	-	-

109.65:Nd2

111.73:Nd2

Table 8.5: Chemical shift assignments of isolated PAsp R93A (citrate-bound)

	H	N	HA	HB	HG	HD	HE	C	CA	CB	CG	CD	CE
112 Lys	7.87	120.08	3.73	1.71,1.86	1.29,1.44	1.65	2.94	178.95	61.12	32.57	24.82	29.3	41.91
113 Glu	8.85	115.97	-	-	-	-	-	178.86	58.66	29.12	-	-	-
114 Val	7	120.02	4.66	1.88	0.67	-	-	180.35	63.54	31.1	22.35	-	-
115 Leu	7.52	118.2	3.91	1.41,1.73	1.53	0.64,0.76	-	177.92	56.93	41.15	27.26	25.12,22.62	-
116 Lys	7.01	116.26	4.29	1.84,2.06	1.60,1.39	1.61	2.82	176.86	56.57	32.56	25.19	29.47	42.01
117 Gly	8.31	107.26	-	-	-	-	-	173.43	45.44	-	-	-	-
118 Lys	7.63	122.25	4.58	1.46,1.65	1.32	1.62	2.9	174.1	55.07	34.06	24.71	28.95	42.29
119 Ser	8.09	116.82	5.24	3.97	-	-	-	175.16	57.3	64.5	-	-	-
120 Ile	8.94	117.3	4.79	1.74	0.96,0.69,1.19	0.83	-	173.49	59.54	43.09	25.94,17.60	14.31	-
121 Ile	8.08	121.73	4.87	1.51	1.62,0.78,0.76	0.75	-	176.29	60.93	39.66	29.11,18.13	13.97	-
122 Ser	9.41	122.22	4.83	3.48	-	-	-	173.29	55.69	65.28	-	-	-
123 Glu	8.45	128.03	5.34	1.84,1.94	2.17,1.99	-	-	175.22	55.08	30.94	36.87	-	-
124 Ala	8.6	126.4	4.55	1.08	-	-	-	174.77	51.02	22.21	-	-	-
125 Val	8.41	120	3.92	1.94	0.76,0.80	-	-	175.67	62.44	31.09	20.96,21.72	-	-
126 Gly	6.87	112.98	-	-	-	-	-	-	44.59	-	-	-	-
128 Leu	10.78	123.34	4.3	1.61	0.69	0.86	-	176.73	55	42.07	25.9	22.79	-
129 Gly	7.16	105.35	-	-	-	-	-	-	44.08	-	-	-	-
130 Pro	-	-	4.67	1.94,2.35	2.21,1.94	3.74,3.66	-	176.66	63.76	32.09	27.87	49.94	-
131 Ala	9.13	128.01	5.05	1.36	-	-	-	175.22	52.03	24.59	-	-	-
132 Ile	8.54	118.29	4.85	1.53	0.84,1.00,1.39	0.79	-	173.73	59.21	41	16.97,29.23	14.13	-
133 Arg	9.26	123.53	5.58	1.52,1.78	1.41	3.18,2.98	-	175.21	54.21	33.84	28.22	44.95	-
134 Gly	9.1	110.8	2.83,4.94	-	-	-	-	171.86	44.03	-	-	-	-
135 Lys	9.09	122.92	5.89	1.33	-	-	2.71	173.78	54.35	34.66	26.48	29.48	41.47
136 Ala	8.85	122.55	5.06	1.13	-	-	-	-	48.07	22.18	-	-	-
137 Pro	-	-	4.31	2.05,0.68	1.78,1.59	3.65,3.44	-	174.24	60.91	31.66	26.66	50.36	-
138 Ile	7.4	117.95	3.93	0.73	0.60,0.43	0.6	-	175.11	59.82	39.72	27.43,17.05	16.02	-
139 Phe	8.81	126.48	5.36	3.02,2.67	-	-	-	177.03	56.69	42.39	-	-	-
140 Asp	8.8	118.93	4.59	2.69,3.17	-	-	-	178.22	51.89	41.11	-	-	-
141 Glu	9.56	118.13	-	-	-	-	-	176.59	58.92	28.55	-	-	-
142 Asn	-	-	-	-	-	6.89,7.69	-	-	-	39.57	-	-	114.62:Nd2
142 Asn	8.11	116.3	-	-	-	-	-	175.77	52.76	-	177.38	-	-
143 Gly	7.98	108.09	-	-	-	-	-	174.28	45.88	-	-	-	-
144 Ser	8.54	118.5	4.63	3.74	-	-	-	173.94	57.85	63.45	-	-	-
145 Val	8.81	124.82	3.94	1.87	0.66,0.77	-	-	177.4	63.67	31.44	22.39,22.24	-	-
146 Ile	8.89	120.96	4.44	1.91	0.31,0.78,0.53	0.44	-	175.19	60.9	39.85	18.53,25.43	14.02	-
147 Gly	7.26	107.2	3.82,3.95	-	-	-	-	169.91	46.2	-	-	-	-
148 Ile	8.52	118.61	4.43	1.07	1.03,0.61,0.56	0.56	-	173.93	60.38	45.15	17.62,27.16	14.16	-
149 Val	9.04	125.12	4.92	1.96	0.96,0.89	-	-	174.26	60.94	33.86	22.02,21.75	-	-
150 Ser	9.44	122.25	5.27	3.77,3.11	-	-	-	173.76	55.31	65.67	-	-	-

Table 8.5: Chemical shift assignments of isolated PAsp R93A (citrate-bound)

	H	N	HA	HB	HG	HD	HE	C	CA	CB	CG	CD	CE
151 Val	9.14	128.81	4.88	2.22	0.86,0.72	-	-	174.68	60.63	32.93	20.40,21.11	-	-
152 Gly	7.21	112.75	5.29	-	-	-	-	171.29	43.66	-	-	-	-
153 Phe	8.46	118.28	4.48	2.5	-	-	-	174.95	57	42.75	-	-	-
154 Leu	9.04	121.05	4.48	1.61,1.83	-	0.72,0.88	-	178.36	55.2	40.9	27.12	25.45,22.20	-
155 Leu	8.25	122.25	4.11	1.43,1.46	1.42	0.76,0.77	-	178.35	56.18	41.95	27.24	25.42,23.34	-
156 Glu	8.44	118.69	-	-	-	-	-	-	57.64	-	-	-	-
157 Asp	-	-	4.63	2.75,2.60	-	-	-	176.71	54.83	41.47	-	-	-
158 Ile	7.63	118.87	4.04	1.84	1.08,1.49,0.79	0.74	-	176.11	62.04	38.67	17.50,27.18	13.81	-
159 Gln	8.15	121.69	-	-	-	-	-	-	55.95	-	-	-	-
159 Gln	-	-	4.27	-	2.29	-	-	175.51	-	29.05	33.98	-	-
160 Arg	8.04	122.38	4.36	1.86,1.77	-	3.17	-	175.71	56.25	30.8	27.26	43.43	-
161 Thr	7.74	120.63	4.09	4.18	1.11	-	-	-	63.36	70.71	22.14	-	-

Table 8.6: Chemical shift assignments of wild-type CitApc

	N	C	CA	CB	CG	CD	CE	
8 Met	-	-	58.97	32.08	-	-	-	
9 Val	120.9	176.94	65.67	30.88	-	-	-	
10 Ile	116.87	177.76	66.24	37.97	-	-	-	
11 Ile	121.45	177.85	66.62	37.91	17.88	-	-	
12 Cys	116.47	180.1	65.54	27.1	-	-	-	
31 Ala	121.44	179.52	55.53	18.64	-	-	-	
32 Ala	119.14	180.96	55.09	18.25	-	-	-	
33 Thr	116.01	176.07	66.72	68.43	-	-	-	
34 Leu	123.37	178.61	58.09	41.72	29.14	24.33,27.14	-	
35 Lys	-	178.31	60.72	-	-	-	-	
36 Glu	118.17	179.02	59.32	29.54	36.9	-	-	
37 Gln	118.49	178.91	58.74	28.4	-	-	-	
38 Ile	123.13	177.86	65.26	37.28	-	-	-	
39 Gly	107.67	174.61	47.96	-	-	-	-	
40 Met	119.69	179.07	58.86	32.85	32.84	-	-	
41 Arg	-	-	59.26	30.09	-	-	-	
42 Ala	121.55	179.49	55.62	17.86	-	-	-	
43 Leu	117.82	177.81	57.77	40.95	26.84	25.36,23.25	-	
44 Asn	117.27	178.86	56.61	38.78	175.42	-	-	112.07:Nd2
45 Val	121.45	177.25	67.86	31.74	-	-	-	
46 Ala	124.12	179.74	56.06	18.2	-	-	-	
47 Glu	114.84	180.12	58.9	30.13	37.8	-	-	
48 Thr	118.97	176.05	66.67	68.23	20.88	-	-	
49 Val	-	178.1	67.39	31.98	22.80,24.54	-	-	
50 Ala	118.94	178.13	55.17	18.75	-	-	-	
51 Ser	111.87	-	59.53	64.83	-	-	-	
53 Ser	-	-	62.68	63.67	-	-	-	
54 Leu	120.17	177.09	58.24	42.19	27.18	24.63	-	
55 Val	114.83	175.83	65.52	30.97	23.74,21.88	-	-	
56 Arg	114.87	180.42	59.85	29.88	-	43.5	-	
57 Glu	117.09	179.19	59.17	29.41	36.49	182.83	-	
58 Ala	120.55	179.26	53.89	18.11	-	-	-	
59 Phe	115.98	177.05	61.63	38.84	-	-	-	
60 Arg	116.77	176.72	56.13	29.84	28.56	43.39	-	
61 Asp	121.26	175.92	53.88	40.8	-	-	-	
62 Ser	116.44	175.68	61.35	62.4	-	-	-	
63 Asn	114.15	174.07	49.63	38.4	177.73	-	-	111.39:Nd2
64 Pro	-	175.83	64.69	33.39	26.86	50.78	-	
65 Ser	106.93	176.17	61.81	64.47	-	-	-	
66 Val	119.46	178.99	66.8	30.58	22.77,20.99	-	-	
67 Arg	114.5	179.24	58.74	32.73	28.13	45.06	-	
68 Leu	117.18	177.49	57.83	42.98	27.42	24.18,26.13	-	
69 Gln	120.09	174.87	60.29	24.61	30.91	-	-	
70 Pro	-	178.08,180.17	65.35	30.7	28.78	50.09	-	
71 Phe	117.99	176.13	61.08	39.5	-	-	-	
72 Ala	122.24	179.68	55.81	18.3	-	-	-	
73 Glu	117.05	178.82	57.83	-	-	-	-	
74 Arg	121.5	178.78	59.14	29.54	27.34	43.69	-	
75 Ile	117.48	179.62	62.03	34.66	19.08,26.03	10.52	-	
76 Arg	125.62	178.14	61.06	29.41	26.51	42.45	-	
77 Gln	116.5	178.69	58.71	28.38	34.1	-	-	
78 Lys	-	178.52	58.58	32.94	24.52	29.12	42.12	
79 Thr	106.03	175.85	63.01	71.29	22.58	-	-	
80 Gly	108.79	173.73	45.36	-	-	-	-	
81 Ala	121.8	175.6	51.53	18.37	-	-	-	
82 Glu	120.97	176.46	57.63	28.97	35.27	181.77	-	
83 Tyr	104.31	172.61	54.59	38.94	-	-	-	
84 Val	121.07	174.18	62.47	31.9	19.65,19.65	-	-	
85 Val	126.53	175.78	60.93	34.43	24.16,19.72	-	-	
86 Ile	124.01	175.17	59.51	40.73	27.82,18.54	14.78	-	
87 Gly	116.39	172.61	43.72	-	-	-	-	
88 Asn	116.67	176.53	50.92	38.41	175.89	-	-	109.87:Nd2
89 Arg	115.69	176.38	58.78	29.93	27.36	43.17	-	

Table 8.6: Chemical shift assignments of wild-type CitApc

	N	C	CA	CB	CG	CD	CE	
90 Gln	115.74	175.92	56.04	28.57	34.91	-	-	
91 Gly	108.36	172.67	45.09	-	-	-	-	
92 Ile	120.16	176.46	58.27	35.18	26.67,17.09	9.25	-	
93 Arg	122.06	177.53	57.58	32.41	29.59	43.51	-	
94 Tyr	121.05	174.1	55.1	40.67	-	-	-	
95 Ala	119.5	175.7	51.74	22.69	-	-	-	
96 His	122.15	172.01	56.65	33.65	-	-	-	
97 Pro	-	177.79	64.56	31.43	27.84	49.17	-	
98 Leu	124.09	177.31	53.47	41.01	27.57	23.74,25.70	-	
99 Thr	118.46	177.89	65.68	68.14	22.52	-	-	
100 Glu	121.58	177.01	58.39	28.32	35.98	-	-	
101 Arg	116.67	178.12	55.58	29.81	28.96	42.08	-	
102 Ile	123.39	176.88	64.74	37.19	17.26,29.96	13.17	-	
103 Gly	114.83	173.4	45.12	-	-	-	-	
104 Lys	119.31	175.65	54.21	34.63	25.9	29.23	42.31	
105 Ser	116.03	174.23	59.42	64.02	-	-	-	
106 Met	122.55	176.28	57.46	36.45	34.57	-	-	
107 Ile	127.18	175.01	60.11	40.9	16.48,27.23	12.17	-	
108 Gly	113.68	175.94	44.99	-	-	-	-	
109 Gly	108.63	174.8	46.57	-	-	-	-	
110 Asp	116.48	176.62	52.09	38.14	182.12	-	-	
111 Asn	115.42	177.62	53.94	38.97	-	-	-	111.94:Nd2
112 Lys	120.63	179.09	61.2	32.7	25.03	-	-	
113 Glu	115.82	178.96	58.63	29.27	36.4	-	-	
114 Val	120.02	180.65	63.38	31.08	22.48,22.48	-	-	
115 Leu	118.63	178.33	56.99	41.24	27.39	22.73,25.27	-	
116 Lys	116.34	176.87	56.5	32.69	25.23	29.46	42.13	
117 Gly	107.54	173.48	45.14	-	-	-	-	
118 Lys	122.14	173.91	55.45	33.75	25.31	-	-	
119 Ser	116.82	175.3	57.29	64.08	-	-	-	
120 Ile	117.48	173.62	59.31	43	17.69,25.71	14.56	-	
121 Ile	121.57	176.47	60.95	39.36	29.38,18.39	14.17	-	
122 Ser	122.45	173.58	55.39	65.22	-	-	-	
123 Glu	129.5	175.25	54.81	30.81	37.09	183.08	-	
124 Ala	126.99	174.75	50.7	22.36	-	-	-	
125 Val	120.32	175.76	62.5	30.29	21.06,21.91	-	-	
126 Gly	111.96	176.61	44.66	-	-	-	-	
127 Ser	121.42	176.55	62.43	62.04	-	-	-	
128 Leu	123.49	176.66	54.66	42.25	26.54	22.53,25.97	-	
129 Gly	105.54	-	43.88	-	-	-	-	
130 Pro	-	177.31	63.55	32.31	28.2	50	-	
131 Ala	-	174.99	52.26	25.07	-	-	-	
132 Ile	118.02	174	59.94	40.7	28.78	-	-	
133 Arg	123.06	175.2	54.31	34.17	28.98	44.86	-	
134 Gly	110.98	171.74	44.09	-	-	-	-	
135 Lys	123.08	173.54	54.34	34.15	26.65	29.33	41.42	
136 Ala	123.1	173.77	47.59	22.02	-	-	-	
137 Pro	-	174.53	60.76	31.77	26.77	50.69	-	
138 Ile	118.24	175.24	59.79	39.75	27.60,17.32	16.31	-	
139 Phe	126.31	177.18	56.65	42.53	-	-	-	
140 Asp	119.04	178.34	51.83	41.11	179.22	-	-	
141 Glu	118.25	176.8	58.84	28.62	36.06	-	-	
142 Asn	116.33	175.89	52.65	39.65	-	-	-	
143 Gly	108.53	173.99	45.75	-	-	-	-	
144 Ser	117.82	174.17	57.72	63.55	-	-	-	
145 Val	125.06	177.51	63.56	31.53	22.06,22.06	-	-	
146 Ile	120.86	175.45	60.88	39.71	18.66,25.36	14.16	-	
147 Gly	107.25	169.95	45.9	-	-	-	-	
148 Ile	119.14	174.12	60.65	45.45	27.34,18.12	14.39	-	
149 Val	124.95	174.34	60.88	33.72	21.91,21.91	-	-	
150 Ser	122.07	173.84	55.25	65.86	-	-	-	
151 Val	129.4	174.93	60.31	33.03	20.28,21.25	-	-	
152 Gly	112.15	170.8	43.72	-	-	-	-	

Table 8.6: Chemical shift assignments of wild-type CitApc

	N	C	CA	CB	CG	CD	CE
153 Phe	116.38	175.08	57.15	43.24	-	-	-
154 Leu	120.66	-	55.32	40.57	27.19	25.54,21.92	-
156 Glu	119.05	178.07	59.25	29.63	-	-	-
157 Asp	118.88	178.58	57.28	41.39	-	-	-
158 Ile	122.44	178.11,178.08	65.23	38.09	16.60,28.36	14.47	-
159 Gln	117.8	178.91	58.64	29.19	-	-	-
160 Arg	120.29	179.47	60.18	30.01	-	-	-
161 Thr	119.33	176.93	67.04	68.34	-	-	-
162 Val	122.29	179.8	67.76	31.62	-	-	-
178 Leu	123.31	178.37	58.38	41.08	-	-	-
179 Phe	116.53	178.39	60.65	38.31	-	-	-
180 Gly	105.74	174.57	47.85	-	-	-	-
181 Ala	124.62	179.37	55.81	19.83	-	-	-
182 Val	117.18	178.72	67.03	31.22	-	-	-
183 Gly	105.12	-	45.79	-	-	-	-
184 Ala	122.85	181.15	55.03	18.28	-	-	-
185 Val	117.34	177.68	66.7	31.62	-	-	-
186 Ala	121.12	180.56	55.47	18.73	-	-	-
187 Ile	118.62	180.09	65.85	38.43	15.89,29.61	13.73	-
222 Val	-	173.55	60.75	35.93	22.36,21.12	-	-
223 Ala	-	176.62	50	23.35	-	-	-
224 Ile	-	-	58.27	42.93	18.24,24.89	15.26	-
227 Glu	-	-	56.16	29.61	36.64	-	-
229 Thr	-	174.32	61.69	68.91	22.95	-	-
230 Ile	-	-	62.99	38.03	17.96,29.36	14.51	-
231 Thr	-	-	61.44	69.44	23.03	-	-
234 Asn	-	-	50.09	41.03	-	-	-
236 Thr	-	-	66.24	68.74	-	-	-
237 Ala	-	-	55.64	19.12	-	-	-
241 Leu	-	-	55.71	43.38	26.92	23.31,25.17	-
244 Asp	-	-	53.73	41.81	-	-	-
252 Thr	-	-	60.64	70.15	21.51	-	-
253 Pro	-	178.96	62.88	32.65	28.28	51.92	-
255 Leu	-	-	56.27	40.61	27.01	23.06,25.50	-
258 Ile	-	-	57.75	38.55	25.97	-	-
259 Pro	-	-	65.02	32	27.29	50.04	-
261 Ser	-	-	58.96	64.44	-	-	-
264 Pro	-	-	65.68	30.84	29.15	49.58	-
266 Val	-	-	65.09	30.88	22.69,21.26	-	-
268 Arg	-	-	59.15	31.02	27.57	43.08	-
269 Thr	-	177.72	62.54	70.11	21.83	-	-
270 Gly	-	172.98	46.63	-	-	-	-
271 Gln	-	174.31	53.88	30.28	33.38	-	-
272 Ala	125.79	176.29	51.85	20.88	-	-	-
273 Glu	-	-	54.81	32.49	35.55	-	-
275 Asp	-	-	55.61	39.54	-	-	-
276 Asp	-	-	53.86	42.81	-	-	-
277 Glu	-	-	56.41	30.56	37.3	-	-
279 Val	-	-	61.46	32.63	21.10,21.10	-	-
281 Gly	-	175.4	47.14	-	-	-	-
283 Glu	-	-	54.57	31.99	35.63	-	-
284 Thr	-	-	63.13	68.73	22.21	-	-
286 Ile	-	-	59.19	38.24	-	-	-
287 Ala	-	-	50.36	23.11	-	-	-
291 Pro	-	-	61.75	31.89	26.28	50.23	-
293 Lys	-	-	54.29	36.45	26.37	29.48	42.19
294 Asn	-	-	50.61	38.86	-	-	-
296 Gln	-	-	56.38	28.42	34.92	-	-
300 Ile	-	-	60.55	38.96	26.42,18.18	14	-
301 Gly	-	170.82	45.68	-	-	-	-
302 Ala	-	-	52.32	22.48	-	-	-
305 Thr	-	-	57.97	70.77	22.73	-	-
307 Arg	-	-	53.49	33.53	27.59	43.72	-

Table 8.6: Chemical shift assignments of wild-type CitApc

	N	C	CA	CB	CG	CD	CE
--	---	---	----	----	----	----	----

Table 8.7: Chemical shift assignments of CitApc R93A (citrate-free)

	N	C	CA	CB	CG	CD	CE
35 Lys	-	178.98	60.31	-	-	-	-
36 Glu	118.94	-	59.42	29.78	-	-	-
38 Ile	-	-	-	-	-	-	-
39 Gly	108.52	174.61	47.97	-	-	-	-
40 Met	118.83	-	58.6	31.88	-	-	-
41 Arg	121.5	-	59.06	29.67	-	-	-
42 Ala	-	179.24	55.96	18.23	-	-	-
43 Leu	116.65	-	57.77	41.79	-	-	-
44 Asn	117.64	-	56.45	39.05	176.19	-	-
45 Val	121.38	177.21	67.57	31.62	-	-	-
46 Ala	122.28	179.28	55.92	18.17	-	-	-
47 Glu	115.92	180.11	59.48	29.84	-	-	-
48 Thr	118.79	-	66.68	68.31	20.91	-	-
49 Val	123.62	177.72	67.38	31.74	22.78,24.44	-	-
50 Ala	119.04	178	55.02	19.22	-	-	-
51 Ser	109.72	174.97	58.3	64.23	-	-	-
52 Thr	119.87	-	64.18	-	-	-	-
53 Ser	-	-	62.94	63.98	-	-	-
54 Leu	119.85	-	58.22	42.02	-	-	-
55 Val	116.59	-	65.57	31.1	21.75,23.53	-	-
56 Arg	-	-	-	-	-	-	-
57 Glu	117.8	179.83	58.98	29.34	-	-	-
58 Ala	122.15	179.45	54.17	18.3	-	-	-
59 Phe	115.19	177.03	61.57	38.87	-	-	-
60 Arg	117.03	176.58	56.17	30.4	28.08	43.57	-
61 Asp	121.38	175.86	54.01	41.14	-	-	-
62 Ser	116.61	175.49	61.38	62.53	-	-	-
63 Asn	114.41	-	49.74	38.57	177.7	-	-
64 Pro	-	176.02	64.48	33.54	26.77	50.79	-
65 Ser	107.84	175.74	62.12	64.25	-	-	-
66 Val	120.01	178.59	66.56	30.89	22.64,20.94	-	-
67 Arg	114.27	179.26	57.92	32.49	27.95	44.47	-
68 Leu	117.02	177.36	57.85	43.06	27.24	25.96,24.14	-
69 Gln	119.64	-	60.37	-	32.19	-	-
69 Gln	-	-	-	24.9	-	-	-
70 Pro	-	179.87	65.28	30.63	28.56	50.06	-
71 Phe	117.9	175.94	60.67	39.73	-	-	-
72 Ala	121.88	179.17	55.56	18.44	-	-	-
73 Glu	115.99	-	58.28	29.91	-	-	-
74 Arg	120.72	178.97	59.06	29.45	27.34	43.56	-
75 Ile	118.38	-	62.14	34.82	26.28,18.37	10.12	-
76 Arg	124.72	178.05	60.85	29.56	-	-	-
77 Gln	116.61	178.79	58.82	28.69	34.01	179.86	-
78 Lys	117.49	178.44	58.62	32.95	24.86	29.15	42.24
79 Thr	104.6	-	62.46	72.13	-	-	-
80 Gly	109.45	174.01	45.81	-	-	-	-
81 Ala	122.9	176.24	52.02	18.63	-	-	-
82 Glu	121.48	-	57.38	29.77	-	-	-
83 Tyr	-	-	56.09	40.55	-	-	-
84 Val	-	173.77	62.72	32.82	19.76,20.18	-	-
84 Val	119.77	-	-	-	-	-	-
85 Val	127.27	175.25	60.23	34.84	21.24,22.37	-	-
86 Ile	124.21	175.15	59.94	40.98	18.52,27.42	14.52	-
87 Gly	116.1	172.35	44.87	-	-	-	-
88 Asn	116.74	-	50.93	38.84	-	-	-
89 Arg	115.88	-	59.24	30.28	-	-	-
90 Gln	115.87	175.97	56.12	28.67	34.87	-	-

111.38:Nd2

Table 8.7: Chemical shift assignments of CitApc R93A (citrate-free)

	N	C	CA	CB	CG	CD	CE
91 Gly	107.05	173.14	45.33	-	-	-	-
92 Ile	121.01	176.05	58.83	36.38	17.01,27.17	10.3	-
93 Ala	126.66	176.95	52.46	18.9	-	-	-
94 Tyr	122.71	-	55.59	40.68	-	-	-
95 Ala	120.01	175.44	51.34	22.38	-	-	-
96 His	124.15	-	58.12	-	-	-	-
97 Pro	-	-	64.15	31.84	27.45	49.97	-
98 Leu	-	-	-	-	-	-	-
99 Thr	118.53	-	-	-	-	-	-
99 Thr	-	-	65.57	68.26	22.42	-	-
100 Glu	-	-	-	28.84	36.17	-	-
101 Arg	-	-	-	26.46	28.28	-	-
102 Ile	-	-	63.85	37.29	29.32,17.35	13.18	-
103 Gly	-	-	-	-	-	-	-
104 Lys	-	-	-	-	-	-	-
105 Ser	-	-	-	-	-	-	-
106 Met	-	-	-	-	-	-	-
107 Ile	-	-	-	38.64	17.69,27.34	13.04	-
109 Gly	110.35	173.7	45.09	-	-	-	-
111 Asn	-	-	54.4	38.86	-	-	-
111 Asn	-	-	-	-	-	-	-
112 Lys	120.61	-	60.82	32.27	-	29.35	-
113 Glu	116.66	178.91	58.66	29.34	-	-	-
114 Val	120.99	180.37	63.45	31.46	22.31	-	-
115 Leu	118.35	177.85	56.77	40.99	27.25	25.25,22.66	-
116 Lys	116.66	176.91	56.49	32.72	25.28	29.59	42.12
117 Gly	107.46	173.38	45.35	-	-	-	-
118 Lys	122.26	174.13	55.38	34.15	24.97	-	42.31
119 Ser	116.47	174.99	57.45	64.31	-	-	-
120 Ile	120.5	-	59.25	42.9	17.88	-	-
121 Ile	124.52	175.71	59.82	40.65	18.47,28.36	-	-
122 Ser	120.32	172.65	56.78	65.99	-	-	-
123 Glu	122.63	-	55.91	32	36.92	-	-
124 Ala	124.93	-	51.11	22.39	-	-	-
125 Val	120.71	-	62.58	32.44	21.18,21.18	-	-
126 Gly	115.36	-	44.81	-	-	-	-
127 Ser	-	-	61.15	63.03	-	-	-
128 Leu	-	176.26	54.19	42.34	27.05	23.01,25.40	-
129 Gly	107.14	-	44.35	-	-	-	-
130 Pro	-	-	64.16	32.36	27.77	49.88	-
131 Ala	-	175.58	51.31	23.54	-	-	-
133 Arg	125.96	-	54.2	-	-	-	-
134 Gly	110.3	171.34	44.05	-	-	-	-
135 Lys	122.67	173.79	54.18	37.18	-	-	-
136 Ala	122.87	-	47.65	22.27	-	-	-
137 Pro	-	174.38	60.78	31.92	26.74	50.59	-
138 Ile	117.89	174.92	59.88	39.76	17.50,27.36	15.92	-
139 Phe	126.59	176.93	56.68	42.1	-	-	-
140 Asp	119.51	178.34	51.96	41.12	-	-	-
141 Glu	118.26	-	58.94	28.69	-	-	-
142 Asn	116.39	175.71	52.7	39.58	177.21	-	-
143 Gly	108.16	174.3	45.8	-	-	-	-
144 Ser	118.76	173.9	57.93	63.5	-	-	-
145 Val	124.83	177.52	63.44	31.54	22.32,22.32	-	-
146 Ile	121.23	175.12	60.79	39.69	18.57,25.56	14.22	-
147 Gly	107.03	169.99	45.92	-	-	-	-
148 Ile	118.17	173.92	60.25	44.34	-	-	-
149 Val	125.61	174.44	60.71	34.26	21.96,21.47	-	-
150 Ser	121.49	173.8	55.38	65.15	-	-	-
151 Val	-	174.25	60.49	34.72	21.43,21.43	-	-
152 Gly	112.34	172.37	44.28	-	-	-	-
153 Phe	-	-	57.7	44.2	-	-	-
154 Leu	-	-	54.69	42.35	27.24	25.34,23.23	-

Table 8.7: Chemical shift assignments of CitApc R93A (citrate-free)

	N	C	CA	CB	CG	CD	CE
155 Leu	-	-	-	-	-	-	-
157 Asp	-	-	-	-	-	-	-
179 Phe	-	-	-	-	-	-	-
180 Gly	-	-	-	-	-	-	-
210 Lys	-	-	-	-	-	-	-
216 Ala	-	-	-	-	-	-	-
220 Gly	-	172.44	45.07	-	-	-	-
222 Val	-	173.21	61.03	35.77	20.56,22.16	-	-
223 Ala	128.11	176.39	49.85	23.26	-	-	-
224 Ile	110.98	-	58.23	42.82	24.86,18.13	15.28	-
225 Asn	119.34	-	50.85	38.8	-	-	-
226 Gln	-	176.59	59	-	-	-	-
227 Glu	116.77	-	56.33	29.73	-	-	-
229 Thr	-	174.26	61.52	69.07	22.96	-	-
230 Ile	-	177.36	63.03	38.16	29.28,18.09	14.51	-
231 Thr	121.08	-	61.43	69.4	-	-	-
234 Asn	-	-	50.25	40.26	-	-	-
235 Gln	119.64	-	59.75	28.04	-	-	-
236 Thr	-	-	66.31	68.62	22.35	-	-
239 Lys	117.68	-	58.91	32.14	25.05	-	-
240 Leu	120.69	-	57.69	42.16	27	25.01,23.78	-
241 Leu	-	-	55.59	43.03	27.12	25.30,22.97	-
242 Gly	106.48	174.06	45.69	-	-	-	-
243 Tyr	119.02	-	-	42.15	-	-	-
244 Asp	-	-	54.02	42.02	-	-	-
245 Asn	115.27	-	-	-	-	-	-
246 Glu	-	-	58.3	29.06	35.56	-	-
247 Arg	121.01	-	58.3	-	-	-	-
250 Leu	-	177.9	56.52	41.43	26.78	25.23,23.10	-
251 Gly	109.65	173.94	45.33	-	-	-	-
252 Thr	-	-	60.68	69.96	21.44	-	-
253 Pro	-	-	62.76	32.55	28.17	51.73	-
255 Leu	-	-	56.31	40.62	27	25.34,22.88	-
256 Gln	114.77	-	57.38	29.07	34.2	-	-
257 Leu	-	-	55.81	44.2	27.13	-	-
258 Ile	-	-	58.32	38.16	25.92	13.67	-
259 Pro	-	-	65.06	31.93	27.24	50.12	-
261 Ser	115.02	-	58.57	64.28	-	-	-
263 Leu	122.85	-	-	39.57	-	-	-
264 Pro	-	-	65.68	30.82	29.3	49.82	-
265 Glu	-	178.08	58.5	-	-	-	-
266 Val	120.68	-	65.25	30.91	22.38,21.26	-	-
268 Arg	118.31	178.9	59.34	30.97	27.46	43.16	-
269 Thr	106.65	177.36	62.51	70.31	21.82	-	-
270 Gly	112.2	173.2	46.52	-	-	-	-
271 Gln	119.7	174.01	53.92	30.23	33.4	-	-
272 Ala	125.59	176.5	51.89	20.88	-	-	-
273 Glu	119.44	-	54.84	32.04	35.62	-	-
275 Asp	-	174.49	55.73	39.62	-	-	-
276 Asp	120.77	-	53.94	42.88	-	-	-
277 Glu	126.42	-	56.56	30.49	37.19	-	-
278 Met	124.31	-	54.6	37.01	30.89	-	-
279 Val	121.78	-	61.27	32.37	21.07,21.07	-	-
280 Leu	-	-	53.8	45.08	27.03	-	-
282 Gly	-	173.52	45.03	-	-	-	-
283 Glu	-	-	54.35	31.94	35.53	-	-
284 Thr	118.75	-	62.86	68.94	22.36	-	-
285 Val	-	-	-	35.39	21.19,19.40	-	-
286 Ile	-	-	59.33	38.42	27.27	-	-
287 Ala	-	-	50.19	23.15	-	-	-
291 Pro	-	-	62.32	32.21	26.25	50.33	-
292 Ile	-	-	60.48	39.13	27.3	-	-
293 Lys	125.95	-	54.22	36.61	25.97	29.54	42.18

Table 8.7: Chemical shift assignments of CitApc R93A (citrate-free)

	N	C	CA	CB	CG	CD	CE
294 Asn	-	-	50.25	38.42	176.29	-	-
295 Lys	118.67	-	59.01	31.97	-	28.97	-
296 Gln	116.08	175.96	56.38	28.49	34.88	-	-
297 Gly	107.46	173.55	45.3	-	-	-	-
298 Arg	-	-	54.78	30.84	27.27	-	-
300 Ile	119.86	175.43	60.55	39.06	18.16,26.48	13.93	-
301 Gly	108.42	170.74	45.51	-	-	-	-
302 Ala	120.04	173.43	51.99	22.98	-	-	-
303 Val	118.29	-	-	-	-	-	-
304 Ser	-	174.36	55.58	66.06	-	-	-
305 Thr	-	-	57.94	70.95	22.84	-	-
306 Phe	-	-	54.71	41.94	-	-	-
307 Arg	-	174.96	53.49	33.4	26.98	-	-
309 Lys	-	-	-	33.98	25.6	29.94	-

Table 8.8: Chemical shift assignments of CitApc R93A (citrate-bound)

	N	C	CA	CB	CG	CD	CE
34 Leu	123.37	-	-	-	-	-	-
35 Lys	117.21	-	60.88	31.85	-	-	-
36 Glu	118.38	-	59.08	29.62	-	-	-
37 Gln	118.61	179.38	58.85	28.62	34.04	-	-
39 Gly	107.64	174.79	47.84	-	-	-	-
40 Met	119.1	178.84	58.88	32.1	-	-	-
41 Arg	121.4	-	58.95	29.52	-	-	-
42 Ala	121.77	179.1	55.49	18.09	-	-	-
43 Leu	117.74	177.63	57.78	41.14	26.93	23.19,25.46	-
44 Asn	117.72	-	56.57	38.85	-	-	-
45 Val	120.94	-	67.08	31.64	22.02,22.02	-	-
46 Ala	123.89	179.76	56.23	18.24	-	-	-
47 Glu	-	-	59.41	29.75	-	-	-
48 Thr	118.62	177.63	66.66	68.46	20.95	-	-
49 Val	123.92	-	67.34	31.91	22.97,24.60	-	-
50 Ala	118.98	178.35	55.03	18.74	-	-	-
51 Ser	112.03	-	59.56	64.87	-	-	-
52 Thr	-	176.04	-	-	-	-	-
53 Ser	-	-	62.22	-	-	-	-
54 Leu	119.64	177.6	58.33	42.29	27.11	24.78	-
55 Val	-	175.95	65.4	31.06	23.61,21.78	-	-
56 Arg	115.59	-	59.73	30.1	-	-	-
57 Glu	-	-	-	-	-	182.8	-
57 Glu	118.4	-	59.1	29.29	36.39	-	-
58 Ala	122.29	179.41	54.11	18.2	-	-	-
59 Phe	114.98	177.17	61.58	38.86	-	-	-
60 Arg	117.06	-	56.15	29.79	-	-	-
61 Asp	121.24	176.03	54	40.98	-	-	-
62 Ser	116.54	175.68	61.36	62.54	-	-	-
63 Asn	114.22	-	49.71	38.46	-	-	-
64 Pro	-	175.85	64.45	33.61	26.85	50.84	-
65 Ser	107.29	175.84	62.3	64.24	-	-	-
66 Val	119.08	178.88	66.66	30.85	22.76,20.99	-	-
67 Arg	114.54	179.43	58.14	32.6	28.11	44.66	-
68 Leu	116.87	177.15	57.87	43.36	27.39	24.03,25.93	-
69 Gln	119.72	-	60.36	24.76	31.06	178.43	-
70 Pro	-	180.1	65.33	30.71	28.65	50.1	-
71 Phe	117.2	176.06	60.92	39.63	-	-	-
72 Ala	122.26	179.65	55.84	18.42	-	-	-
73 Glu	115.81	-	57.84	-	-	-	-
74 Arg	-	-	59.12	29.81	27.43	-	-
75 Ile	-	179.87	62.03	34.69	26.10,19.06	10.05	-
76 Arg	125.4	177.97	60.98	29.36	26.21	42.71	-

Table 8.8: Chemical shift assignments of CitApc R93A (citrate-bound)

	N	C	CA	CB	CG	CD	CE	
77 Gln	116.9	178.74	58.7	28.42	34.05	-	-	
79 Thr	106.13	176.05	62.93	71.46	22.44	-	-	
80 Gly	110.08	173.74	45.32	-	-	-	-	
81 Ala	121.29	175.56	51.42	18.43	-	-	-	
82 Glu	121.13	176.72	57.65	29.01	35.28	181.66	-	
83 Tyr	104.43	-	-	-	-	-	-	
83 Tyr	-	172.86	54.57	39.22	-	-	-	
84 Val	121.17	174.24	62.37	32.02	19.74,19.74	-	-	
85 Val	127.22	-	60.91	34.38	19.82,23.59	-	-	
86 Ile	124.63	175.34	59.65	40.33	27.70,18.78	14.77	-	
87 Gly	116.16	172.89	44.06	-	-	-	-	
88 Asn	116.58	176.63	50.83	38.78	176.08	-	-	110.06:Nd2
89 Arg	115.7	176.25	58.5	30.24	28.04	43.61	-	
90 Gln	115.83	176.06	55.85	28.68	34.78	-	-	
91 Gly	108.02	172.66	45.5	-	-	-	-	
92 Ile	120.1	175.82	58.12	36.11	17.01,26.73	9.81	-	
93 Ala	125.62	177.09	52.5	19.14	-	-	-	
94 Tyr	122.68	174.85	55.47	40.7	-	-	-	
95 Ala	120.1	175.38	51.31	22.45	-	-	-	
96 His	-	172.65	-	-	-	-	-	
96 His	124.09	-	55.98	34.44	-	-	-	
97 Pro	-	178.18	64.51	31.68	27.99	49.45	-	
98 Leu	123.76	177.21	53.17	41.04	27.25	25.48	-	
99 Thr	120.93	177.62	66.06	68.2	22.45	-	-	
100 Glu	120.07	176.53	58.23	28.7	36.16	-	-	
102 Ile	122.3	177.45	64.06	37.2	29.58,17.33	13.15	-	
103 Gly	115.65	173.66	45.03	-	-	-	-	
104 Lys	118.81	-	53.81	35.08	25.43	28.83	42.42	
105 Ser	117.41	173.38	60.05	64.01	-	-	-	
106 Met	122.69	-	56.66	-	-	-	-	
107 Ile	130.42	175.59	59.71	40.09	16.87,26.96	11.2	-	
108 Gly	112.74	176.47	45.07	-	-	-	-	
109 Gly	108.77	175.03	46.59	-	-	-	-	
110 Asp	116.5	-	52.16	38.44	181.88	-	-	
110 Asp	-	176.82	-	-	-	-	-	
111 Asn	115.48	-	-	-	-	-	-	
111 Asn	-	-	54.17	39	175.52	-	-	111.91:Nd2
112 Lys	120.25	178.89	61.23	32.73	25.13	29.55	42.01	
113 Glu	115.86	178.97	58.72	29.28	36.54	-	-	
114 Val	120.27	180.63	63.36	31.17	22.48,22.48	-	-	
115 Leu	118.49	178.04	56.84	41.22	27.29	25.33,22.73	-	
116 Lys	116.31	176.94	56.5	32.8	25.26	29.65	42.14	
117 Gly	107.4	173.62	45.33	-	-	-	-	
118 Lys	122.91	174.11	55.24	33.82	24.99	29.22	-	
119 Ser	116.83	175.2	57.29	64.16	-	-	-	
120 Ile	117.15	-	59.33	43.11	25.68,17.64	14.5	-	
121 Ile	121.55	-	60.96	39.47	18.40,29.31	14.2	-	
122 Ser	122.63	173.53	55.38	65.48	-	-	-	
123 Glu	129.29	175.3	54.84	30.96	37.07	-	-	
124 Ala	126.7	174.77	50.87	22.45	-	-	-	
125 Val	120.15	175.73	62.32	30.84	21.02,21.78	-	-	
126 Gly	112.61	176.79	44.75	-	-	-	-	
127 Ser	-	-	62.12	63.14	-	-	-	
128 Leu	123.51	176.87	55.07	41.81	26.15	22.95,22.95	-	
129 Gly	105.34	-	43.84	-	-	-	-	
130 Pro	-	-	63.61	32.27	28.13	49.91	-	
131 Ala	130.19	175.18	52.35	24.96	-	-	-	
132 Ile	117.96	173.8	59.58	40.74	-	-	-	
133 Arg	123.21	175.03	54.36	34.17	28.9	45.07	-	
134 Gly	110.77	172.01	43.94	-	-	-	-	
135 Lys	122.98	173.6	54.28	34.26	26.63	29.37	41.42	
136 Ala	123.04	174.46	47.67	22.14	-	-	-	
137 Pro	-	174.59	60.75	31.74	26.82	50.71	-	

Table 8.8: Chemical shift assignments of CitApc R93A (citrate-bound)

	N	C	CA	CB	CG	CD	CE
138 Ile	118.2	175.25	59.77	39.88	27.54,17.50	16.05	-
139 Phe	126.44	177.29	56.73	42.46	-	-	-
140 Asp	119.3	178.24	51.88	41.17	-	-	-
140 Asp	-	-	-	-	179.22	-	-
141 Glu	118.06	176.85	58.84	28.62	35.89	-	-
142 Asn	116.43	175.82	52.71	39.65	177.26	-	-
143 Gly	108.03	174.27	45.71	-	-	-	-
144 Ser	118.91	174.2	57.91	63.51	-	-	-
145 Val	125.07	177.46	63.52	31.47	22.34,22.34	-	-
146 Ile	120.97	175.19	60.78	39.77	25.58,18.65	14.33	-
147 Gly	107.12	170.08	46	-	-	-	-
148 Ile	119.05	173.93	60.46	45.61	17.93,27.27	14.39	-
149 Val	125.1	173.7	61	33.77	22.00,22.00	-	-
150 Ser	122.7	173.82	55.25	65.81	-	-	-
151 Val	129.13	175.03	60.32	32.87	21.33,20.32	-	-
152 Gly	112.4	171.15	43.66	-	-	-	-
153 Phe	-	174.91	57.07	-	-	-	-
154 Leu	120.47	-	55.34	40.65	27.13	25.68,21.79	-
222 Val	-	-	60.47	-	-	-	-
223 Ala	-	-	50.04	-	-	-	-
224 Ile	-	176.85	58.35	42.75	18.29,24.90	15.19	-
225 Asn	119.06	-	50.6	38.83	-	-	-
229 Thr	-	-	61.69	68.99	22.94	-	-
230 Ile	124.37	177.55	62.9	38.16	18.02,29.35	14.45	-
231 Thr	121.05	-	61.51	69.45	23.12	-	-
232 Met	-	-	56.6	32.9	35.83	-	-
233 Val	-	-	60.3	-	-	-	-
234 Asn	-	-	50.04	-	-	-	-
236 Thr	-	-	66.44	68.65	22.16	-	-
236 Thr	115.41	-	-	-	-	-	-
237 Ala	121.59	178.76	55.54	19.05	-	-	-
239 Lys	117.86	-	59.08	32.23	25.18	29.31	41.96
240 Leu	120.52	-	57.62	42.09	27.01	23.76,24.92	-
241 Leu	-	-	55.51	43.33	27.17	23.19	-
242 Gly	-	174.16	45.71	-	-	-	-
243 Tyr	-	175.05	57.31	42.6	-	-	-
246 Glu	-	-	58.4	28.95	-	-	-
247 Arg	120.49	-	58.43	29.19	-	-	-
248 Asn	115.01	-	54.14	39.16	-	-	-
249 Val	-	-	62.69	-	-	-	-
250 Leu	120.8	-	56.69	41.51	-	-	-
251 Gly	-	173.95	45.32	-	-	-	-
253 Pro	-	-	62.91	32.56	28.19	51.84	-
254 Ile	-	-	-	37.91	30.19,17.99	15.3	-
255 Leu	118.95	-	56.29	40.88	-	-	-
256 Gln	115.42	-	57.53	29.11	34.23	-	-
257 Leu	-	-	55.98	44.09	27.09	-	-
258 Ile	-	-	-	38.46	26.04	13.8	-
259 Pro	-	-	65.23	31.95	27.3	50.29	-
261 Ser	-	-	58.88	64.43	-	-	-
264 Pro	-	-	65.76	30.38	29.04	-	-
265 Glu	117.57	-	-	-	-	-	-
268 Arg	117.38	-	59.11	31.04	27.53	43.14	-
269 Thr	107.41	-	62.58	70.33	21.64	-	-
270 Gly	111.94	173.12	46.62	-	-	-	-
271 Gln	119.23	-	53.87	30.31	33.5	-	-
272 Ala	125.37	-	51.94	20.95	-	-	-
273 Glu	119.83	173.77	54.76	32.05	35.69	-	-
274 Tyr	-	-	56.53	-	-	-	-
275 Asp	-	174.45	55.45	39.48	-	-	-
276 Asp	120.77	-	53.85	-	-	-	-
277 Glu	-	-	56.28	30.62	37.54	-	-
278 Met	124.47	-	-	-	-	-	-

Table 8.8: Chemical shift assignments of CitApc R93A (citrate-bound)

	N	C	CA	CB	CG	CD	CE
280 Leu	-	176.07	54.02	44.92	26.85	-	-
281 Gly	116.65	-	-	-	-	-	-
282 Gly	-	173.5	45.02	-	-	-	-
283 Glu	120.67	-	54.59	31.91	35.6	-	-
288 Asn	-	-	52.07	-	-	-	-
289 Arg	119.17	-	-	-	-	-	-
291 Pro	-	-	61.97	32.63	26.05	50.23	-
293 Lys	126.06	176.62	54.25	36.48	26.29	29.57	42.25
294 Asn	-	177.93	50.65	38.81	-	-	-
296 Gln	-	-	56.25	28.22	-	-	-
297 Gly	-	173.55	45.18	-	-	-	-
298 Arg	121.88	-	54.93	31.01	-	-	-
300 Ile	120.14	-	60.73	39.02	18.20,26.33	13.9	-
301 Gly	-	170.7	45.69	-	-	-	-
302 Ala	-	173.79	52.23	22.96	-	-	-
303 Val	118.85	-	59.25	35.81	-	-	-

Table 8.9: Residues of PAsC visible in spectra of CitApc R93A.

residue	citrate-free		citrate-bound	
	citrate-free	citrate-bound	citrate-free	citrate-bound
200	-	-	255	x
201	-	-	256	x
202	-	-	257	x
203	-	-	258	x
204	-	-	259	x
205	-	-	260	-
206	-	-	261	x
207	-	-	262	-
208	-	-	263	-
209	-	-	264	x
210	-	-	265	-
211	-	-	266	x
212	-	-	267	-
213	-	-	268	x
214	-	-	269	x
215	-	-	270	x
216	-	-	271	x
217	-	-	272	x
218	-	-	273	x
219	-	-	274	-
220	x	-	275	x
221	-	-	276	x
222	x	-	277	x
223	x	-	278	-
224	x	x	279	-
225	x	x	280	x
226	-	-	281	-
227	x	-	282	x
228	-	-	283	x
229	x	x	284	-
230	x	x	285	-
231	x	x	286	-
232	-	x	287	-
233	-	-	288	-
234	x	-	289	-
235	x	-	290	-
236	x	x	291	x
237	-	x	292	-
238	-	-	293	x
239	x	x	294	x
240	x	x	295	-

241	x	x	296	x	x
242	x	x	297	x	x
243	-	x	298	x	x
244	-	-	299	-	-
245	-	-	300	x	x
246	x	x	301	x	x
247	-	-	302	x	x
248	-	-	303	-	x
249	-	-	304	x	-
250	x	x	305	x	-
251	x	x	306	x	-
252	x	-	307	x	-
253	x	x	308	-	-
254	-	x	309	-	-
total	62	45			

8.4 Pulse programs

8.4.1 Liquid-state NMR

¹⁵N-HSQC

```
;hsqc15N.new
```

```
;D. Lee, Nov. 2002
```

```
;15N-1H HSQC correlations without water saturation
```

```
;The delay for 3-9-19 watergate (d5) should be matched
```

```
;with 1/d;d=distance of next null point (in Hz).
```

```
;S. Mori et al, JMR B108, 94-98 (1995)
```

```
;p1 : power for 1H
```

```
;p2 : power for 13C
```

```
;p3 : power for 15N
```

```
;p13 : power for 15N waltz16 decoupling
```

```
;p1 : 90 degree hard pulse 1H
```

```
;p3 : 90 degree hard pulse 13C
```

```
;p4 : 180 degree hard 13C pulse (225d for 5/600)
```

```
;p5 : 90 degree hard pulse 15N
```

```
;pcpd3 : 90 deg cpd-pulse15N(waltz16,160u)
```

```
;d1 : relaxation delay
```

```
;d2 : INEPT delay ( 2.7m)
```

```
;d5 : delay for 3-9-19=1/(Hz between nulls)
```

```
;in0 : 1/(2 SW) (Hz)
```

```

;p21 : 500u (Gradient in first INEPT)
;p22 : 500u (Gradient for z-filter)
;p23 : 1m (Gradient for second INEPT)
;gpz1 : 19%
;gpz2 : 30%
;gpz3 : 65%

# include <Avance.incl>

define delay INEPT_W
define delay INEPT_D

define GRADIENT1 10u p21:gp1 200u
define GRADIENT2 10u p22:gp2 200u
define GRADIENT3 10u p23:gp3 200u

"p2=2*p1"
"p6=2*p5"

"in0=inf1/2"
"d0=in0/2-p5*2/3.14159-p1"
"d3=d5/2-p5"
"INEPT_D=d2-p21-210u"
"INEPT_W=d2-(p23+210u+p1*2.3846+d5*2.5)"

1 10u ze
2 1m do:f3
d1 p1:f1
20u p3:f3
20u LOCKH_ON
;-----first INEPT
(p1 ph20):f1
GRADIENT1
INEPT_D
(center(p2 ph21):f1 (p6 ph1):f3)
GRADIENT1
INEPT_D
(p1 ph21):f1
GRADIENT2
;-----15N evolution
(p5 ph1):f3
(refalign (d0 p2 ph23 d0):f1 center (p3 ph23 1.5u p4 ph20 1.5u p3 ph23):f2)
(p5 ph20):f3
GRADIENT2
;-----second INEPT

```

```

(p1 ph22):f1
GRADIENT3
INEPT_W
(p1*0.2308 ph21 d5 p1*0.6923 ph21 d5 p1*1.4615 ph21):f1
(d3 p6 ph1 d3):f3
(p1*1.4615 ph23 d5 p1*0.6923 ph23 d5 p1*0.2308 ph23):f1
GRADIENT3
INEPT_W p13:f3 LOCKH_OFF
;-----acquisition
go=2 ph31 cpd3:f3
1m do:f3 mc 0 to 2 F1PH(ip1,id0)
10u do:f1
10u do:f2
10u do:f3
;10u do:f4
10u LOCKH_OFF
exit

ph1 =0 2
ph31=2 0

ph20=0
ph21=1
ph22=2
ph23=3

```

¹⁵N-NOESY-HSQC

```

;hsqc15N.new
;D. Lee, Nov. 2002

;15N-1H HSQC correlations without water saturation
;The delay for 3-9-19 watergate (d5) should be matched
;with 1/d;d=distance of next null point (in Hz).

;S. Mori et al, JMR B108, 94-98 (1995)

;p1 : power for 1H
;p2 : power for 13C
;p3 : power for 15N
;p13 : power for 15N waltz16 decoupling

;p1 : 90 degree hard pulse 1H
;p3 : 90 degree hard pulse 13C
;p4 : 180 degree hard 13C pulse (225d for 5/600)

```

```
;p5 : 90 degree hard pulse 15N
;pcpd3 : 90 deg cpd-pulse15N(waltz16,160u)

;d1 : relaxation delay
;d2 : INEPT delay ( 2.7m)
;d5 : delay for 3-9-19=1/(Hz between nulls)
;d8 : NOESY mixing
;in0 : 1/(2 SW) (Hz)

;p20 : 1m (Gradient in cleaning)
;p21 : 500u (Gradient in first INEPT)
;p22 : 500u (Gradient for z-filter)
;p23 : 1m (Gradient for second INEPT)
;p24 : 500u (Gradient for z-filter)
;p25 : 1m (Gradient for mixing)
;gpz0 : 80%
;gpz1 : 19%
;gpz2 : 30%
;gpz3 : 65%
;gpz4 : 37%
;gpz5 : 60%

;cnst22: 13C betw. CO and C(ali) [100ppm]
;cnst23: 13C betw. C(ali) and C(aro) [70ppm]
include <Avance_dl.incl>

define delay INEPT_W
define delay INEPT_D

define GRADIENT0 10u p20:gp0 200u
define GRADIENT1 10u p21:gp1 200u
define GRADIENT2 10u p22:gp2 200u
define GRADIENT3 10u p23:gp3 200u
define GRADIENT4 10u p24:gp4 200u
define GRADIENT5 10u p25:gp5 200u

"p2=2*p1"
"p6=2*p5"

"in0=inf1/2"
"in10=inf2/2"

"d0=in0/2-p1*2/3.14159"
"d10=in10/2-p5*2/3.14159"
"d7=d8-(p25+210u)"
```

```

"d3=d5/2-p5"
"INEPT_D=d2-p21-210u"
"INEPT_W=d2-(p23+210u+p1*2.3846+d5*2.5)"

aqseq 312

1 10u ze
2 1m
10u do:f3
d1
10u p1:f1
10u p2:f2
20u p3:f3
20u LOCKH_ON
10u
GRADIENT0
4m
10u fq=cnst23(bf ppm):f2
20u
(refalign (p1 ph1 d0 d0 p1 ph2):f1 center (p6 ph20):f3 center(p3 ph21 1.5u p4 ph20 1.5u p3 ph21):f2)
GRADIENT5
d7 fq=cnst22(bf ppm):f2
;-----first INEPT
(p1 ph20):f1
GRADIENT1
INEPT_D
(center(p2 ph21):f1 (p6 ph20):f3)
GRADIENT1
INEPT_D
(p1 ph21):f1
GRADIENT2
;-----15N evolution
; (p5 ph3):f3
(refalign (p5 ph3 d10 d10 p5 ph20):f3 center (p2 ph23):f1 center (p3 ph23 1.5u p4 ph20 1.5u p3 ph23):f2)
; (p5 ph20):f3
GRADIENT4
;-----second INEPT
(p1 ph22):f1
GRADIENT3
INEPT_W
(p1*0.2308 ph21 d5 p1*0.6923 ph21 d5 p1*1.4615 ph21):f1
(d3 p6 ph20 d3):f3
(p1*1.4615 ph23 d5 p1*0.6923 ph23 d5 p1*0.2308 ph23):f1
GRADIENT3
INEPT_W p13:f3 LOCKH_OFF

```


-----acquisition

go=2 ph31 cpd3:f3

1m do:f3 mc #0 to 2

F1PH(ip1,id0)

F2PH(rp1 & rd0 & ip3,id10)

10u do:f1

10u do:f2

10u do:f3

10u LOCKH_OFF

exit

ph1 =0 0 2 2

ph2 =0 0 0 0 2 2 2 2

ph3 =0 2

ph31=2 0 0 2 0 2 2 0

ph20=0

ph21=1

ph22=2

ph23=3

HCCH-TOCSY

Bruker standard pulse program: hcchdigp3d2

HNCO

Bruker standard pulse program: hncogp3d

¹³C-NOESY-HSQC

Bruker standard pulse program: noesyhsqcetgp3d

HNCA

Bruker standard pulse program: hncagpwg3d

CBCACONH

Bruker standard pulse program: cbcaconhgpwg3d

8.4.2 Solid-state NMR

PDSB

```
;sd.ksei

;=====
; Pulse program
;=====

1 ze
2 d1 do:f2
1u fq=0:f2

; set initial power levels
2u pl2:f2

;90 f2
p2:f2 ph1

;CP f2-f1, uses sp0 power level
(p15 pl5 ph2):f1 (p15:sp0 ph0):f2

;t1 evolution
1u pl12:f2
1u cpds2:f2
d0

;SD
(p1 pl1 ph3):f1
d11 do:f2
(p1 pl1 ph4):f1

;decoupling
1u pl12:f2
1u cpds2:f2

;acquisition
go=2 ph3 l
1m do:f2
100m wr #0 if #0 zd
1m id0
1m ip2
lo to 2 times td1

Halt Acq, 1m
```

```
exit
```

```
ph0 = 0
ph1 = 1 1 1 1 1 1 1 1
3 3 3 3 3 3 3 3
ph2 = 0
ph3 = 1 1 1 1 3 3 3 3
ph4 = 0 1 2 3
ph31= 0 1 2 3 2 3 0 1
2 3 0 1 0 1 2 3
```

CANCO

```
; CXNCY_3D.suva
```

```
;3D version of CXNCY (N-CY) correlation experiment (TPPI in both indirect dimensions)
;H to CX CP ==> CX evolution ==> CX to N CP ==> N evolution ==> N to CY CP ==> C evolution
;CW decoupling on protons during N from/to C transfer
;Similar Proton decoupling during both acquisition dimensions
; N (J) decoupling using 180 pulse in the indirect F1 dimension
; C (J) decoupling using 180 pulse in the indirect F2 dimension
```

```
;=====
; Variables introduction
;=====
```

```
;p2 H 90 pulse power
;p2 H 90 pulse length
;l31 (=2) HCX CP ramp on H, (=3) HCX CP ramp on C
;p15 HCX CP build up time
;p15 (=sp1) HCX CP power on CX
;p16 (=sp0) HCX CP power on H
;cnst10 HCX CP offset on C
;cnst20 HN CP offset on H
;p11 C 90 pulse power
;p1 C 90 pulse length
;p4 (= 2*p1) X 180 pulse length
;l29 (=1) CXN CP ramp on CX, (=3) CXN CP ramp on N, (=13) CXN CP ramp on both NC
;p35 CXN CP build up time
;p19 (=sp5) CXN CP power on N
;p110 (=sp6) CXN CP power on C
;l30 (=1) NCY CP ramp on CY, (=3) NCY CP ramp on N, (=13) NCY CP ramp on both NC
;cnst11 NCY CP offset on C
;cnst12 C offset for C j decoupling during N evolution
;p25 NCY CP build up time
```

```

;p17 (=sp2) NCY CP power on C
;p18 (=sp3) NCY CP power on N
;p13 N 90 pulse power
;p3 N 90 pulse length
;p5 (= 2*p3) N 180 pulse length
;p11 H CW decoupling during NC CP
;p12 H decoupling during both acquisitions
;cpds2 H decoupling program
;p31 H decoupling pulse length
;cnst21 H decoupling offset

```

```

;=====
; Set variables
;=====

```

```

;"l31 = 2"
;"sp0 = p16"
;"sp1 = p15"
;"l30 = 1"
;"sp2 = p17"
;"sp3 = p18"
;"sp4 = p110"
;"sp5 = p19"
;"p4 = 2*p1"
;"p5 = 2*p3"
;"cnst63 = p112"
;"cnst62 = p111"

```

```

"d0 = 1u"
"in0 = inf1/2"

```

```

"d10 = 1u"
"in10 = inf2/2"

```

```

;=====
; Begin Pulse program
;=====

```

```

1 ze

```

```

;— Relaxation & reset parameters —

```

```

2 d1 do:f2

```

```

2u p1:f1 p2:f2 p5:f3

```

```

2u fq=cnst10:f1
2u fq=cnst20:f2
2u fq=cnst30:f3

;--- 90 on H ---

(p2 pl2 ph1):f2

;--- HCX CP ---

if (l31 == 2)
{
(p15 pl5 ph2):f1 (p15:sp0 ph0):f2
}

if (l31 == 1)
{
(p15:sp1 ph2):f1 (p15 pl6 ph0):f2
}

;--- t1(C) evolution ---

2u pl12:f2 pl3:f3
1u cpds2:f2
d0*0.5
(p5 pl3 ph0):f3
d0*0.5
2u do:f2
1u pl10:f1 pl11:f2 pl9:f3

;--- CXN CP ---

if (l29 == 1)
{
(p35:sp4 ph4):f1 (p35 pl11 ph0):f2 (p35 pl9 ph3):f3
}

if (l29 == 3)
{
(p35 pl10 ph4):f1 (p35 pl11 ph0):f2 (p35:sp5 ph3):f3
}

if (l29 == 13)
{
(p35:sp4 ph4):f1 (p35 pl11 ph0):f2 (p35:sp5 ph3):f3
}

```

}

;— t2(N) evolution —

```

1u pl1:f1 pl12:f2
1u cpds2:f2
2u fq=cnst12:f1
d10*0.5
(p4 pl1 ph0):f1
d10*0.5
2u do:f2
2u pl7:f1 pl11:f2 pl8:f3

```

;— NCY CP —

2u fq=cnst11:f1

```

if (l30 == 1)
{
(p25:sp2 ph5):f1 (p25 pl11 ph0):f2 (p25 pl8 ph6):f3
}

```

```

if (l30 == 3)
{
(p25 pl7 ph5):f1 (p25 pl11 ph0):f2 (p25:sp3 ph6):f3
}

```

```

if (l30 == 13)
{
(p25:sp2 ph5):f1 (p25 pl11 ph0):f2 (p25:sp3 ph6):f3
}

```

;— acquisition with H decoupling —

```

2u fq=0:f1
1u pl12:f2
1u cpds2:f2
go=2 ph3 l
1m do:f2

```

;— write data —

10m wr #0 if #0 zd

1m id10

```
1m ip3
lo to 2 times td2
```

```
1m rd10
1m rp3
1m id0
1m ip2
lo to 2 times td1
```

```
HaltAcqu, 1m
exit
```

```
;--- Phase cycling ---
```

```
ph0 = 0
ph1 = 1 3
ph2 = 0
ph3 = 0 0 2 2
ph4 = 0
ph5 = 1 1 1 1 1 1 1 1
ph6 = 0 0 0 0 2 2 2 2
ph31 = 0 2 2 0 2 0 0 2
```

```
=====
; END Pulse program
=====
```

CA(NCO)CA

```
; CXNCYCZ_BSHCP_CC_2D.suva
```

```
;2D (CC) version of CXNCYCZ correlation experiment (TPPI in both indirect dimensions)
```

```
;H to CX CP ==> CX evolution ==> CX to N CP ==> N to CY CP ==> CYCZ BSHCP ==> C evolution
```

```
;CW decoupling on protons during N from/to C transfer
```

```
;Similar Proton decoupling during both acquisition dimensions
```

```
; N (J) decoupling using 180 pulse in the indirect F1 dimension
```

```
; C (J) decoupling using 180 pulse in the indirect F2 dimension
```

```
=====
; Variables introduction
=====
```

```
;p2 H 90 pulse power
```

```
;p2 H 90 pulse length
```

```
;l31 (=2) HCX CP ramp on H, (=3) HCX CP ramp on C
```

```

;P15 HCX CP build up time
;p15 (=sp1) HCX CP power on CX
;p16 (=sp0) HCX CP power on H
;cnst10 HCX CP offset on C
;cnst20 HN CP offset on H
;p11 C 90 pulse power
;p1 C 90 pulse length
;p4 (= 2*p1) X 180 pulse length
;l29 (=1) CXN CP ramp on CX, (=3) CXN CP ramp on N, (=13) CXN CP ramp on both NC
;p35 CXN CP build up time
;p19 (=sp5) CXN CP power on N
;p110 (=sp4) CXN CP power on C
;l30 (=1) NCY CP ramp on CY, (=3) NCY CP ramp on N, (=13) NCY CP ramp on both NC
;cnst11 NCY CP offset on C
;P25 NCY CP build up time
;p17 (=sp2) NCY CP power on C
;p18 (=sp3) NCY CP power on N
;p13 N 90 pulse power
;p3 N 90 pulse length
;p5 (= 2*p3) N 180 pulse length
;p111 H CW decoupling during NC CP
;p113 H CW decoupling during COCA BSHCP
;cpd1 H decoupling during COCA BSHCP
;p117 COCA BSH CP power on C
;p17 13C COCA CP contact time
;p18 CO flip pulse ca. 60 grad
;cnst13 COCA BSHCP offset on CA
;p19 CO flip to Y, ca. 4.5u
;p112 H decoupling during both acquisitions
;cpds2 H decoupling program
;p31 H decoupling pulse length
;cnst21 H decoupling offset

;=====
; Set variables
;=====

;l31 = 2"
;sp0 = p16"
;sp1 = p15"
;l30 = 1"
;sp2 = p17"
;sp3 = p18"
;sp4 = p110"
;sp5 = p19"

```



```

;"p4 = 2*p1"
;"p5 = 2*p3"
;"cnst63 = pl12"
;"cnst62 = pl11"
;"sp17 = pl17"
;"cnst61 = pl13"

"d0 = 0.4u"
"in0 = inf1/2"

;=====
; Begin Pulse program
;=====

1 ze

;--- Relaxation & reset parameters ---

2 d1 do:f2

2u pl1:f1 pl2:f2 pl5:f3
2u fq=cnst10:f1
2u fq=cnst20:f2
2u fq=cnst30:f3

;--- 90 on H ---

(p2 pl2 ph1):f2

;--- HCX CP ---

if (l31 == 2)
{
(p15 pl5 ph2):f1 (p15:sp0 ph0):f2
}

if (l31 == 1)
{
(p15:sp1 ph2):f1 (p15 pl6 ph0):f2
}

;--- t1(C) evolution ---

2u pl12:f2 pl3:f3
1u cpds2:f2

```

d0*0.5

(p5 p13 ph0):f3

d0*0.5

2u do:f2

1u pl10:f1 pl11:f2 pl9:f3

;— CXN CP —

if (l29 == 1)

{

(p35:sp4 ph4):f1 (p35 pl11 ph0):f2 (p35 pl9 ph3):f3

}

if (l29 == 3)

{

(p35 pl10 ph4):f1 (p35 pl11 ph0):f2 (p35:sp5 ph3):f3

}

if (l29 == 13)

{

(p35:sp4 ph4):f1 (p35 pl11 ph0):f2 (p35:sp5 ph3):f3

}

;— NCY CP —

1u fq=cnst11:f1

1u pl7:f1 pl11:f2 pl8:f3

if (l30 == 1)

{

(p25:sp2 ph5):f1 (p25 pl11 ph0):f2 (p25 pl8 ph6):f3

}

if (l30 == 3)

{

(p25 pl7 ph5):f1 (p25 pl11 ph0):f2 (p25:sp3 ph6):f3

}

if (l30 == 13)

{

(p25:sp2 ph5):f1 (p25 pl11 ph0):f2 (p25:sp3 ph6):f3

}

;— COCA BSH CP & CW during CP —

```

0.8u pl1:f1 pl13:f2
0.8u cpds1:f2

(p18 pl1 ph18):f1

1u fq=cnst13:f1
(p17:sp17 ph17):f1

(p19 pl1 ph19):f1

1u do:f2

;--- acquisition with H decoupling ---

2u fq=0:f1
1u pl12:f2
1u cpds2:f2
go=2 ph31
10u do:f2

;--- write data & 2D increments ---

10m wr #0 if #0 zd
1m id0
1m ip2
lo to 2 times td1

HaltAcqu, 1m
exit

;--- Phase cycling ---
ph0 = 0
ph1 = 1 3
ph2 = 0
ph3 = 0
ph4 = 0 0 2 2
ph5 = 1 1 1 1 1 1 1 1 3 3 3 3 3 3 3 3
ph6 = 0 0 0 0 2 2 2 2
ph17 = 1 1 1 1 1 1 1 1 3 3 3 3 3 3 3 3
ph18 = 2 2 2 2 2 2 2 2 0 0 0 0 0 0 0 0
ph19 = 3 3 3 3 3 3 3 3 1 1 1 1 1 1 1 1
ph31 = 0 2 2 0 2 0 0 2 2 0 0 2 0 2 2 0

;=====
; END Pulse program

```

```
=====
```

NCACB

```
;NCACB_3D.cshi
```

```
;DREAM for N-CA-CB, protonated sample
```

```
"p4=2*p1"
```

```
"p6=2*p3"
```

```
"d0=0.2u"
```

```
"d10=0.2u"
```

```
"in0=inf1/2"
```

```
"in10=inf2/2"
```

```
1 ze
```

```
2 d1 do:f2
```

```
1u do:f3
```

```
1u fq=0:f2
```

```
; 1u fq=cnst13:f3 ; 15N freq
```

```
; 1u pl13:f3 ; 15N/13C GARP/W16
```

```
2u fq=cnst10:f1 ; C0 freq.
```

```
1u pl2:f2 pl5:f3
```

```
; H 90
```

```
p2:f2 ph1
```

```
; HN CP
```

```
(p15:sp1 ph0):f2 (p15 pl5 ph2):f3
```

```
; t1(N) evolution
```

```
1u pl12:f2
```

```
1u cpds2:f2
```

```
d0*0.5
```

```
(p4 pl1 ph0):f1
```

```
d0*0.5
```

```
1u do:f2
```

```
; NC CP
```

```
if (l30 == 1)
```

```
{ (p25:sp2 ph4):f1 (p25 pl11 ph0):f2 (p25 pl8 ph3):f3
```

```
}
```

```
if (l30 == 2)
```

```
{ (p25 pl7 ph4):f1 (p25 pl11 ph0):f2 (p25:sp3 ph3):f3
```

```
}
```

```
;--- Second t2(CO) evolution ---
1u pl12:f2 pl3:f3
1u cpds2:f2
d10*0.5
(p6 pl3 ph0):f3
d10*0.5
1u do:f2

; DREAM for CACB transfer
1u fq=cnst25:f1
(p17:sp17 ph17):f1 (p17 pl14 ph0):f2

;--- acquisition with H decoupling ---

1u pl12:f2
1u cpds2:f2
; 1u cpds3:f3 ;
go=2 ph31
10u do:f2
; 10u do:f3

;--- write data & 3D increments ---

10m wr #0 if #0 zd

1m id10
1m ip4
lo to 2 times td2
1m rd10
1m rp4

1m id0
1m ip2
lo to 2 times td1

HaltAcqu, 1m
exit

ph0= 0 2 ; 1H cp
ph1= 1 1 1 1 3 3 3 3 ; 1H p90 excite
ph2= 0 0 2 2 ; 15N in 1Hto15N cp
ph3= 0 ; 15N in NCA dcp
ph4= 0
ph17=0 0 0 0 0 0 0 2 2 2 2 2 2 2 2 2
```

```

ph18=1 1 1 1 1 1 1 1 3 3 3 3 3 3 3
ph19=2 2 2 2 2 2 2 2 0 0 0 0 0 0 0 ; CO along Y
ph31=0 2 2 0 2 0 0 2

```

```

;p2 H 90 pulse length
;p2 H 90 pulse power
;p15 X CP power (constant)
;p15 CP contact time
;p112 acq. decoupling power
;sp17 13C CACB cp pl
;p17 13C CACB cp time
;cnst10 CA freq offset
;cnst25 CA-CB freq offset

```

```

;p1 X 90 pulse length (calibration)
;p11 X 90 pulse power (calibration)
;p16 1H CP power
;p113 15N w16 decoupling
;cnst12 1H SPINAL fq
;p114 1H cw for DREAM
;p111 1H cw for NCA dcp

```

NCACO

```
; NCACO_BSHCP_3D.suva
```

```

;3D version of NCACO correlation experiment (TPPI in both indirect dimensions)
;H to N CP ==> N evolution ==> N to CA CP ==> CO evolution ==>CACO BSHCP ==> C evolution
;CW decoupling on protons during N to C transfer and CACO BSH CP
;Similar Proton decoupling during both acquisition dimensions
; C (J) decoupling using 180 pulse in the indirect F1 dimension
; N (J) decoupling using 180 pulse in the indirect F2 dimension

```

```

;=====
; Variables introduction
;=====

```

```

;p12 H 90 pulse power
;p2 H 90 pulse length
;l31 (=2) HN CP ramp on H, (=3) HN CP ramp on N
;P15 HN CP build up time
;p15 (=sp1) HN CP power on N
;p16 (=sp0) HN CP power on H
;cnst30 HN CP offset on N
;cnst20 HN CP offset on H

```

```

;p11 X 90 pulse power
;p1 X 90 pulse length
;p4 (= 2*p1) X 180 pulse length
;cnst10 NCO CP offset on CO
;l30 (=1) NC CP ramp on C, (=3) NC CP ramp on N, (=13) NC CP ramp on both NC
;P25 NC CP build up time
;p17 (=sp2) NC CP power on C
;p18 (=sp3) NC CP power on N
;p11 H CW decoupling during NC CP
;p13 H CW decoupling during CACO BSHCP
;cpd1 H decoupling during CACO BSHCP
;p17 CACO BSH CP power on C
;p17 13C CACO CP contact time
;cnst11 CACO BSHCP offset on CA
;p19 CO flip to Y, ca. 4.5u
;p12 H decoupling during both acquisitions
;cpd2 H decoupling program
;p31 H decoupling pulse length
;cnst21 H decoupling offset

;=====
; Set variables
;=====

;"l31 = 2"
;"sp0 = pl6"
;"sp1 = pl5"
;"sp2 = pl7"
;"sp3 = pl8"
;"p4 = 2*p1"
;"p6 = 2*p3"
;"cnst63 = pl12"
;"cnst62 = pl11"
;"sp17 = pl17"
;"cnst61 = pl13"

"d0 = 0.2u"
"in0 = inf1/2"

"d10 = 0.2u"
"in10 = inf2/2"

;=====
; Begin Pulse program
;=====

```

1 ze

;— Relaxation & reset parameters —

2 d1 do:f2

2u pl1:f1 pl2:f2 pl5:f3

2u fq=0:f1

2u fq=cnst20:f2

2u fq=cnst30:f3

;— 90 on H —

(p2 pl2 ph1):f2

;— HN CP —

if (l31 == 2)

{

(p15:sp0 ph0):f2 (p15 pl5 ph2):f3

}

if (l31 == 3)

{

(p15 pl6 ph0):f2 (p15:sp1 ph2):f3

}

;— First t1(N) evolution —

2u pl1:f1 pl12:f2

2u cpds2:f2

d0*0.5

(p4 pl1 ph5):f1

d0*0.5

2u do:f2

2u fq=cnst10:f1

;— NC CP —

if (l30 == 1)

{

(p25:sp2 ph4):f1 (p25 pl11 ph5):f2 (p25 pl8 ph3):f3

}


```

if (l30 == 3)
{
(p25 pl7 ph4):f1 (p25 pl11 ph5):f2 (p25:sp3 ph3):f3
}

```

```

if (l30 == 13)
{
(p25:sp2 ph4):f1 (p25 pl11 ph5):f2 (p25:sp3 ph3):f3
}

```

;--- Second t2(CO) evolution ---

```

1u pl12:f2 pl3:f3
1u cpds2:f2
d10*0.5
(p6 pl3 ph5):f3
d10*0.5
2u dof2

```

;--- CACO BSH CP & CW during CP ---

```

0.8u pl1:f1 pl13:f2
0.8u cpds1:f2

(p17:sp17 ph17):f1

```

```

1u fq=cnst11:f1
(p19 pl1 ph19):f1

```

```

1u dof2

```

;--- acquisition with H decoupling ---

```

1u pl12:f2
1u cpds2:f2
go=2 ph31
10u dof2

```

;--- write data & 3D increments ---

```

10m wr #0 if #0 zd

```

```

1m id10
1m ip4
lo to 2 times td2

```

```
1m rd10
```

```
1m rp4
```

```
1m id0
```

```
1m ip2
```

```
lo to 2 times td1
```

```
HaltAcqu, 1m
```

```
exit
```

```
;— Phase cycling —
```

```
ph0 = 0 2
```

```
ph1 = 1 1 1 1 3 3 3 3
```

```
ph2 = 0 0 2 2
```

```
ph3 = 0
```

```
ph4 = 0
```

```
ph5 = 0
```

```
ph17 = 0 0 0 0 0 0 0 2 2 2 2 2 2 2 2
```

```
ph19 = 1 1 1 1 1 1 1 3 3 3 3 3 3 3 3
```

```
ph31 = 0 2 2 0 2 0 0 2
```

```
;=====
```

```
; END Pulse program
```

```
;=====
```

NCOCA

```
;NCOCA_BSH_3d.cshi
```

```
; BSH for N-CO-CA, protonated sample
```

```
; v2 for CO flip along Y axis
```

```
"p4=2*p1"
```

```
"p6=2*p3"
```

```
"in0=inf1/2"
```

```
"in10=inf2/2"
```

```
"d0=1u"
```

```
"d10=1u"
```

```
; Pulse program
```

```
;=====
```

```
1 ze
```

```
2 d1 do:f2
```

```
; 1u do:f3
```

```

1u fq=0:f2
; 1u fq=cnst13:f3 ; 15N freq
; 1u pl13:f3 ; 15N/13C GARP/W16
1u fq=cnst10:f1 ; C0 freq.
10u pl2:f2 pl5:f3

; H 90
p2:f2 ph1

; HN CP
(p15:sp1 ph0):f2 (p15 pl5 ph2):f3

; t1(N) evolution
1u pl12:f2
1u cpds2:f2
d0*0.5
(p4 pl1 ph0):f1
d0*0.5
1u do:f2

; NC CP
1u fq=cnst11:f1
if (l30 == 1)
{ (p25:sp2 ph4):f1 (p25 pl11 ph0):f2 (p25 pl8 ph3):f3
}
if (l30 == 2)
{ (p25 pl7 ph4):f1 (p25 pl11 ph0):f2 (p25:sp3 ph3):f3
}

; t2(CX) evolution
1u pl12:f2 pl3:f3
1u cpds2:f2
d10*0.5
(p6 pl3 ph0):f3
d10*0.5
1u do:f2

; flip CO for COCA cp
1u pl1:f1
(p18 ph18):f1

; COCA cp
1u fq=cnst25:f1
(p17:sp17 ph17):f1 (p17 pl14 ph3):f2
; (p19 ph19):f1 ; CA lock on X, CO flip to Y

```

```
; Acquisition with H decoupling
1u pl12:f2
1u cpds2:f2
go=2 ph31
10u do:f2

; Write data & 3D increments
10m wr #0 if #0 zd
1m id10
1m ip4
lo to 2 times td2
1m rd10
1m rp4
1m id0
1m ip2
lo to 2 times td1

HaltAcqu, 1m
exit

ph0= 0 2 ; 1H cp
ph1= 1 1 1 1 3 3 3 3 ; 1H p90 excite
ph2= 0 0 2 2 ; 15N in 1Hto15N cp
ph3= 0 ; 15N in NCA dcp
ph4= 0
ph17=0 0 0 0 0 0 0 2 2 2 2 2 2 2 2
ph18=1 1 1 1 1 1 1 1 3 3 3 3 3 3 3 3
ph19=2 2 2 2 2 2 2 0 0 0 0 0 0 0 0
ph31=0 2 2 0 2 0 0 2

;p2 H 90 pulse length
;p2 H 90 pulse power
;p15 X CP power (constant)
;p15 CP contact time
;p12 acq. decoupling power
;p17 13C COCA cp pl
;p17 13C COCA cp time
;p18 = pl1, CO flip pulse
;p18 CO flip pulse ca. 60 grad
;cnst10 CO freq offset
;cnst25 CA freq offset

;p1 X 90 pulse length (calibration)
;p4 X 180 pulse length (calibration)
```

```

;p11 X 90 pulse power (calibration)
;p3 N 90 pulse length (calibration)
;p6 N 180 pulse length (calibration)
;p13 N 90 pulse power (calibration)
;p16 1H CP power
;p113 15N w16 decoupling
;cnst12 1H SPINAL fq
;p114 1H cw for BSH
;p111 1H cw for NCA dcp
;p18 15N in NCO dcp
;p19 CO flip to Y, ca. 4.5u

```

NCOCACB

```

;NCOCACB_3D.cshi
; BSH for N-CO-CACB

"p4=2*p1"
"in0=inf1/2"
"in10=inf2/2"

1 ze
2 d1 do:f2
1u do:f3
2u fq=0:f2
2u fq=cnst10:f1 ; C0 freq.
2u pl2:f2 pl5:f3

; H 90
p2:f2 ph1

; HN CP
(p15:sp1 ph0):f2 (p15 pl5 ph2):f3

; t1(N) evolution
1u pl12:f2
1u cpds2:f2
d0*0.5
(p4 pl1 ph0):f1
d0*0.5
1u do:f2

; NC CP
if (l30 == 1)
{ (p25:sp2 ph4):f1 (p25 pl11 ph0):f2 (p25 pl8 ph3):f3

```

```

}
if (l30 == 2)
{ (p25 pl7 ph4):f1 (p25 pl11 ph0):f2 (p25:sp3 ph3):f3
}

; t2(CO) evolution
1u pl12:f2 pl3:f3
1u cpds2:f2
d0*0.5
(p6 pl3 ph0):f3
d0*0.5
1u do:f2

; BSH for COCA transfer
(p18 pl1 ph18):f1 ; flip CO
1u fq=cnst25:f1 ; CA freq.
(p17:sp17 ph17):f1 (p17 pl14 ph0):f2 ; BSH CP with cw proton dec.
; (p19 ph19):f1 ; CA lock on X, CO flip to Y

; DREAM for CACB transfer
;; 1u fq=cnst26:f1
(p21:sp21 ph21):f1 (p21 pl21 ph0):f2

; Acquisition
1u pl12:f2 pl13:f3
1u cpds2:f2
; 1u cpds3:f3 ;
go=2 ph31
10u do:f2
; 10u do:f3

; Write data & 3D increments
10m wr #0 if #0 zd

1m id10
1m ip4

lo to 2 times td2
1m rd10
1m rp4

1m id0
1m ip4
lo to 2 times td1

```

HaltAcqu, 1m

exit

ph0= 0 2 ; 1H cp

ph1= 1 1 1 1 3 3 3 3 ; 1H p90 excite

ph2= 0 0 2 2 ; 15N in 1Hto15N cp

ph3= 0 ; 15N in NCA dcp

ph4= 0 ; 13C in NCO

ph17=0 0 0 0 0 0 0 2 2 2 2 2 2 2 2 ;BSH-CP

ph18=1 1 1 1 1 1 1 3 3 3 3 3 3 3 3 ; trim before BSH-CP

ph19=2 2 2 2 2 2 2 0 0 0 0 0 0 0 ; CO along Y

ph21=0 0 0 0 0 0 0 2 2 2 2 2 2 2 2

ph31=0 2 2 0 2 0 0 2

;p2 H 90 pulse length

;p12 H 90 pulse power

;p15 X CP power (constant)

;p15 CP contact time

;p12 acq. decoupling power

;p17 13C COCA cp pl

;p17 13C COCA cp time

;p18 = p11, CO flip pulse

;p18 CO flip pulse ca. 60 grad

;cnst10 CO freq offset

;cnst25 CA freq offset

;cnst26 CA freq offset

;p1 X 90 pulse length (calibration)

;p11 X 90 pulse power (calibration)

;p16 1H CP power

;p13 15N w16 decoupling

;cnst12 1H SPINAL fq

;p14 1H cw for BSH

;p11 1H cw for NCA dcp

;p18 15N in NCO dcp

;p19 CO flip to Y, ca. 4.5u

HC-INEPT

; inept1D.hh

; based on cp.ksei

; last change: 30-Oct-2006, 31.Oktober: with 13c-decoupling

;cnst2=145

;cnst3=6

```

;echo delays
;OWNER=nmrsl
"d4=1/(4*cnst2)"
"d3=1/(cnst3*cnst2)"
"in0=infl/4"
;compensation delays
;p1>p2
;"d5=p1-p2"
;"d6=d5/2"

;=====
; Pulse program
;=====

1 ze ;accumulate into an empty memory
2 d1 do:f2
1u fq=0:f2

;90 1H
2u pl2:f2 pl1:f1
p2:f2 ph1

d0
p1*2:f1 ph0
d0
;spinecho
d4
(p2*2 ph2):f2 (p1*2 ph4):f1
; (d5 p2*2 ph2):f2 (p1*2 ph4):f1
d4

;PT
(p2 ph3):f2 (p1 ph5):f1
; (d6 p2 ph3):f2 (p1 ph5):f1

;spinecho
d3
(p2*2 ph2):f2 (p1*2 ph6):f1
; (d5 p2*2 ph2):f2 (p1*2 ph6):f1
d3

;acquisition with decoupling (choose GARP)
1u pl12:f2
1u cpds2:f2

```

```
;lu pl12:f2
go=2 ph31
1m do:f2 ;decoupler off
100m wr #0 if #0 zd
1m id0
1m ip1
lo to 1 times td1
HaltAcqu, 1m ;jump address for protection files
exit ;quit
```

```
ph0= 0 2
;ph1 = 0 0 0 0 0 0 0 0 2 2 2 2 2 2 2 2
ph1 = 0 2
ph2 = 0 2
;ph3 = 1 1 3 3
ph3 = 1
ph4 = 0 2
;ph5 = 0 0 0 0 1 1 1 1 2 2 2 2 3 3 3 3
ph5 = 0 0 2 2
;ph6 = 0 2 0 2 1 3 1 3
ph6 = 1 3
;ph31= 0 0 2 2 1 1 3 3
ph31= 1 3 3 1
```


Curriculum Vitae

Personal data

Name Benjamin Schomburg

Date of Birth 11.06.1985

Place of Birth Löhne

Nationality German

Education

1991-1995 Primary school Grundschule Gohfeld

1995-2004 Secondary school Städtisches Gymnasium Löhne

2004-2005 Community Service at the City Environmental Office Löhne

2005-2010 Biochemistry Studies at the University of Bielefeld

2010 Master thesis at the University of St. Andrews, United Kingdom.
Subject: *Monitoring structural changes in an FbaB-CnaB2 mutant by NMR spectroscopy*, supervisor: Dr. Uli Schwarz-Linek.

2010-2014 Ph.D. student at the Max Planck Institute for Biophysical Chemistry in Göttingen, Germany. Subject: *Transmembrane Signalling: Structural and functional Studies on Histidine Kinase CitA*, supervisor: Prof. Dr. Christian Griesinger.

Göttingen, December 2014